REPORT DOCUMENTATION PAGE

Form Approved
OMB No. 0704-0188

1. AGENCY USE ONLY (Leave Blank)	2. REPORT DATE	3. REPORT TYPE AND DATES COVERED
	02 November 25	FINAL 00 February 01 through 02 August 31

4. TITLE AND SUBTITLE
Micro Laser Plasma Thrusters for Small Satellites

5. FUNDING NUMBERS
F49620-00-C-0005

6. AUTHOR(S)
Claude R. Phipps, Ph.D.

7. PERFORMING ORGANIZATION NAME (S) AND ADDRESS(ES)
Photonic Associates
200A Ojo de la Vaca Road
Santa Fe, NM 87508

8. PERFORMING ORGANIZATION REPORT NUMBER
PHO0003

9. SPONSORING/MONITORING AGENCY NAME(S) AND ADDRESS(ES)
Department of the Air Force
Air Force Office of Scientific Research
801 North Randolph St. Room 732
Arlington, VA 22203-1977

10. SPONSORING/MONITORING AGENCY REPORT NUMBER
0002AC

11. SUPPLEMENTARY NOTES

12a. DISTRIBUTION/AVAILABILITY STATEMENT
Distribution Statement A: Approved for public release; distribution is unlimited.

12b. DISTRIBUTION CODE

13. ABSTRACT (Maximum 200 words) Final Report, STTR Phase II contract

We developed and tested a preprototype micro laser plasma thruster (μLPT). This is a new departure in sub-kilogram micropropulsion modules, which we believe can compare favorably with the μPPT in total impulse/dry mass and thrust/power ratios. A lens focuses the light output of a group of fiber-coupled diode lasers onto a special ablatant tape. The tape is composed of a transparent supporting layer through which the light passes without perforating it, and a proprietary absorbing fuel layer which is ignited and further heated by the laser to produce a miniature jet. The device is repetitively pulsed, operates on spacecraft bus voltage, and weighs 0.85 kg.The diodes have 50% electrical to optical efficiency. Best performance from a non-energetic fuel material was obtained with black polyvinyl chloride (PVC), which produced an average of 66 μN thrust and coupling coefficient (C_m) of 80μN/W. A proprietary energetic material was also tested, in which the laser initiates a non-propagating detonation. This material produced 500 μN of thrust and C_m was 300μN/W. Data are summarized from over 200 single-shot and full thrust tests on dozens of combinations of ablatant materials and supporting transparent polymers.

14. SUBJECT TERMS
Final STTR Report

plasma, microsatelite, nanosatellite, picosatellite, micropropulsion, laser ablation, thruster, micro-PPT

15. NUMBER OF PAGES
76

16. PRICE CODE

17. SECURITY CLASSIFICATION OF REPORT	18. SECURITY CLASSIFICATION OF THIS PAGE	19. SECURITY CLASSIFICATION OF ABSTRACT	20. LIMITATION OF ABSTRACT
UNCLASSIFIED	UNCLASSIFIED	UNCLASSIFIED	

F49620-00-C-0005
0002-AC

REPORT TITLE

Micro Laser Plasma Thrusters for Small Satellites

Prepared By:

Dr. Claude Phipps, Principal Investigator
PHOTONIC ASSOCIATES
200A Ojo de la Vaca Road
Santa Fe, NM 87508

Prepared For:

Dr. Mitat Birkan, Program Manager
AFOSR/NA
Directorate of Aerospace and Material Sciences
801 North Randolph St. Room 732
Arlington, VA 22203-1977

Prime Contract Number:	F49620-00-C-0005
Contract Type:	STTR Phase II
Contract Date:	February 1, 2000
Status report for Period:	1 February 2000 through 31 August 2002

Acknowledgments

The **New Mexico Engineering Research Institute** (NMERI), a unit of the University of New Mexico (UNM), Albuquerque, NM was subcontractor for the majority of this effort. Toward the end of the contract period, the name was changed to **Institute for Engingeering Research and Applications** (IERA), when the parent organization changed to New Mexico Institute for Mining and Technology (NMT) in Socorro, NM. NMERI/IERA provided the experimental facilities used in obtaining the results reported herein. The work would not have been possible without these facilities, and the enthusiastic and skilled cooperation of NMERI/IERA personnel, especially the co-PI, **Dr. James Luke**. Throughout the program, his dedication, creativity and technical knowledge were crucial. He built a large part of our test setup, and was an active participant in all tests. Dr. Luke was co-author of this report.

Other technical contributors included **Mr. Wesley Helgeson**, our fine electronics technician, **Mr. Ryan McNeal**, our CADCAM expert, and **Dr. Glen McDuff**, who helped significantly with the digital electronics and target tape creation. The tireless support of the laboratory director, **Mr. John Marquis,** was also critical for our success. We also deeply appreciate many instances of helpful advice from **Dr. Greg Spanjers**, AFRL Edwards.

Executive Summary

Major accomplishments under this STTR Phase II contract were:

1) Construction and testing the first model of a unique new microthruster which can meet Air Force requirements for the attitude control system of 100-kg-class spacecraft.

2) Building and testing a unique type of thrust stand with 5mN/rad response and 20μN resolution.

3) Completing an ablatant R&D program in which over 200 single-shot and full thrust tests were conducted. In this program, single-shot "static" tests gave I_{sp} up to 1800 seconds and thrust-to-power ratio C_m up to 1200 μN/W, and full thrust tests gave I_{sp} up to 300 seconds with C_m of 350 μN/W. The discrepancy is mainly due to differing illumination geometries as explained in the text.

4) Achieving 75μN thrust and C_m = 120μN/W with a passive ablatant that we developed.

5) Achieving 560μN thrust, C_m = 275μN/W and I_{sp} = 300 seconds with an exothermic ablatant developed by Paul Scherrer Institut, Villigen, Switzerland.

6) Designing, building and testing a unique optical system (the "R-mode optic") which facilitates grazing incidence target illumination in order to study R-mode target illumination without optic contamination.

7) Combining the outputs of four JDSU 6380-A fiber-coupled diode lasers for 15W peak power and 2W average power in repetitive-pulse operation.

8) Completing a concept-level design of a commercial product thruster's component subsystems, and identifying some commercial components for these.

9) Measuring the angular distribution of carbonaceous deposits resulting from preprototype operation

10) Discovering and solving a plume steering problem associated with continuous operation

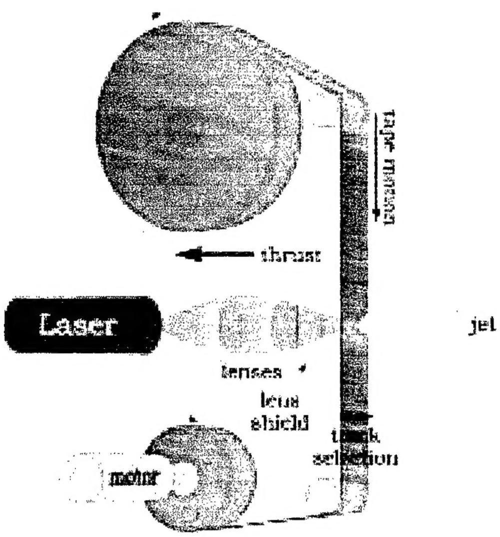

Figure 1. The μLPT concept

Program Objectives

The μLPT is designed towards the Attitude Control System requirements in a 100kg spacecraft (TechSat21-class). Related requirements are:

- Four thrust axes
- 75μN thrust per axis
- 100N-s impulse per axis
- 320 N-s total lifetime impulse

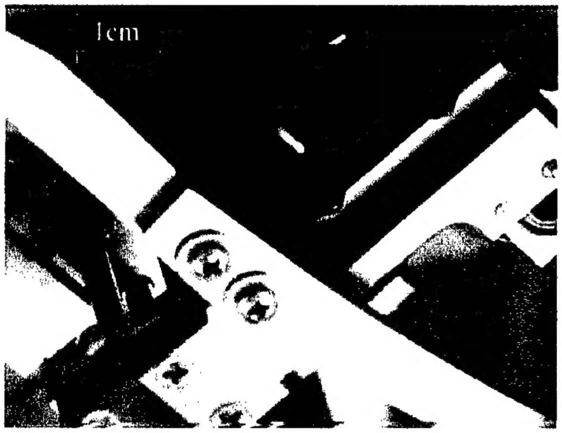

Figure 2. The μLPT jet

Its sub-kg mass is about 10% of the reaction-wheel/torque-rod mass currently installed on TechSat 21. With engineering development, the μLPT can exceed the AFRL μPPT in total impulse/dry mass and thrust/power ratio.

1. Overview of the LPT Program

The micro-Laser Plasma Thruster (μLPT) is a sub-kg micropropulsion option invented and developed by Photonic Associates.

The Air Force has identified this technology as an alternative to the micro pulsed plasma

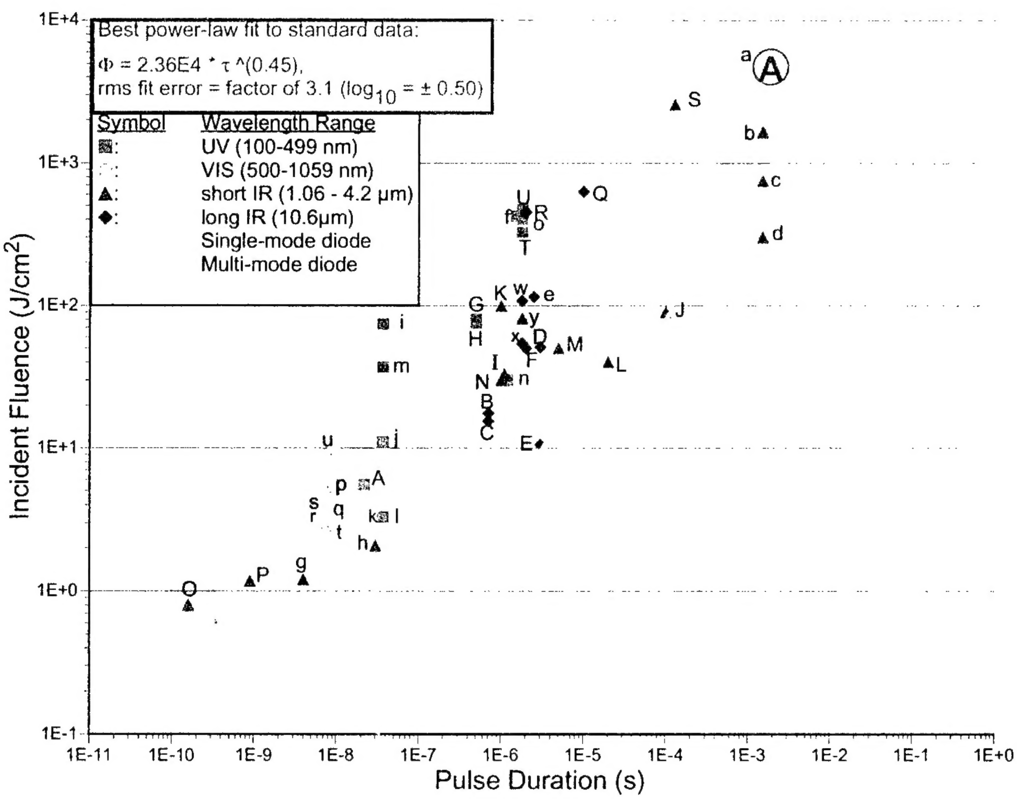

Figure 3. Optimum coupling fluence vs. pulse duration. The gold bar is a best fit to data from 46 experiments reported in the literature in which this parameter was given or could be deduced, covering wavelengths from the long infrared to the ultraviolet. The solid and dashed grey lines represent, respectively, the capability of a single-mode, 1W diode laser and a multi-mode 4W diode laser focused with standard optics. Our operating point is shown at "A".

thruster (μPPT) for micro-propulsion applications.

Four JDS Uniphase 6380-A multi-transverse-mode diode lasers operating at 920 nm drive the ms-pulse μLPT. Standard 0.68NA aspheric lenses focus the 14W laser peak output to a 500μm^2 spot, giving 3 MW/cm^2 on target. These intensities are sufficient to form a plasma jet. [Figure 1].

The diodes are low-voltage devices with electrical efficiency in excess of 50%. The laser light is focused on the transparent side of a double-layer fuel tape [Figure 5]. Passing through the transparent, acetate-base backing without damaging it, the beam heats a specially prepared absorbing coating on the opposite side of the tape to high temperature, producing the ablation jet. This is highly collimated due to confining electrostatic forces involved in the plasma formation and expansion [Figure 2].

Figure 3 is a plot of optimum incident fluence for plasma formation, using literature data. [See Phipps and Luke 2002 for a detailed discussion and references]. The μLPT became realistic when laser diodes developed adequate power and brightness for their essentially constant-power operating characteristic to intersect the best fit gold bar in the Figure at a useful operating point. The Figure predicts that 1-W diodes with pulse durations of at least 0.2 to 1ms will be able to produce plasma jets.

The target fuel tape is 1 inch wide. For passive targets, that is, those in which the coating material itself is not exothermic, we typically use 160μm total thickness, including 60μm of ablatant and 100μm of transparent acetate backing.

TABLE 1. Preprototype specifications

Item	**Value**
Weight with fuel	850 g
Tape dimensions	50.5cm x 2.54cm
Backing thickness	100μm
Ablative coating thickness	90μm
Laser power (P_{avg}, P_{pk})	2 W, 14W
Laser target illumination area	500 μm^2
Tape speed	20 mm/s
Pulse duration	2 ms
Pulse repetition frequency	100 Hz
Track width	100μm
Tracks	254
Tape lifetime	1.8 hours
Coupling coefficient C_m	80 μN/W
Force output §	150 μN
Q*	11 kJ/g
I_{sp}	400 s
Minimum impulse bit	0.6 μN-s †

§ using C_m and P_{avg}, †: at 1ms pulsewidth

Typical thrust was 75μN for the passive polyvinyl chloride (PVC) target with up to 14W peak incident optical power, but, for the designer material, 560μN, 7.5 times what is required by the program objectives.

TABLE 2. Passive vs. designer coating performance		
Coating (measurement type)	C_m (μN/W)	I_{sp} (seconds)
Passive (dynamic)	120	160
Designer (dynamic)	350	360
Passive (static)	200	1800
Designer (static)	1200	550

The minimum impulse bit we measured was is 0.4 nano N-s in a 100μs pulse. Mass of the preprototype [Figure 4] and associated electronics is 850g.

In addition to transmission ("T-mode) illumination, we have studied Reflection mode, [Figure 5] in which the jet and the laser are located on the same side of the target. R-mode gives about 2 times better I_{sp} and 50% better C_m, but also offers significant design challenges to limit contamination of the illumination optics to acceptable levels [see section 5.1.3 of this report].

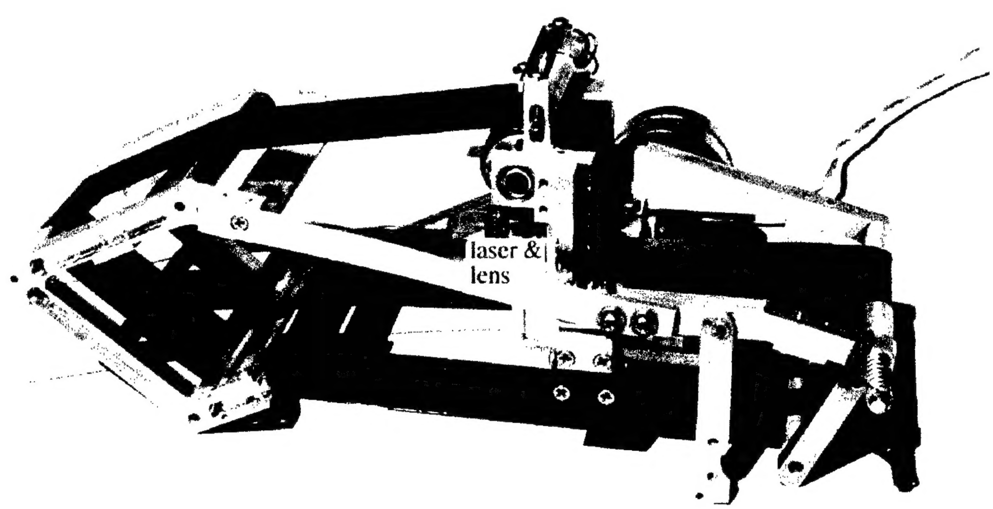

Figure 4. The preprototype microthruster. Pictured is an earlier version using a single JDSU 6380-A laser, rather than the current bundle of 4 fiber-coupled 6380-A(L2) lasers. A spring-loaded tape-tensioning arm is located at the right-hand end of the device.

Our Phase I work demonstrated feasibility of the micro Laser Plasma Thruster (μLPT) [Phipps & Luke 1999]. It is expected to show good performance in system specific impulse I_{ssp}, defined as [Koppel 1999]:

$$I_{ssp} = I_{sp}(1+k) \quad [1]$$

where

$$k = M_{dry}/M_{fuel} \quad [2]$$

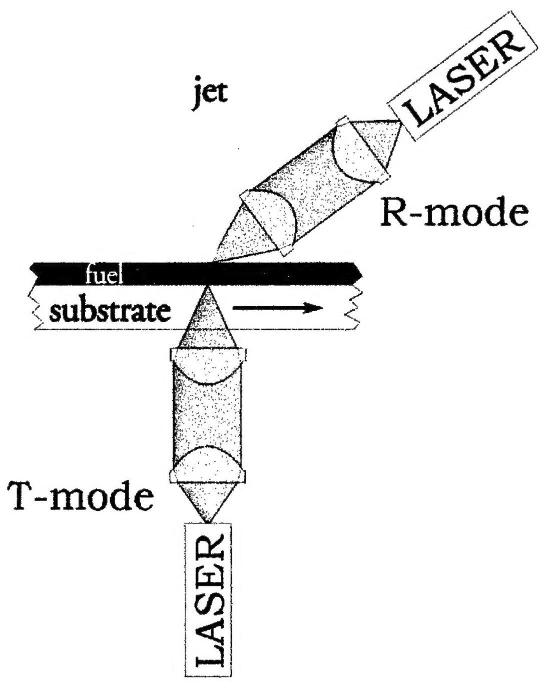

Figure 5. Defining R- and T-mode

because $k \approx 4$ for this thruster. Dry mass consists of the package, a laser diode, two tiny lenses, an electronics board and two tiny motors to move the fuel tape past the laser diode focus and change tracks. The μLPT requires no neutralizers, heaters, high voltage supply, high voltage switches, magnetic fields, nozzle, gas, tanks, or valves. It is also free of mysterious small-scale physics.

Most importantly, nothing erodes during operation except the ablation fuel. The μLPT can operate pulsed or CW, and power density on target is optically variable in an instant, so I_{sp} can be adjusted "on the fly" to match mission requirements.

We believe the μLPT will benefit civilian as well as Air Force microsatellite propulsion applications.

This is the final report of work completed on Photonic Associates' AFOSR Phase II STTR prime contract F49620-00-C-0005. The objective of this contract was to build a laser plasma microthruster. Phase I was completed 31 July 1999 under AFOSR contract F49620-98-C-0038. Our subcontractor throughout both contracts has been the University of New Mexico's New Mexico Engineering Research Institute (NMERI). Toward the end of the contract period, NMERI changed its name to the Institute for Engineering Research and Applications, and its parent organization changed to New Mexico Institute for Mining and Technology (NMT) in Socorro, NM. NMERI/IERA provided the experimental facilities used in obtaining the results reported herein.

Table 3. How thermal diffusion losses affect target heating with 2ms pulses [a]			
Material	**x_{2th}(2ms)/d_s(100μm)** [Ratio of thermal diffusion depth at 2ms to spot size]	**ΔT(2ms)** [Temperature rise at τ=2ms (K)]	**Δt (2000K)** [Time to reach 2000K (s)]
PMMA	4.98E-2	3.81E+3	1.38E-4
Polyvinylidene chloride (Saran™)	8.88E-2	1.54E+3	8.47E-4
PVC	1.40E-1	1.31E+3	1.17E-3
Polystyrene	1.65E-1	1.22E+3	1.33E-3
Celluloid	1.38E-1	1.00E+3	1.99E-3
Teflon	1.49E-1	9.50E+2	2.21E-3
Cellulose acetate	1.68E-1	8.11E+2	3.04E-3
Graphite	5.62E+0	5.56E+2	6.48E-3
Silica	4.10E-1	5.28E+2	7.18E-3
Tungsten	1.09E+0	1.04E+2	1.84E-1
Titanium	1.10E+0	8.79E+1	2.59E-1
Nylon	1.30E+0	8.66E+1	2.67E-1
Tantalum	2.43E+0	5.23E+1	7.31E-1
Aluminum	3.92E+0	3.12E+1	2.05E+0
Copper	4.77E+0	1.98E+1	5.08E+0

[a] 4W laser input assumed, with 25% absorption

2. Theoretical Considerations

2.1 Impulse Generation

Laser impulse production by pulsed-laser-induced ablation in vacuum is well understood [Phipps, *et al.* 1988; Phipps & Michaelis 1994]. The maximum momentum per joule of incident laser light is produced at a fluence Φ_{opt} which is close to the threshold for plasma formation since, above this level, plasma inhibits coupling [Figure 3]. Even with laser spot size d_s as small as 5μm, impulse coupling efficiency C_m and Φ_{opt} are well-predicted. Apart from slowly varying factors related to dimensionality of the expansion and the ratio of d_s to thermal penetration depth during the pulse, estimates based on the large existing literature apply.

Relative to the values shown in Figure 3, from 2-20 times greater laser power will be required to compensate thermal conductance with very small spots and long pulses when

highly thermally conductive materials are used [Table 3]. With 1 to 4W CW laser power in our research setup, it has been necessary to use ablatants with low thermal conductivity such as PVC. As expected, we were not able to produce a spark on aluminum [Table 3].

The momentum coupling coefficient C_m is defined as the ratio of target momentum $m\Delta v$ produced to incident laser pulse energy W during the ejection of laser-ablated material (the photoablation process). For continuous lasers, it is the ratio of thrust F to incident power P:

$$C_m = \frac{m\Delta v}{W} = \frac{F}{P} \quad . \tag{3}$$

In the ablation process, Q* joules of laser light (the asterisk is customary notation: Q* is not a complex number) are consumed to ablate each kg of target material:

$$Q^* = \frac{W}{\Delta m} \quad . \tag{4}$$

Energy conservation prevents C_m and Q* from being arbitrary. Increasing one decreases the other. Using Eqs. (1) and (2), energy conservation requires that several constant product relationships exist:

$$2\eta_{AB} = \Delta m v_E^2/W = C_m^2 Q^* = gC_m I_{sp} = C_m v_E. \tag{5}$$

In Eq. [5], $\eta_{AB} \leq 1$ is the efficiency with which laser energy W is converted into exhaust kinetic energy. Choosing combinations of C_m and Q* which exceed the limit expressed in [5] violates physics.

The rate of mass usage is $$\dot{m} = \frac{P}{Q^*} \quad \text{g/s} \qquad [6]$$

where P is laser optical power. When considering C_m and Q* as design variables it must be kept in mind that the ablator lifetime increases with Q* and decreases very rapidly with increasing C_m:

$$\tau_{AB} = \left|M/\dot{m}\right| = \frac{MQ^*}{P} = \frac{2\eta_{AB}M}{P\,C_m^2} \quad , \qquad [7]$$

and that increasing C_m to get more thrust via the relationship

$$F = PC_m \qquad [8]$$

from a given laser entails a serious penalty for ablator lifetime, because $\tau_{AB} \propto 1/C_m^2$ from Eq. [5]. The vacuum coupling coefficient C_m is in the range 10 - 100 μN/W for standard surface-absorbing materials [Phipps *et al.* 1988]. Note that, from Eq. (5), $C_m{*}I_{sp} \leq 2/g = 0.204$. In measurements with exothermic target materials, products $C_m{*}I_{sp} = 0.18$ have been obtained, which is 90% of the theoretical limit for passive materials [Phipps and Michaelis 1994]..

In the laboratory, C_m and Q* are relatively easy quantities to measure, and their product conveniently gives v_E, which is a difficult quantity to measure, requiring, e.g., a laser-induced fluorescence setup or time-resolved shadowgraphy.

The maximum specific impulse of chemical rockets is about 500s, limited by the temperatures available in chemical reactions. Exit velocity v_E > 5km/s (I_{sp} > 5000s) is accessible only by laser ablation, where temperatures can be many times 10,000K, or some other non-chemical process such as ion drives. Specific impulse I_{sp} up to 8000s has been measured with pulsed lasers [Phipps and Michaelis 1994]. Our ultimate goal is to apply these results to microthruster development.

2.2 Inducing Shock in Targets

The classic analysis of high-intensity laser interaction with materials divides into two regimes: laser supported combustion (LSC) and laser supported detonation (LSD) [Pirri, Root & Wu 1978; Raizer 1977]. Although the analysis was originally developed by aerodynamicists for interactions in air, some of these concepts can also apply to a solid target in vacuum.

Table 4. Laser-induced pressure vs. laser parameters

Pulse duration τ	Conditions	Intensity I	Pulse energy W	Pressure (bar)
4ms	Laser welding	13 kW/cm^2	4 mJ	0.43
10 ns	Laser fusion	5.9 GW/cm^2	1800 J	10,000

The transition from the LSC to LSD regime is caused by laser intensity sufficient to produce a shock wave in the material, i.e., wave velocity greater than the particle thermal velocity. For our purposes, it is sufficiently accurate to describe shock formation by the relationship

$$\nabla p = \rho v \cdot \nabla v \qquad [9]$$

from which

$$p = \rho v^2 = \rho c_s^2 \quad . \qquad [10]$$

Taking sound speed c_s=1E5 cm/s and mass density ρ=1 g/cm^3 we find laser-induced pressure p ≅ 1E10 dyn/cm^2 = 10 kbar is necessary. The energy density involved is:

$$u = \frac{3}{2}nkT = \frac{3}{2}p = \frac{3}{2}(1E10)\ \mathrm{erg/cm^3} \qquad [11]$$

In practical terms, the required deposited energy density is u = 1500 J/cm^3 to cause a detonation.

It remains to see what combination of laser intensity I (W/cm^2), pulsewidth τ (s) and wavelength λ(cm) will give the required 10kbar pressure. Vacuum plasma theory adapted from laser fusion [Phipps, *et al.* 1988; Phipps and Dreyfus 1993] well describes the situation above plasma threshold, as has now been generally accepted [Saleres, *et al.* 1992; Fabbro, *et al.* 1990]. The principal results of our earlier work which we will use here is, for the laser-initiated plasma-mediated pressure on a plane surface:

$$p_{AB} = 5.83 \frac{\Psi^{9/16}}{A^{1/8}} \frac{I^{3/4}}{(\lambda\sqrt{\tau})^{1/4}} \qquad [12]$$

and

$$T_e = 2.98\text{x}10^4 \frac{A^{1/8}\, Z^{3/4}}{(Z+1)^{5/8}} (I\lambda\sqrt{\tau})^{1/2} \qquad [13]$$

for the plasma electron temperature (K), where Ψ = the coefficient $(A/2)[Z^2(Z+1)]^{1/3}$, A is the plasma average atomic mass number, Z is the plasma average ionization state number, I is in W/cm^2 and p_{AB} is in dyn/cm^2. Without much loss, we can take Ψ=1 and, for a

Table 5. Summary of Laser Momentum Coupling Literature

Ref.	Target	Laser λ,τ	Max. C_m (μN/W)	Max. C_m*I_{sp}
Phipps, *et al.* 1988	Passive (front illuminated)	various	100	-----
Phipps, *et al.* 1990	Pyroxylin (front illuminated)	10.6 μm, 2μs	950	0.19
Phipps, *et al.* 2000; Yabe, *et al.* 2002	Confined passive absorber	1.06 μm, 85ns	4920	0.009
Fabbro, *et al.* 1990	Confined passive absorber	1.06 μm, 3ns	7000	-----

carbon-hydrogen plasma, A=6. Then, e.g., with λ=970nm, we have the results shown in Table 4.

In other words, it requires laser fusion conditions in an unconfined target to create a shock in the target.

This is a very important consideration when dealing with exothermic ablatant fuels.

In a confined target, on the other hand, it takes far less laser intensity. Fabbro, et al 1990 have shown pressure amplification up to a factor of 70 by confining the plasma between an anvil and a glass plate through which the laser light is introduced to the target. Other workers have replaced the glass plate with a liquid film for industrial applications.

Table 5 provides a summary of laser momentum coupling literature, in order to place the results we report here in perspective.

3. Technical Objectives & Status of Effort

There have been no changes to the technical objectives nor to the statement of work for this contract. All tasks are complete.

4. Technical Accomplishments

4.1 Major Achievements – Hardware

4.1.1 Pre-Preprototype Engineering

The preprototype uses a 50.5-cm continuous-loop tape 2.54 cm wide. At 20mm/s with 100-μm track separation, this offers 254 tracks and 1.8 hours of continuous operation.

The preprototype experimental thruster consists of the optical assembly, the focusing mechanism, track selector mechanism, tape drive mechanism, and the tape guide rollers.

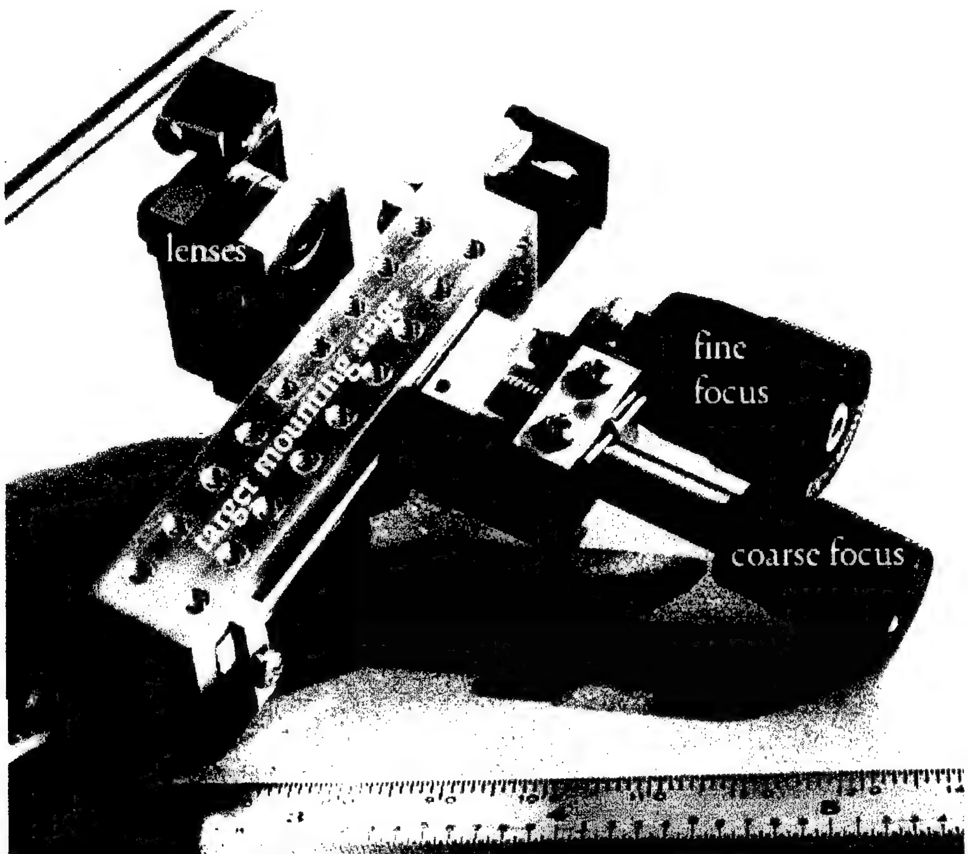

Figure 6. The optical assembly, target mounting stage, and focus mechanism. Shown is the version in which one JDSU 6380-A laser and heatsink is mounted directly behind the collimating and focusing lens pair. In the latest version, the lasers are located remotely and their optical fibers are clamped directly above the word "lenses" in the photo.

The optical assembly includes the laser, laser and fiber mounts, and lens mounts. The optical assembly, shown in Figure 6, is mounted adjacent to the target mounting stage.

The target mounting stage is guided by two pairs of polished steel rods at right angles to each other. It is driven parallel to the optical axis by the focusing mechanism, and perpendicular to the optical axis by the track selector mechanism.

The focusing mechanism acts directly on the target mounting stage, against a return spring. The coarse focus knob has a 0.318mm thread pitch, and the fine focus knob has a 0.254mm thread pitch and acts through a 10:1 lever. The fine focus knob (which can be seen in Figure 6) is marked with 50 divisions around its circumference. Each division corresponds to approximately 0.5μm of travel of the target mounting stage relative to the optical assembly.

4.1.2 Preprototype electromechanical Subsystem

The track selector mechanism drives the target mounting stage with a stepper motor,

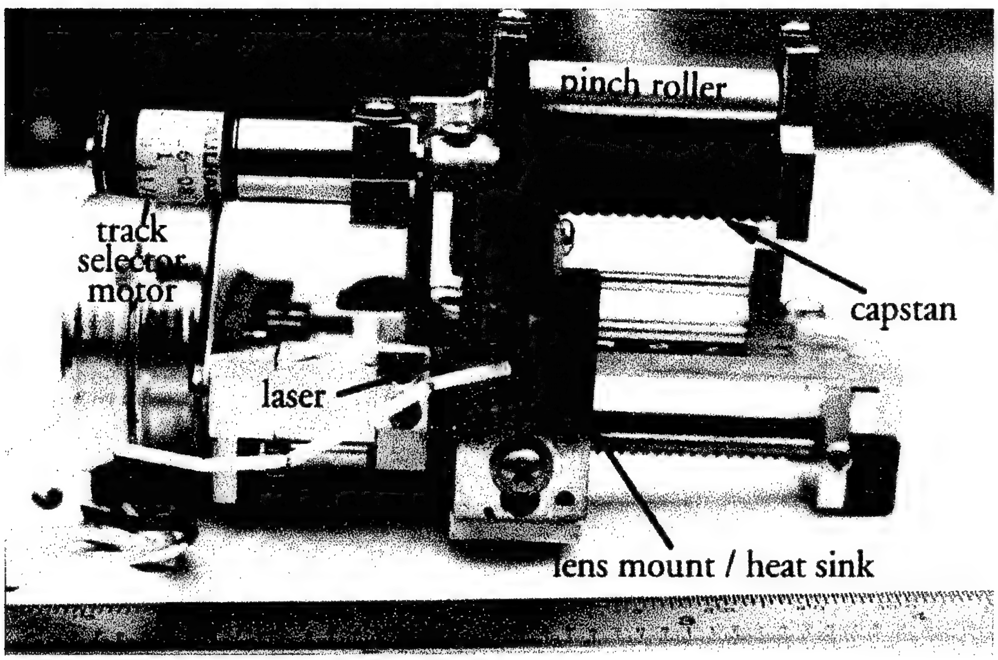

Figure 7. Detail of the tape drive with the single 6380-A laser installed.

which turns a small brass jackscrew through a 3:1 reduction gear. The jackscrew has a 1.5mm thread pitch and runs in acetal (self-lubricating plastic) bearings. In half-stepping mode, the motor can move the target mounting stage in steps as small as 5μm. The track selector mechanism can be seen in Figures 4 and 7.

The tape drive mechanism is mounted on the target mounting stage. In Figure 4, the motor drives the tape vertically through the laser focus. The capstan [Figure 8] is attached directly to the motor shaft, and is covered with viton O-rings which provide traction to grip the tape. The tape is held to the capstan by a pinch roller. The tape drive

mechanism weighs 35g, including the motor and mounting hardware. The entire assembly shown in Figure 7 weighs 250g, including the 120g track selector motor.

The tape guide rollers and frame are shown in Figures 4, 7 and 8. Some of the rollers are mounted in miniature ball bearings, while others have Teflon sleeve bearings. At the right side of the tape guide frame in Figure 4 is a spring-loaded tape tensioning arm. This arm accommodates variations in the tape length. The complete thruster weighs 420g.

Joining the tapes into a continuous loop has proven to be difficult. The evolutionary design process used in the construction of the preprototype thruster has resulted in the

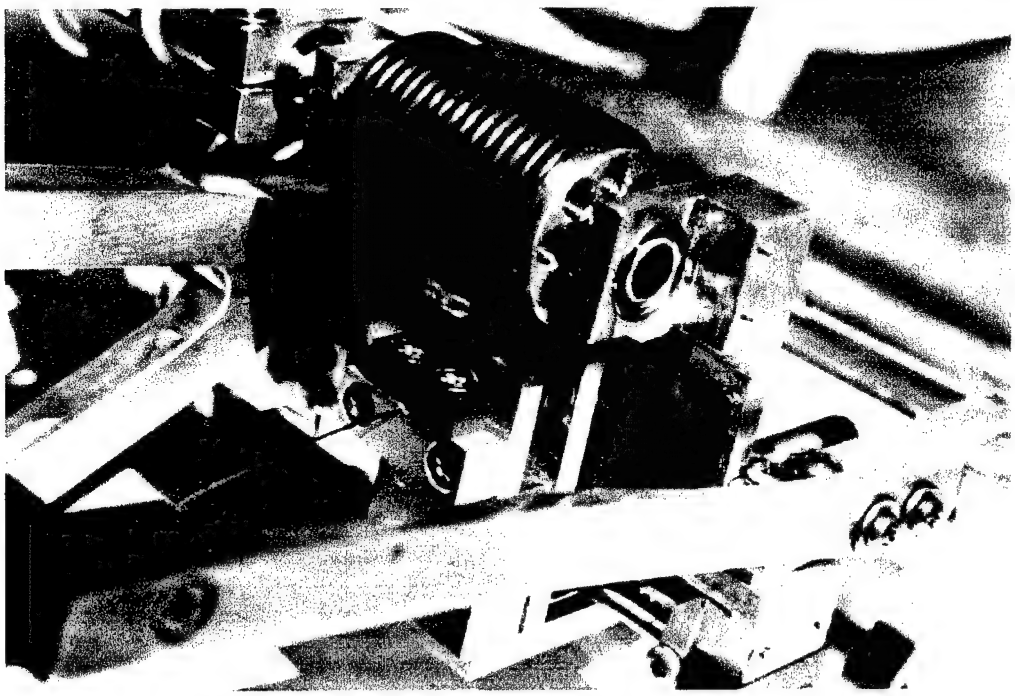

Figure 8. Detail of the preprototype capstan showing the laser fiber clamp.

requirement for several small-radius bends in the tape path. As a result, the tape joint must be very flexible, as well as being very thin. Several tape joining methods have been tested, including self-adhesive splicing tapes and various glues. Mylar splicing tape forms a strong joint, unless it is cut by the laser. One of the more successful glues is made by dissolving the acetate film in acetone. This glue is painted on the ends of the tape and a lap joint is formed. Although tape joints have lasted for hours of operation, a well-made glue joint has not lasted more than several tape passes before failing. The failure invariably occurs next to the lap joint rather than in the joint itself. Kodak film cement is promising, but the tape joint remains an area for further study. The commercial product thruster will not use a continuous tape, and will not require a joint to be made.

As discussed later in this report, we found it necessary to operate the thruster in repetitive-pulse mode, rather than CW, to avoid plume steering. In order to achieve the

required average thrust in this operation mode, it was necessary to dramatically increase the available peak optical power. Figure 9 illustrates the method we used to combine the outputs of four JDSU 6380-A(L2) laser diodes at the input plane of the optics which create the focal spot on target, achieving up to 15W peak optical power at 1ms pulsewidth.

The track selector motor is a salvaged stepper motor. It weighs approximately 120g, but it had the advantage of being readily available for no cost. Although not specifically designed for operation in vacuum, it has operated flawlessly. The tape drive motor is a MicroMo Electronics AM1020 stepping motor with an attached 256:1 planetary gearhead. Both the motor and gearhead were specially ordered with ball bearings and vacuum-compatible lubricants. Combined, the motor and gearhead form a cylinder 10mm in diameter and 36mm long, weighing 15g. This motor is capable of driving the tape 20% faster than the manufacturer's listed maximum speed. A smaller motor is available from the same company, which weighs only 9g. Using two of these small motors for the tape drive and track selector functions, it is possible to reduce the total motor mass to only 18g.

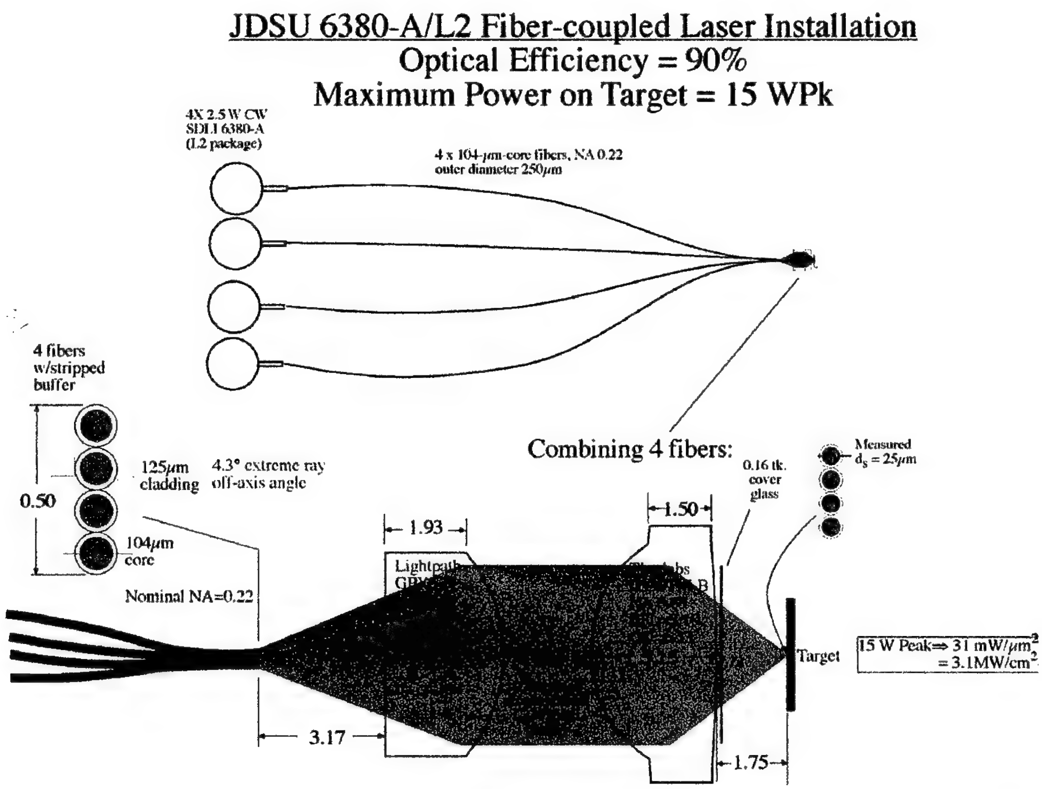

Figure 9. Schematic diagram showing the optical arrangement of the fiber coupled lasers and collimating and focusing optics.

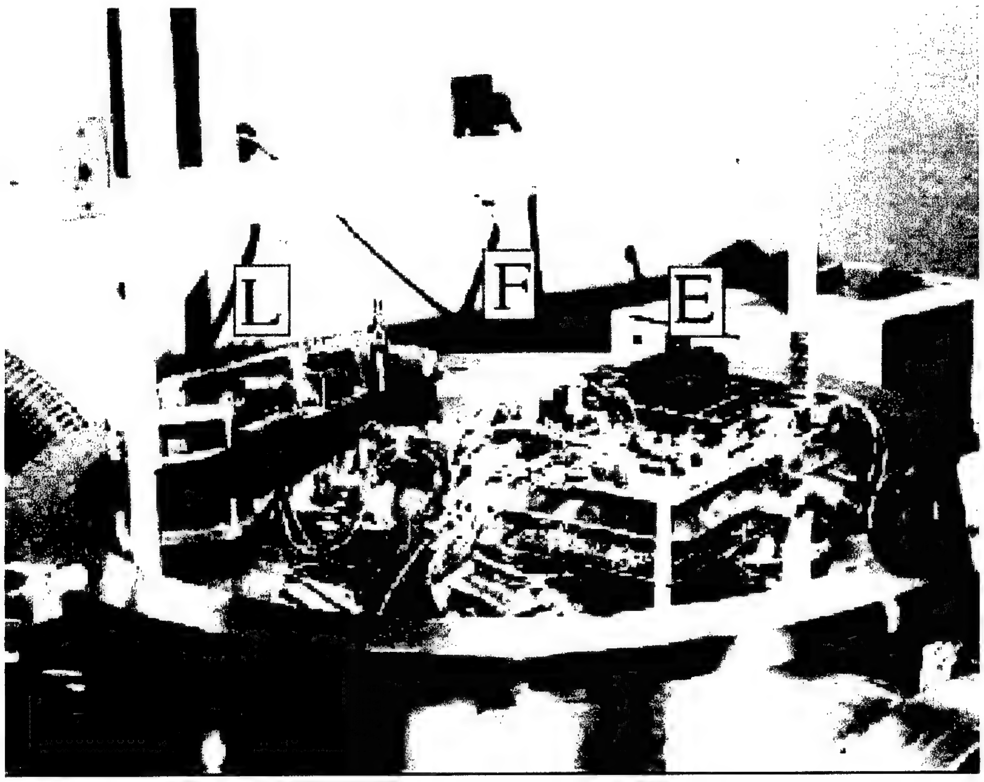

Figure 10. Side view of the thruster and electronics mounted on the force test stand inside our vacuum chamber. "L" is the μLPT; "E" is the Rev. 1 electronics board and "F" is the steel torsion fiber suspending both the μLPT and its electronics for thrust tests. The thrust stand has 17kg capacity and 2μN resolution. Mercury electrical contacts eliminate friction [Figure 13]. A top view is shown in Figure 14. Magnetic field calibration is employed [Figure 15].

4.1.3 Torsion Pendulum Thrust Stand

Figure 10 shows the preprototype thruster and electronics board mounted on the force test stand inside our vacuum chamber.

A torsion balance provides an excellent technique for measuring 1 to 100 μN force range generated by the microthruster. The deflection of the torsion balance we designed under 100 μN applied force is 20 mrad, whereas a standard pendulum of the same length (20 cm) as the span of the torsion balance and supporting 800 g mass would deflect just 13μrad, about 15,000 times less deflection.

At 25% accuracy, its predicted force sensitivity is 20 μN, and its impulse sensitivity is 120 μN-s.

The leading alternative technique is the "swinging gate" type of thruster stand, which requires relatively costly, specialized flexure bearings and also has a force sensitivity at 25% accuracy of 20 μN [Cubbin, *et al.*, 1997; Ziemer, 2000].

The pendulum deflection θ is evaluated by reflecting a probe laser off a micromirror mounted to the center of the torsion mechanism [Figure 13], and pendulum rotation

$$\theta = \theta_b/2 \qquad [14]$$

is half the probe beam deflection. Torque M defines the constant k:

$$M = FR = k\theta \qquad [15]$$

And

$$k = GJ/L, \qquad [16]$$

where L is the fiber effective length, G is the torsion modulus of the fiber

and

$$J = \frac{\pi d^4}{32} \qquad [17]$$

Calibration Theory

The magnetic-torque calibration arrangement is shown in Figure 15. For the situation in which $a_2 >> a_1$ we can write for the magnetic field imposed on the dipole coil

$$B = \frac{2\pi I_2 N_2}{a_2 c} = \text{const.} \qquad [18]$$

throughout the central region of the field coil occupied by the small dipole coil. For example, when $N_2 = 300$ and i_2=800mA [I_2=2.398 E9 esu], a_2=21.9 cm, B =6.885 gauss, which is 17 times the horizontal component of Earth's magnetic field (locally, 0.4 gauss). It is important for this ratio to be large because we want the dipole coil's interaction to be dominated by the large field coil, not the Earth's field.

For the dipole's magnetic moment,

$$m = \frac{\pi N_1 I_1 a_1^2}{c} \qquad [19]$$

from which the torque T is

$$T{=}mB = \frac{2\pi^2 a_1^2}{a_2 c^2} I_1 I_2 N_1 N_2 \qquad [20]$$

Eq. [20] is in cgs units. For currents i in amperes, we have i = (10/c) I, so

$$T{=}mB = \frac{2\pi^2 a_1^2}{100\, a_2} i_1 i_2 N_1 N_2 \qquad \text{dyn-cm.} \qquad [21]$$

In Eq. [21], N_i are the number of turns in each coil. In our case, N_1=300, N_2=20, a_1=3.895 cm, and a_2=21.9 cm, so

$$T = 820\, i_1 i_2 \ \text{dyn-cm.} \qquad [22]$$

We took data on the rotation of the pendulum vs. various combinations of i_1 and i_2.

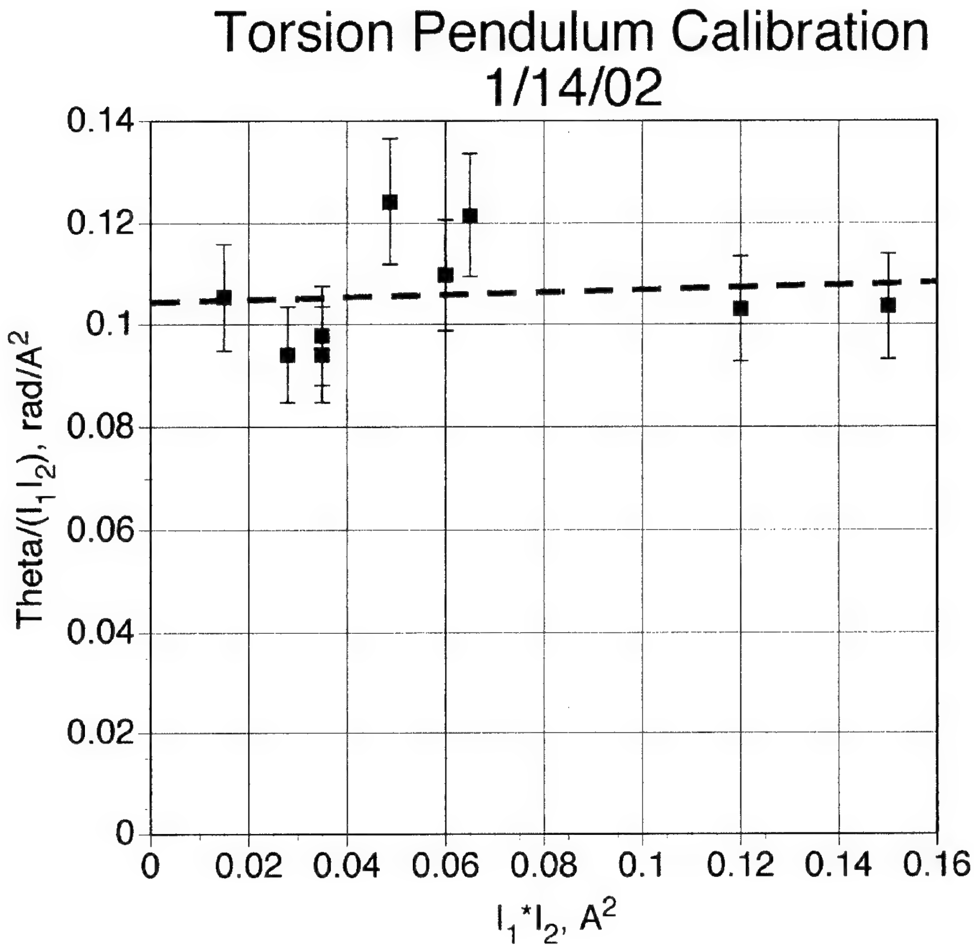

Figure 11. Raw data from torsion pendulum calibration

From Fig. 11, we can say that

$$\theta/(I_1I_2) = 0.106 \pm 10\% \qquad [23]$$

and combining [22] and [23] gives

$$\frac{T}{\theta} = 7.74E\,3\ \text{dyn} - \text{cm}/\text{rad} \pm 10\% \qquad [24]$$

Since the length of the arm from the torsion fiber to the jet centerline $R_1 = 15.5$ cm, it is also true that

$$\frac{F}{\theta} = 500\ \text{dyn}/\text{rad}\ \pm 10\% \qquad [25]$$

which is 2.3 times the value we obtained first-principle calculations. That value was derived by taking the shear modulus G =8.07E11 dyn/cm^2 for the steel fiber, its polar moment $J=\pi d^4/32$ = 4.086E-8 cm^4 and its length L, to get $T/\theta = GJ/L$ = 3297 dyn-cm/rad, 43% of the Eq. [24] value. It is not clear how this discrepancy arose. The fiber is within

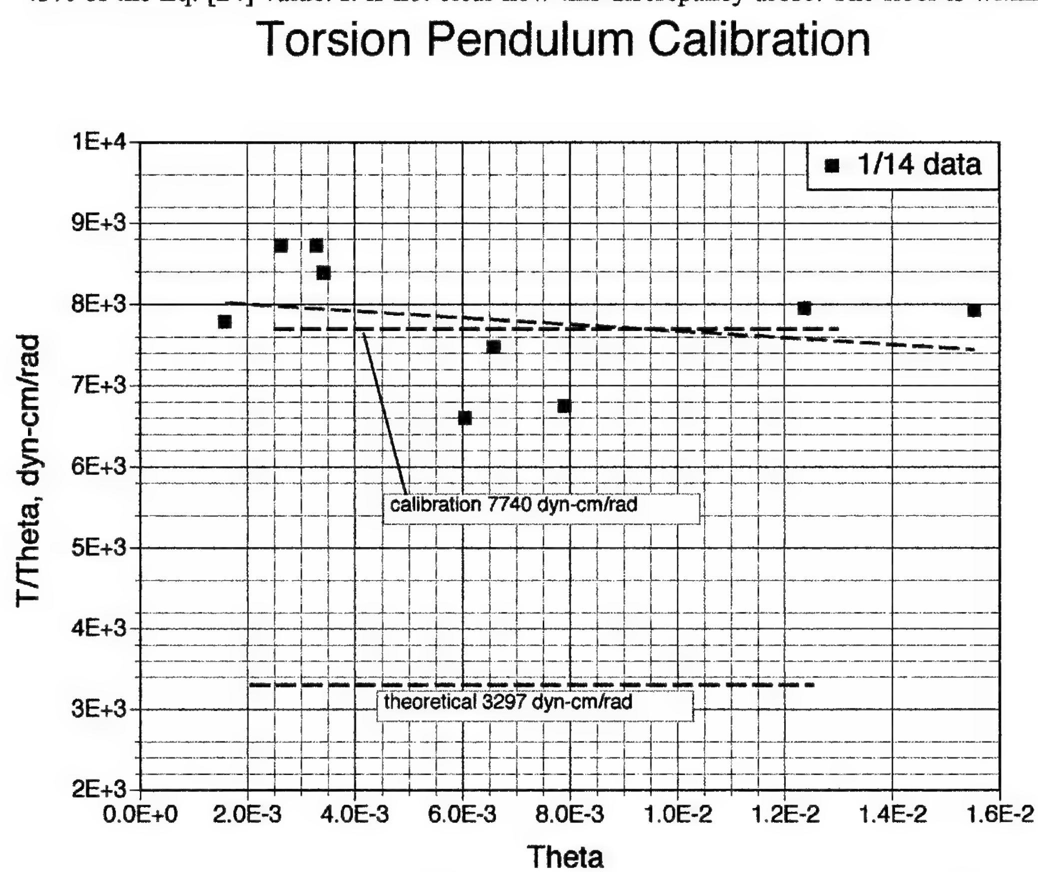

Figure 12. Torsion pendulum calibration compared to theoretical prediction based on published properties of "rocket-wire" fiber

its elastic limit for all stresses. Further calibration results are given in Table 6 and Figure 12.

The torsion pendulum is supported by in an aluminum frame which is mounted in the vacuum chamber. The preprototype thruster and the electronics boards are mounted on opposite ends of the pendulum crossbar. Because of the small forces that we need to measure, it was crucial to eliminate wires, solid commutators, etc. carrying power or signals to the thruster. Therefore the thruster is controlled via an optical data link that is part of the electronics board, and electrical power is sent to the thruster via a mercury contactor cup [Figure 13]. Through the link, command signals are sent to the thruster from the computer, and diagnostic information is sent back from the electronics board. The mercury contactor provides electrical connections that are free of static friction, and the small viscous forces due to the contacts moving in the liquid mercury provide valu-

Table 6: Theoretical predictions for torsion pendulum
(T.P. = Torsion Pendulum)

Parameter	Symbol	Value
T.P. Fiber Length	L	10 cm
T.P. Fiber Dia.	d	0.0254 cm
T.P. Fiber Polar Moment	J	4.086E-8 cm^4
T.P. Fiber Shear Modulus	G	8.07E11 dyn/cm^2
Acceleration of gravity	g	980 cm/s^2
Arm to C.G. thruster	R_1	15.5 cm
Arm to C.G. circuit board	R_2	13.9 cm
Thruster mass	m_1	420 g
Circuit board mass	m_2	470 g
Total mass, thruster and circuit board	m_Σ	890 g
Counterweight mass		40 g
Calculated force response	F/θ	2.12 mN/rad

able damping for the pendulum oscillations. The mercury cup is mounted on a lifting platform which can be operated from outside the vacuum chamber and serves as a pendulum support. During thrust measurements, the cup is lowered until the contact pins are just barely in contact with the mercury.

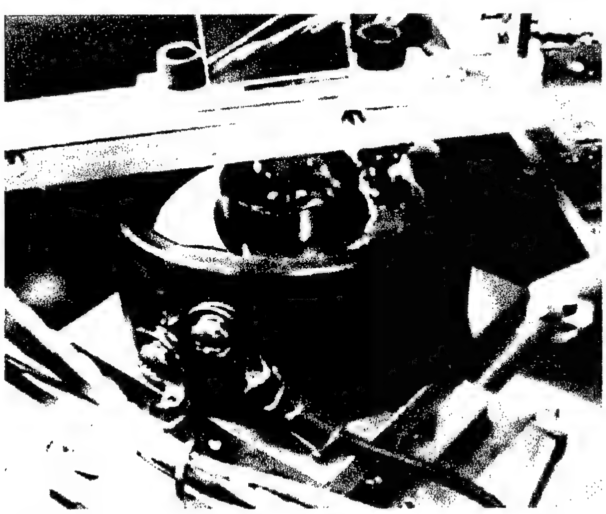

Figure 13. Detail of thrust stand showing mercury cup contactor and small mirror.

Future improvements for the thruster control circuitry are aimed at mass and parts count reduction. For example, the laser temperature monitoring circuitry now composed of three integrated circuits will be replaced with a single chip, resulting in a component mass reduction of about 5 grams and equal reduction in circuit board mass. Along with the mass reduction, the new circuitry will require about one square inch as part of the final mass reduction exercise.

4.1.4 Flag pendulum

Because the resonant period of the torsion pendulum is of order 45 seconds, taking one thrust data point requires as much as 30 minutes, to give the pendulum time to stabilize.

To get data much more rapidly than is possible with our torsion pendulum, we created a tiny (79 mg) flag pendulum to sit in the exhaust stream [Figures 16 and 17].

The flag pendulum is made from 1.1-mil aluminum foil, suspended by 5-mil tungsten wire from a razor-blade fulcrum. A small mirror provides optical deflection readout. A 296 mg washer was glued to the back of the foil to increase the effective mass to the value required to reduce the response to a level appropriate for the forces being measured.

Negatives for the flag pendulum are that it does not intercept the entire exhaust stream, missing significant amounts of detritus outside its acceptance solid angle for some tape speeds and illumination conditions, that it has an unknown sticking fraction for the various components of the stream, and that its motion cannot be conveniently damped, so measurement results must be obtained from the average of several oscillations.

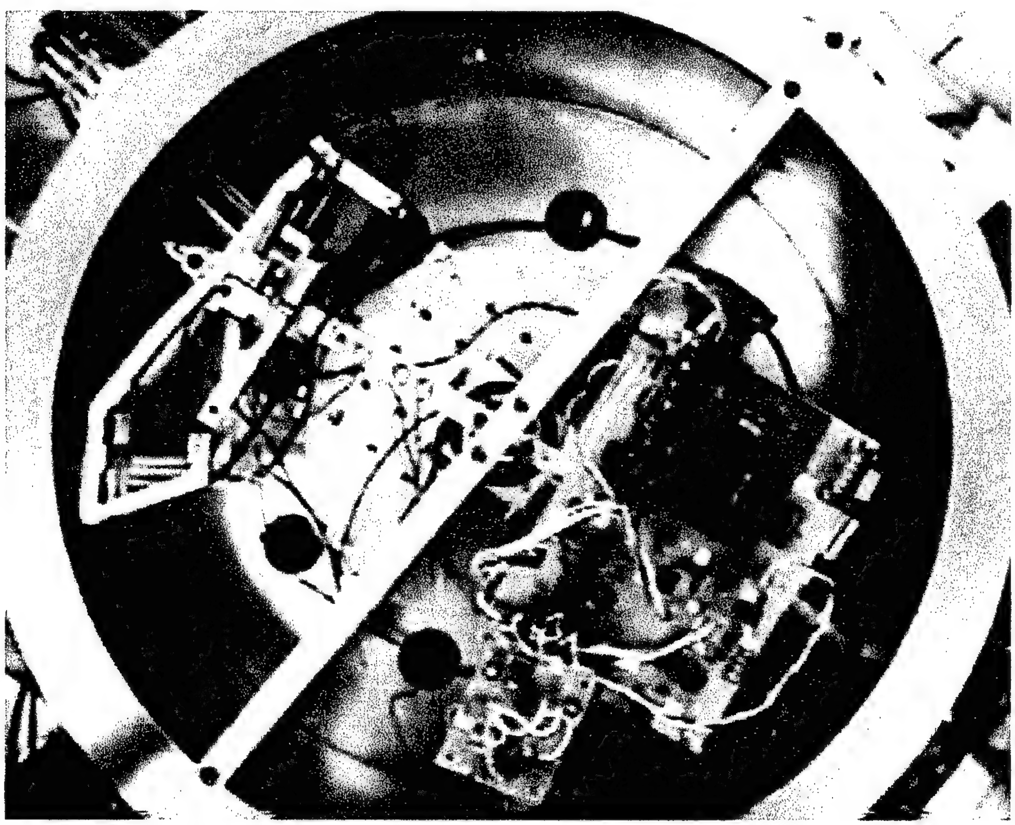

Figure 14. Top view of the thruster and electronics mounted on the force test stand inside our vacuum chamber. The dark grey item on the green board is the Texas Instruments MPS430 microcontroller.

Positive features are:

(a) that it does provide a lower limit for C_m and I_{sp} in the most important part of the μLPT jet [its acceptance angle is 2 to 3 times the divergence angle of the visible jet]

(b) that it gives the highest confidence data we have obtained to date, with much lower scatter than the torsion pendulum in the 50-μN force range, in the latter's current state of development.

(c) that it gives a relatively instantaneous result in 30s versus 30m for the torsion pendulum

(d) that it therefore gives a quick relative indication of the effectiveness of a given power level, pulse duration and target material in producing thrust and

(e) that it is relatively immune to measurement contamination due to outgassing (because of its small size), whereas the torsion pendulum is definitely not so immune. This means that, for the first time, we can obtain believable Q* and I_{sp} measurements. The results we

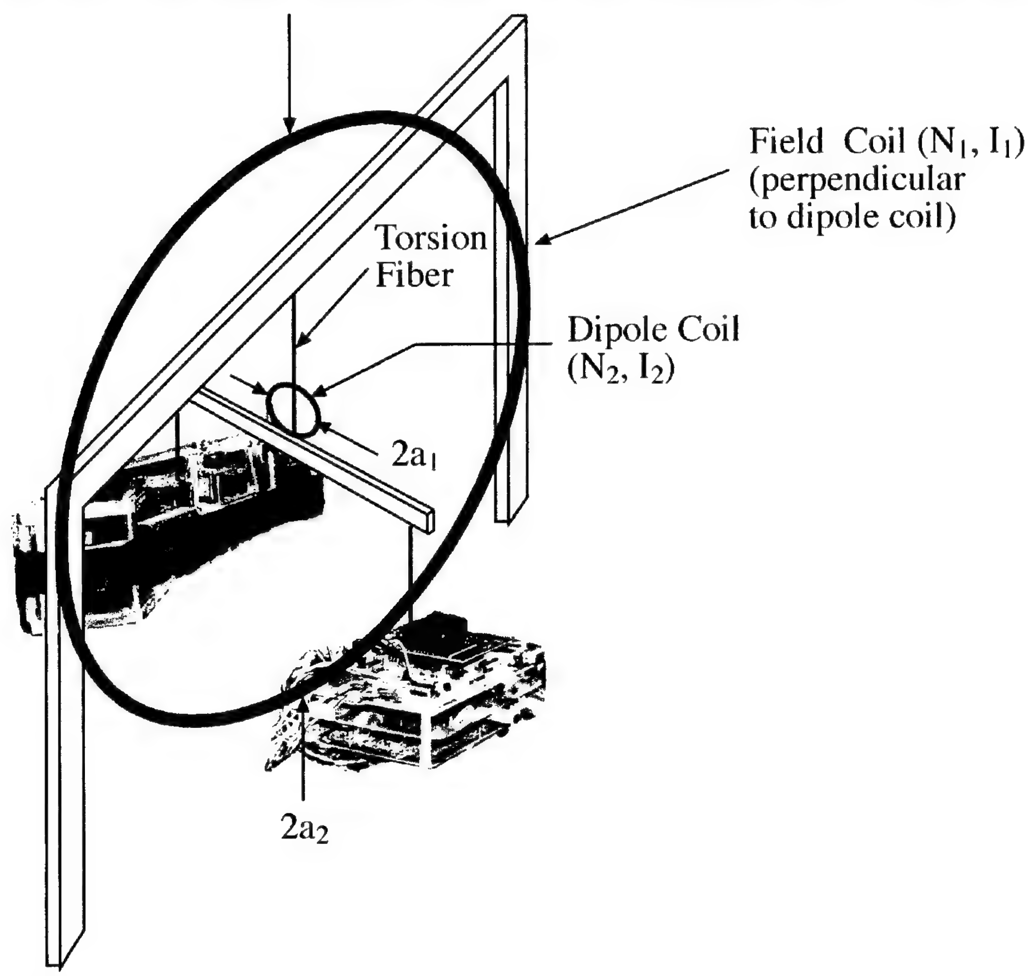

Figure 15. Illustrating magnetic calibration of the torsion thrust stand.

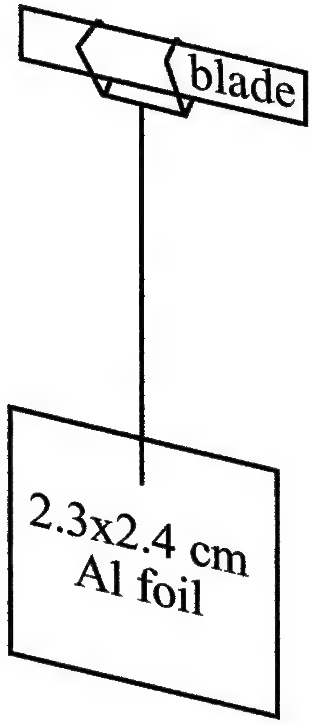

Figure 16. Flag pendulum construction and mounting.

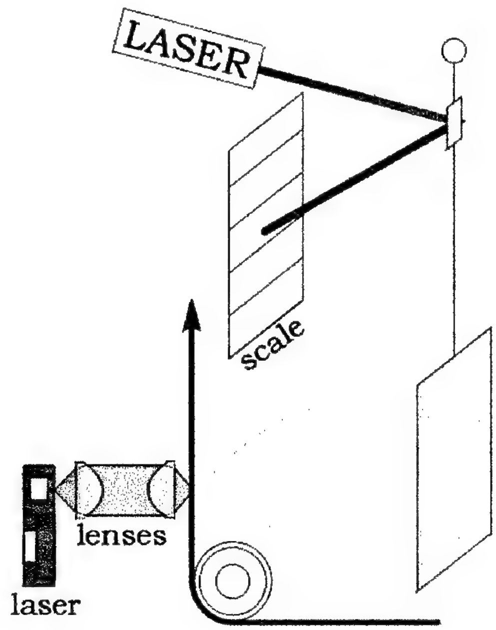

Figure 17. Illustrating the flag pendulum and its data readout. The flag intercepts the central 1.7 sterrad of target plume (75° to 95° full angle for the square flag). Typical jets are 20° full angle. Flag sits in jet 1.5 cm from target tape.

have gotten from the torsion pendulum for specific impulse have been confusing, since with our PVC ablatant, mass loss due to outgassing during preparation for an experiment often exceeds mass loss during laser illumination.

Force calibration for the flag pendulum is calculated from first principles, taking account of all distributed mass to compute an effective mass at the center of the aluminum foil.

The performance of all three data collection methods is compared in Table 7.

Table 7. Three ways of measuring C_m, I_{sp} and thrust in this program

Data type	Pendulum	Quantity measured	Mass capacity	Response	Resolution	Capacity
Static	Small torsion	Impulse	20 mg	6.8μN-s/rad	0.1nN-s	3 μN-s
Dynamic	Torsion thrust stand	Thrust	17 kg	5 mN/rad	20 μN	3 mN
Dynamic	Flag pendulum	Thrust	375 mg	3.4 mN/rad	20 μN	1.5 mN

Data from the two types of thrust sensor agree well, as will be discussed in section 5. Our method for obtaining "static" (single-shot) target data in this program has been adequately described in Phipps and Luke 1999.

4.1.5 Remote control focusing mechanism for thrust stand

A remotely controlled motorized focusing capability was added to the preprototype thruster to facilitate studies of jet behavior vs. position of the focus relative to the fuel tape surface [Figure 18].

Remote control was implemented without having to modify the microcontroller software by creating a control circuit board (upper inset, Figure 18) with two filtered detectors which initiate forward or reverse motion of the focusing motor (lower inset, Figure 18) when one or the other is illuminated by a pointer laser from outside the vacuum chamber.

Data obtained using this setup is described in section 5.

4.1.6 Control system electronics

Control of the micro-Laser Plasma Thruster itself is a straightforward and routine system. Thruster control is divided into three major sections: laser power control, motor speed control, and communications and diagnostics. The heart of the controller is a Texas Instrument MSP430 microcontroller. The MSP430 was chosen for its ultra low power consumption: only 7 mW at full computing speed and only 5uW in standby. With only a 105 mm^2 footprint in its plastic quad flatpack (PQF) package and a mass of only 1.2 grams (unmounted) makes the MPS430 ideal for lightweight low power applications. In/out functions of the MPS430 include; six pulse width modulated channels for motor and laser control, an eight channel 12 bit analog-to-digital, two universal asynchronous receiver transmitter channels for communications and non-volatile memory, and several discrete I/O ports. Total mass for the microcontroller and ancillary electronics is estimated at 2.2 grams.

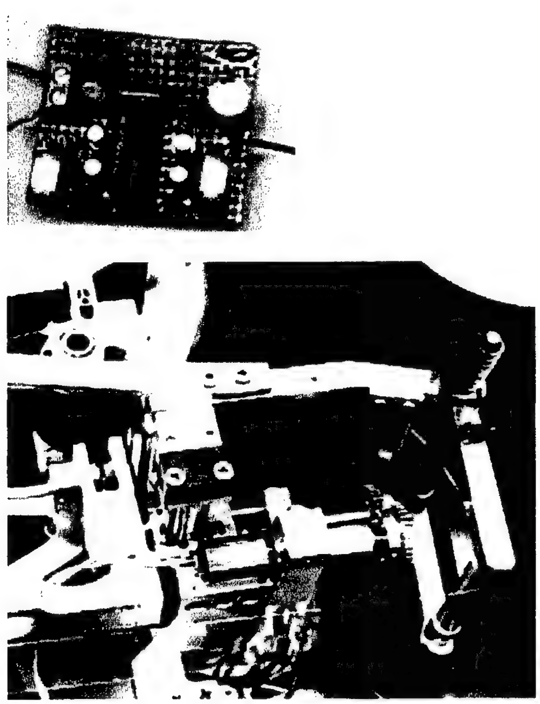

Figure 18. Remote Focusing mechanism (below) and laser-pointer-controlled driver (above)

As mentioned above, there are three major control functions. First and most important is the laser current. Referring to the block diagram [Figure 19], the laser current is set by the user and input to the MPS430. The MPS430 commands the

LTC1624 Switching Regulator to adjust the drive to an external MOSFET that acts as a current source. An International Rectifier IRF9Z34 MOSFET regulates the actual current in the laser diode. Feedback to the LTC1624 provided by a current sensor maintains the current to less than a percent. The LTC1624 is a commonly used regulator in cell phones, PDAs, and laptop computers as a battery charge controller. It too is available in surface mount (SO8 package) with mass of less than a gram. The IRF9Z34 MOSFET is one of the heavier components, weighing 1.9 grams. The total mass for the final design laser current source is less than 5 grams.

Both the tape drive motor and track selector motor are driven by similar circuits. A Motorola MC3479 Stepper Motor Controller is used in both. The motor controllers are directly driven from the microcontroller. Because of the minuscule size of the motors, it is possible for the MC3479 to drive the motors directly with no amplifier stages. Mass of each of the motors is about 20 grams including gear reduction unit. Results from preliminary results indicated that it might be possible to reduce the motor size. There are two motors commercially available smaller than the ones used. This could reduce motor mass from 20 to 10 grams each. Electronics for the motor controls should be approximately 3 grams each giving a total mass of the motor system between 26 to 46

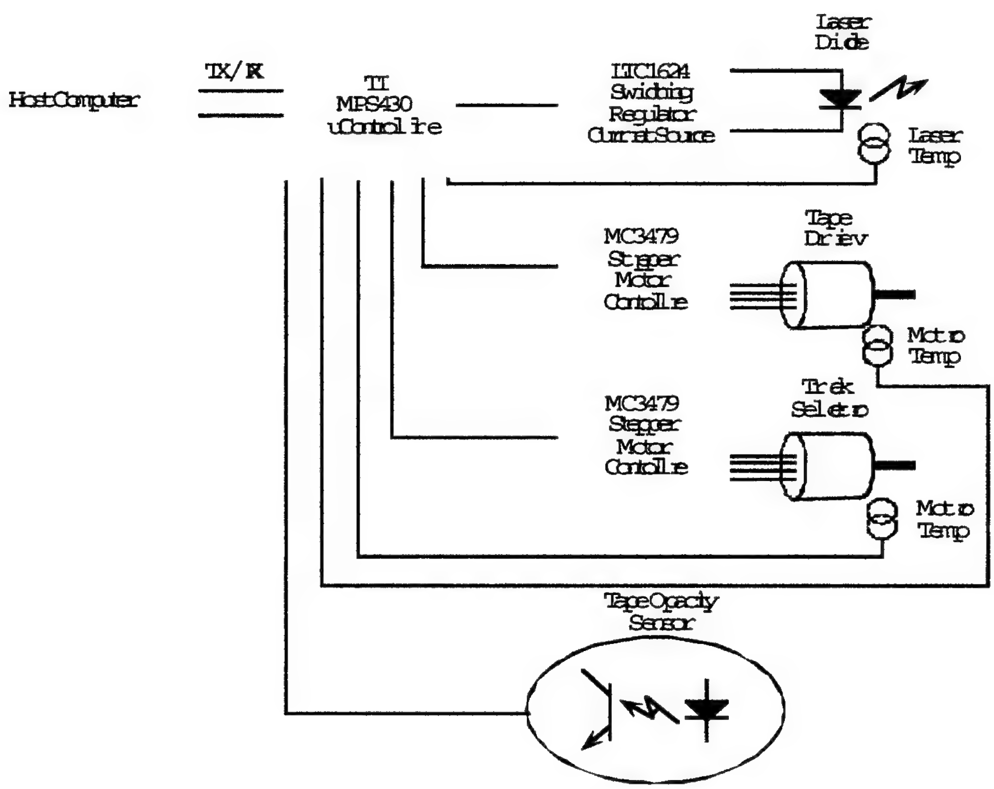

Figure 19. Functional diagram of thruster electromechanical control

grams depending on final motor selection. It should be noted that the mass given are for the components only, no mounting hardware is considered.

4.1.7 Control System Software

Control software for the thruster development was written to expedite development and data acquisition. In its commercial form, the control software will be radically different. Many features of the development software will remain, e.g., tape control algorithms, power monitors, opacity sensors, and burn monitors. Most of the development diagnostic programming will be replaced with the satellite control interface program. The development software is constantly updated and modified to perform new tasks as the development process advances.

The embedded code was written in C and compiled with the supplied TI compiler. Two, interface programs were written to control the thruster. One is text-based and the other is written in National Instruments Lab View. Both perform the same functions but the later is far more user friendly and has data display features. The only critical aspect of the software design is limited on-board memory of the microcontroller. If the program becomes too long, additional memory (another chip) must be added. Addition of a memory chip and support components would only add two or three grams, but should be avoided if possible.

4.1.8 Laser Qualification

In our Phase I effort, we exclusively used a single-transverse mode diode laser with diffraction-limited beam quality, capable of 5.2-μm spot diameter with f/2 (N.A. = 0.47) optics. Early in the Phase II planning, based on the Phase I data, we realized that very fast (large N.A.) optics would still permit us to produce an adequately small focal spot (and adequately high intensity) on the target tape using much less costly multi-mode lasers.

We began Phase II using the least expensive alternative: 2-W optical power Semiconductor Lasers International Corp. model SLI-CW-C-C1-980-2M-R1, costing $308 each. Unfortunately, we determined these are quasi-CW, not true CW lasers, contrary to implications of product advertising. Best power performance was limited to 5ms pulsewidth.

We then switched to JDSU 2W and 4W models 6370-A, 6380-A and 6380-A(L2) lasers costing, respectively $850, $1250 and $1600 each. We have been extremely pleased with their performance and durability throughout the remainder of the program. These have 100x1-μm output facets, as did the SLI Corp parts.

In this section, we discuss life tests we completed on the 6370-A.

The 6370-A laser was set up in the vacuum chamber, mounted on a heat sink, with a collimating lens. The collimated beam was directed into a laser power meter. The laser was set at 1.5W and the life test was begun. Laser and heatsink temperatures, laser output power, and later the input voltage and current were monitored with a chart recorder. The results are shown in Figure 20. Commercial power outages occurred at 1008 hours and 1149 hours. The first outage was very brief and did not cause any noticeable change in the readings. The second outage lasted for about two hours, and

afterwards the laser temperature started to increase slightly, because more current was required to reach 1.5W output. At 1201 hours, the current shunt on the input to the laser failed, resulting in loss of power to the laser. After this was repaired, the laser power output started to decrease, accompanied by an increase in temperature. At the time, it was suspected that the low output could be due to the high temperature. Accordingly, at 1322 hours, the laser was shut off for an hour to cool. The laser was restarted (at a lower current level), but the output did not improve.

The test was terminated after 1780 hours of operation. Microscopic examination did not reveal any damage to the laser optical surface. The life test results were shown to the laser manufacturer, who replied with the opinion that the three loss of power events caused the laser to fail since, during the failure, voltage was not controlled, and it cannot tolerate out-of-limit supply voltage for even a nanosecond. Prior to the power outages, the laser operated for over 1000 hours at 40°C (case temperature, not junction temperature) and 1.5W output in vacuum.

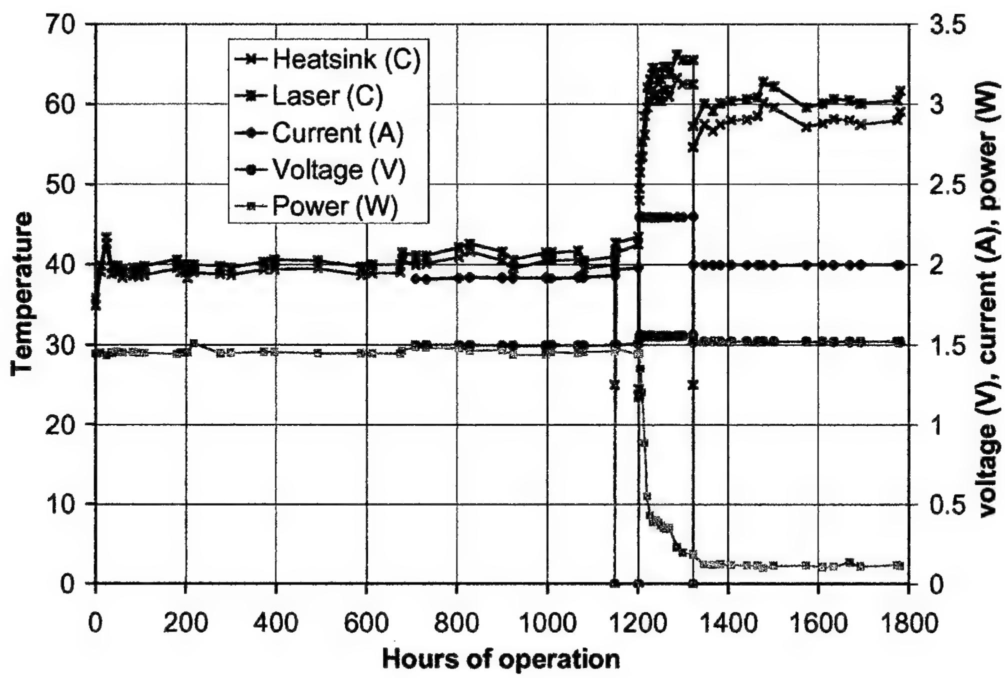

Figure 20. Results of the JDSU 6370-A laser life test.

4.2 Major Achievements – Design

4.2.1 Commercial product Overview and Mechanical Layout

In order to achieve Air Force goals for lifetime impulse, the amount of expendable ablation fuel must be substantially increased from that employed in the microthruster preprototype developed under this contract. Part of the effort under this contract was to design the commercial product which will have 100g of expendable fuel. Figure 21 shows our preliminary functional layout of the commercial product thruster.

Only two electrical motors are used. Major functional components are:

1) Spring motor provides nearly constant tape tension, so that one reversible motor can drive the tape.
2) Track selector motor translates the laser microbench (Figure 23, detail) across the tape.
3) Plasma detector relays information about UV plasma brightness to the master controller
4) Electronics package contains the CPU, system logic, motor controller, programmable laser current source and diagnostics
5) Laser microbench contains the laser, focusing optics and optical laser temperature sensor
6) Laser temperature sensor operates by sensing the 3nm/degC shift in laser output wavelength with temperature or by attachment of a low-mass thermocouple to the laser heat sink.
7) Tape capacity sensor measures the amount of remaining tape on the upper reel
8) Burnthrough sensor detects front (transparent) surface burnthrough in a few ms, so the CPU can turn off the laser before damage to focusing optics occurs.

4.2.2 Burnthrough Sensor

The tape burnthrough sensor is one of the important subsystems in the commercial product. Figure 22 shows the details of the design.

Total mass of the burnthrough sensor components is 7 grams. Power draw is about 13mA at 2.7V.

The 660nm laser beam is normally reflected with 50% efficiency into the PIN diode, which is filtered to reject the ablation laser wavelength as well as room light. Plasma light is also filtered, and attenuates as $1/R^2$. When a dimple first appears on the tape surface, even before burnthrough occurs, the detected signal will effectively go to zero, signalling the CPU to cut laser power.

The laser is driven by the same repetitive-pulse waveform that drives the ablation laser.

The "laser driver" is an automatic power control utilizing a photodiode which is already built into the micro laser module.

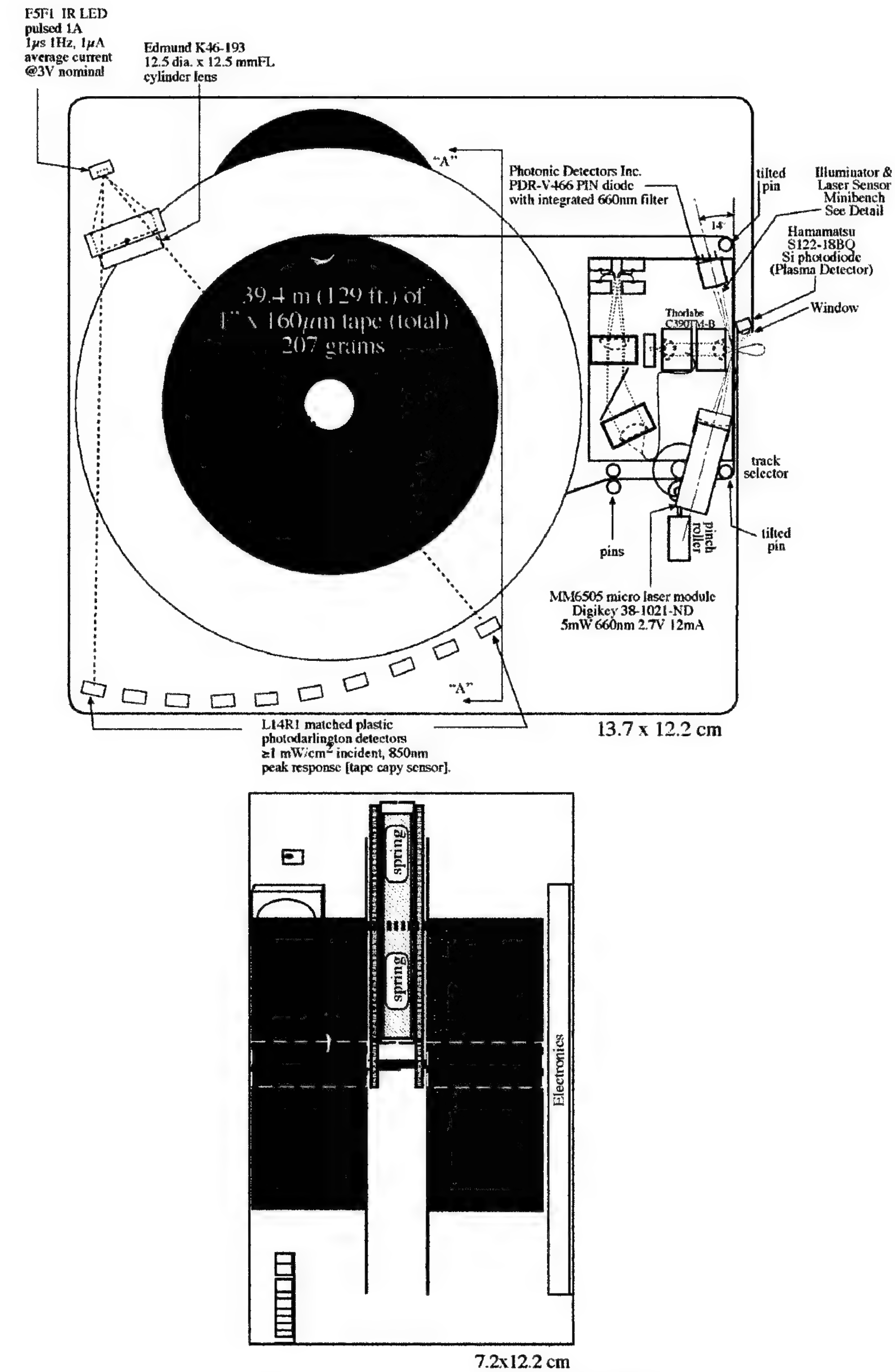

Section "A-A" **Detail: Scale 200%**

Figure 21. Preliminary Commercial product Layout

4.2.3 Plasma & Laser Sensor

Another important subsystem is the plasma plasma and laser sensor. It has 3 functions: 1) to provide a unique signal proportional to laser optical power, 2) to detect laser wavelength shift in 4 bands as a surrogate for laser junction temperature and 3) to provide a separate signal proportional to UV plasma intensity produced by the thruster jet. We will also have a thermocouple available on the laser heat sink, and will decide which to use when the system is built.

The plasma detector is a Hamamatsu S122-18BQ silicon photodiode with extended UV response.

The principle of operation of the laser output detector is that laser output tunes toward the red at a rate of 0.3nm/deg C change in junction temperature. A lens collimates the output of a fiber sampling the laser beam; the holographic grating and second lens together produce a focus which shifts across the inputs of 4 fibers connected to highly sensitive

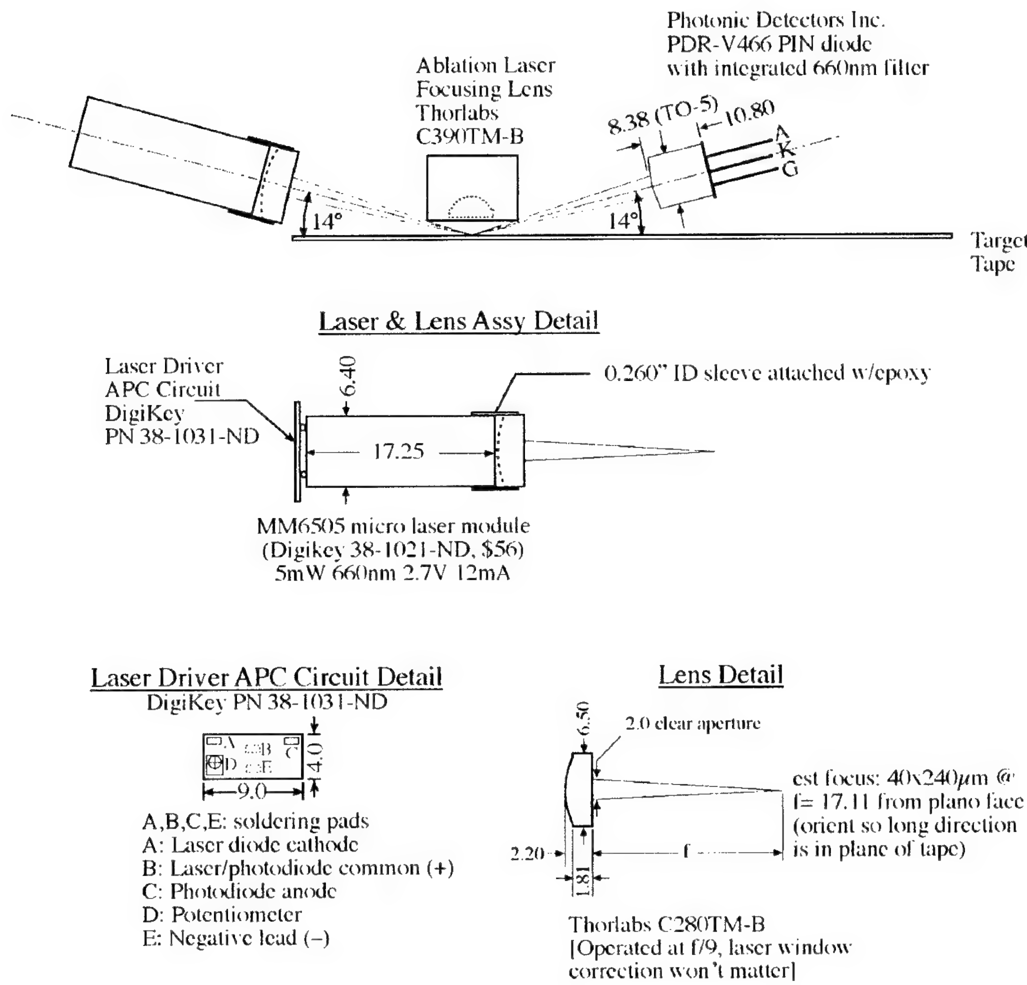

Figure 22. Burnthrough Sensor Detail

L14-9R1 photodarlingtons, one for each of 4 bands designed to span 30 to 90C at 20C per band. The sum of these 4 outputs provides a surrogate for laser output power. The laser power function will be retained even if the junction temperature feature is not used.

Tuning is 0.28 mrad/C. Taking 1.8 cm for the second lens focal length, we obtain 100μm shift in focus position at the focal plane per 20C, compatible with 100μm separation of fiber inputs with 100μm-core fiber allows operation as planned. The grating deviates incident light 62°. At this time, we are considering eliminating the laser sensor from the commercial product in favor of a simple thermocouple, since, with the 20% duty cycle characteristic of repetitive pulse operation, laser junction overheating has never been a problem.

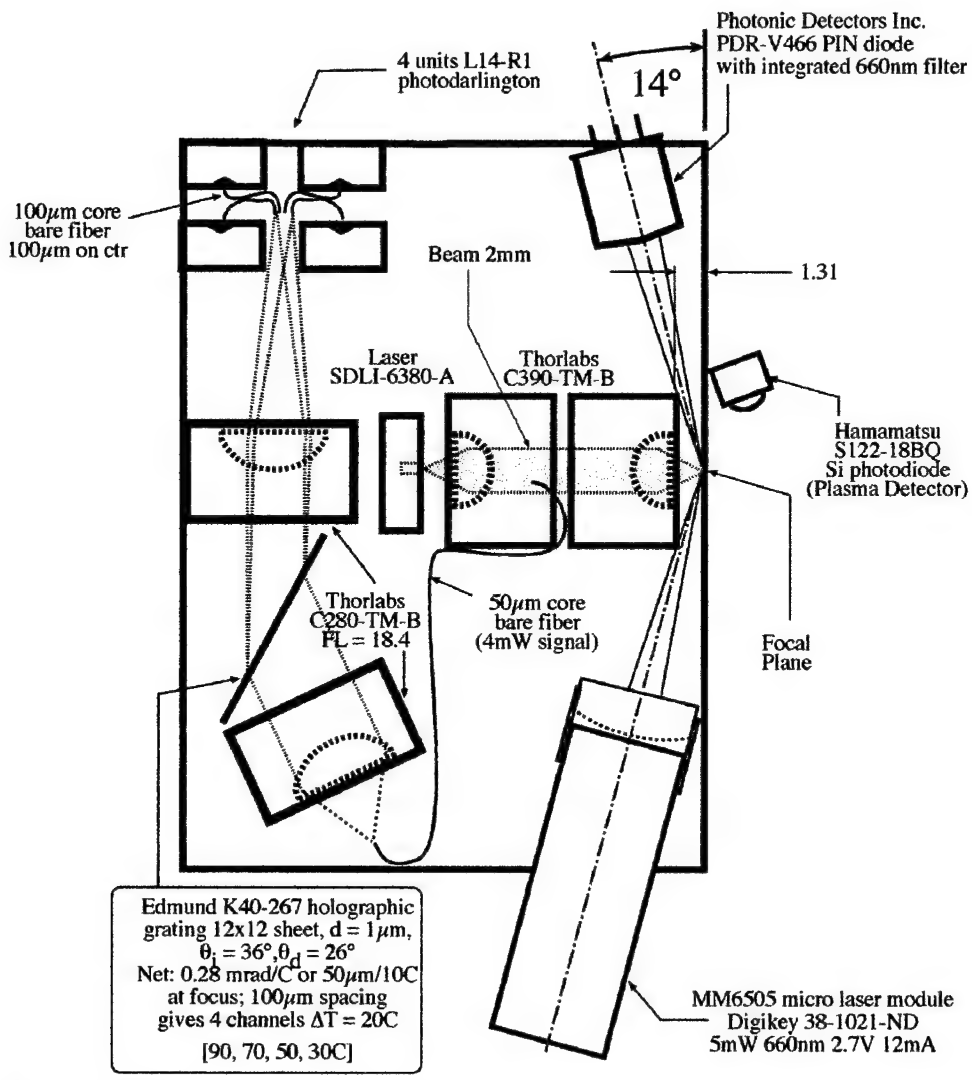

Figure 23. Laser microbench showing plasma and Laser Sensor [see Figure 21]

4.2.4 Spring Motor

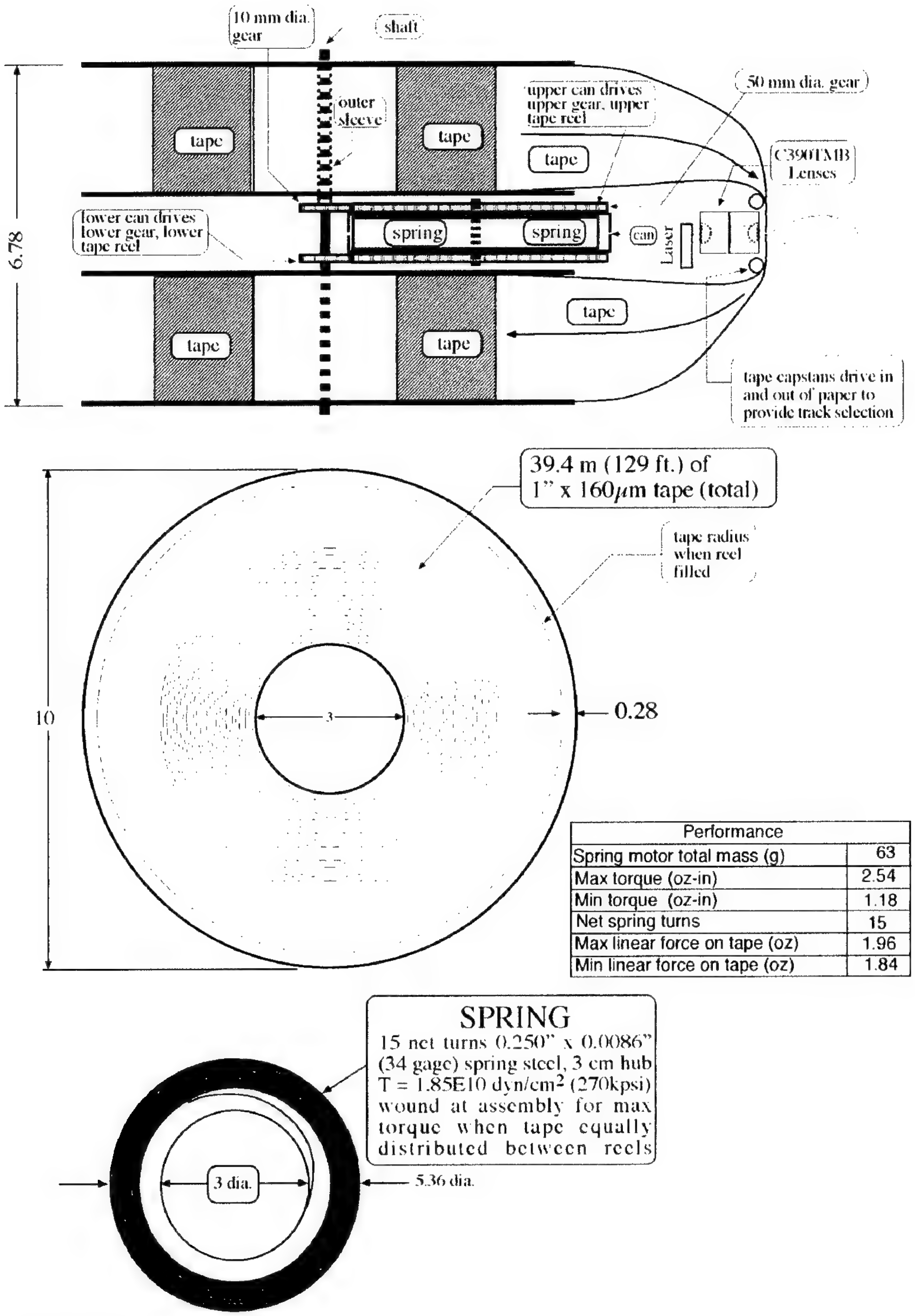

Performance	
Spring motor total mass (g)	63
Max torque (oz-in)	2.54
Min torque (oz-in)	1.18
Net spring turns	15
Max linear force on tape (oz)	1.96
Min linear force on tape (oz)	1.84

SPRING
15 net turns 0.250" x 0.0086" (34 gage) spring steel, 3 cm hub T = 1.85E10 dyn/cm^2 (270kpsi) wound at assembly for max torque when tape equally distributed between reels

Figure 24. Spring motor

Table 8: Springmotor Parameters	
Spring strip thickness	0.0086" [34 Ga.]
Spring strip width	0.25"
Spring strip length	156"
Turns unwound	47
Turns wound	62
Operating range	8 turns
Hub dia.	1.18"
Can I.D.	2.11"
Gear ratio (see Fig. 4)	5:1
Can sheet steel gage	28
Gear sheet steel gage	26
Motor mass	63 grams
Maximum torque in range	2.54 oz.-in.
Minimum torque in range	1.18 oz.-in.
Tape tension	1.9 oz. ± 3%

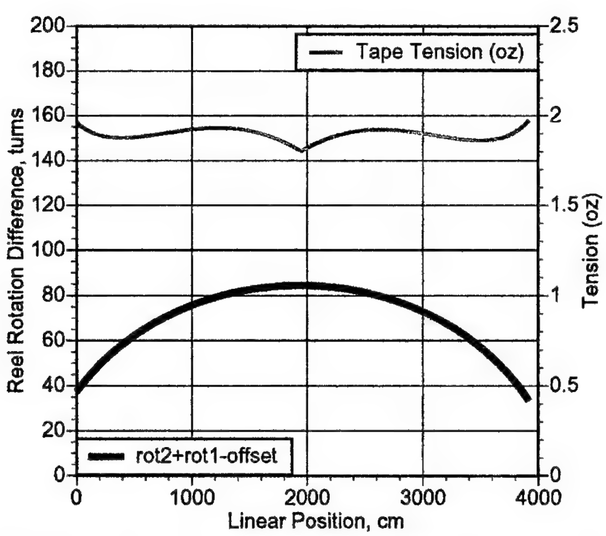

Figure 25. Tape tension and differential reel rotation vs. tape position

Figure 24 shows the function of the springmotor: it is intended to maintain tension in our low-speed tape transport system. By operating against the differential rotation of the tape reels, a minimum of rotation is required of the spring itself. The tape is wound in the opposite sense on the reels so that when they are both exactly half full, they rotate together. In that case, both large gears also rotate equally without causing the spring to wind or unwind. As tape is pulled by the capstan in either direction, one reel fills and the other empties, causing a progressively larger rate of differential rotation. Figure 25 shows the <u>amount</u> of differential rotation vs. tape position as the tape goes from one end to the other. This difference is only about 40 turns. Differential rotation winds or unwinds the spring. The net gear ratio to the spring case is 5:1. So the spring unwinds about 8 turns as this process unfolds. Because the spring winding is symmetrical about the mid-point, so is the Fig. 25 graph. In addition, it is intended to prewind the spring on assembly so that it is most wound up in the middle of the tape. That is, it <u>unwinds whichever way the tape moves</u> from equally full tape reels, applying less torque when it has the most mechanical advantage. That choice, together with some carefully chosen hub sizes, gives (green graph) an almost constant <u>tension</u> of 1.9 oz. on the tape throughout the wind/unwind cycle.

Table 8 gives the principal parameters for the spring motor.

4.2.5 Tape Capacity Sensor

The tape capacity sensor is illustrated adequately in Figure 21. Ten detectors give ten binary channels of output reflecting remaining tape capacity on one takeup reel.

4.3 Commercial Product Performance

Anticipated performance of the commercial product is outlined in Table 9 (compare Table 1).

Table 9. Commercial product Specifications	
Dimensions	14x12x7 cm
Wet mass	0.75 kg
Dry mass	0.65 kg
Tape length	40 m
Tape velocity	2 cm/s
Time per track	33 min
Total lifetime	140 hrs
Lifetime impulse	400 N-s
Q*	10 kJ/kg
C_m	400 μN/W
Laser average power	2 W
Specific impulse	410 s
Thrust	800 μN
Operating temperature	0 - 90C

4.4 R-mode Optics

In view of the improved thrust and I_{sp} characteristics we have measured with R-mode, we were encouraged to consider how to implement it without also sacrificing focusing optic lifetime due to optic contamination.

We completed a unique optical design which takes advantage of the forward peaking of the ablation mass flux by converting the output radiation cone of a single diode laser into a grazing-incidence annulus in which rays are incident on a plane target at angles ranging from 66 to 80 degrees [Figure 26 (Phipps, Luke and McDuff 2002a)].

We estimate the angular distribution of ablation flux by noting that the ablation literature indicates [Dreyfus 1991] this forward peaking can be as pronounced as $\cos^{10}\theta$. This agrees well with our own measurements of angular distribution of contaminant deposits from the plume.

Our data from single-pulse measurements shows 34 s accumulated operation time at 5cm distance from the jet in the forward direction ($\theta=0$) is sufficient to cloud optics.

Taking
$$\dot{x}_v(\theta) = \dot{x}_v\Big|_{\theta=0}\cos^{10}\theta \qquad [26]$$

for the variation of deposition rate with angle, our data point mentioned in the previous paragraph and an inverse-square dependence on range R from the jet to the optic,

we have:
$$t\Big|_{\theta=0} = 1.36\,R^2 \qquad [27]$$

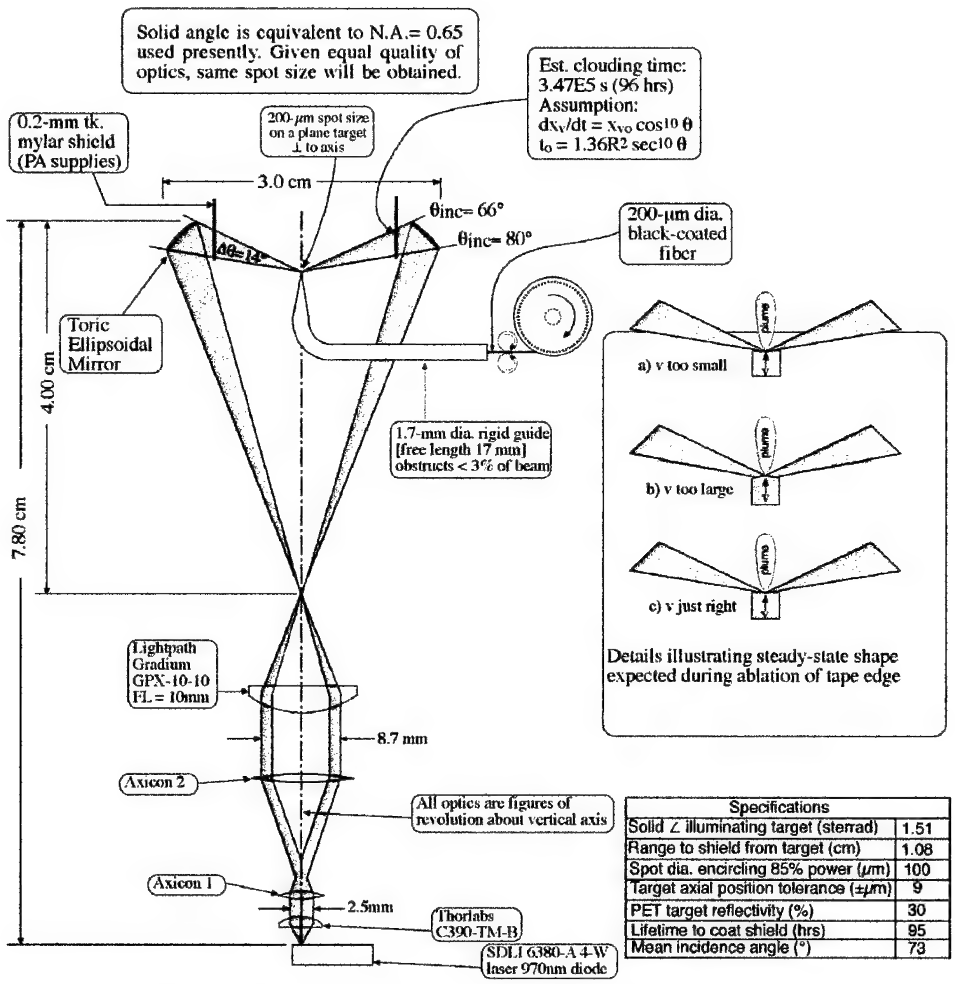

Specifications	
Solid ∠ illuminating target (sterrad)	1.51
Range to shield from target (cm)	1.08
Spot dia. encircling 85% power (μm)	100
Target axial position tolerance (±μm)	9
PET target reflectivity (%)	30
Lifetime to coat shield (hrs)	95
Mean incidence angle (°)	73

Figure 26. R-mode Optic System. Ablation fuel fiber is moving through the focal region of the toric ellipsoidal mirror. All elements are figures of revolution about the vertical axis.

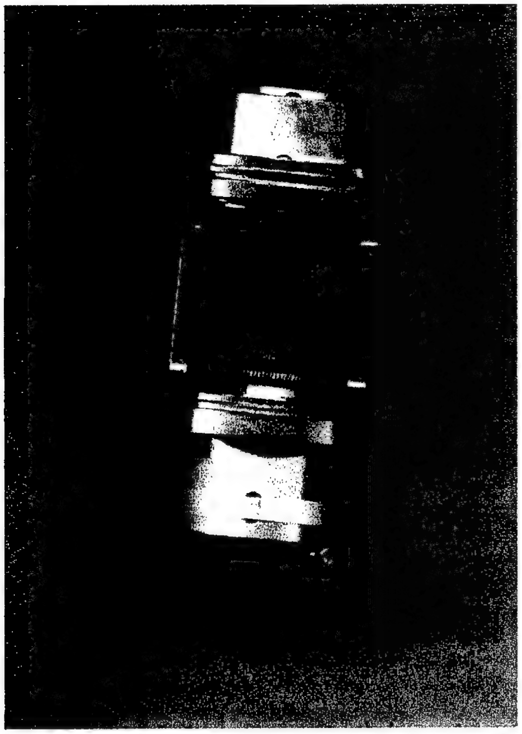

Figure 27. The R-mode optic. The laser is located in the center of the knurled adjustment ring at bottom. The toric ellipsoid reflector is housed in the structure at the top.

and $$t(\theta) = 1.36\, R^2 \sec^{10}\theta \qquad [28]$$

for the predicted clouding time as a function of range R from the jet to the optic and angle θ between the optic centerline and target normal.

To build the device, it was necessary to generate 3 aspheric optics (two axicons and one toric ellipsoid) mounted with the JDSU 6380-A laser in a single unit.

An axicon is a lens whose cross-section is a prism (flat rather than curved surfaces) and whose function is to convert a cylindrical beam into a converging or diverging annulus.

The laser output facet was centered to within 10μm of the optic axis by Applied Physics Specialties staff.

In Figure 26, the laser radiation output is collimated, annularized by the two axicons, then focused on the conjugate focal point of the toric ellipsoidal mirror at the top of the Figure. The latter reimages this irradiation distribution on a 200-μm-diameter spot measured in a plane perpendicular to the vertical axis of the Figure where the target is located in such a way that the average incidence angle θ on this plane is 73°.

Thirteen requests for bid were issued, but only one vendor was capable of making the device we designed. This vendor was Applied Physics Specialties of Don Mills, Ontario, Canada. The design was done under the Phase II contract, and funds to purchase the device were provided through ERC, Inc. by AFRL Edwards.

The axicons were made from ZnSe, since literature data showed the absorption coefficient of that material to be just acceptable for 920nm operation [Figure 28], and its relatively softness compared to glass made it easier to fabricate and polish on a numerically controlled machine.

The finished optic is shown in Figure 27. We tested the R-mode optic onsite with our test apparatus, and the results of these tests showed that 80% of the laser energy at the target location is included within a 200μm diameter circle, which satisfies our requirements for the procurement.

Subsequent measurements showed that the transmission of the entire device was 46%, i.e., that 4W out of the 6380-A diode will generate 1.84W on target. This is a very acceptable result considering the complexity of this radical optical design.

Figure 29 shows the data obtained in the tests conducted at Applied Physics Specialties [Phipps & Luke 2002a].

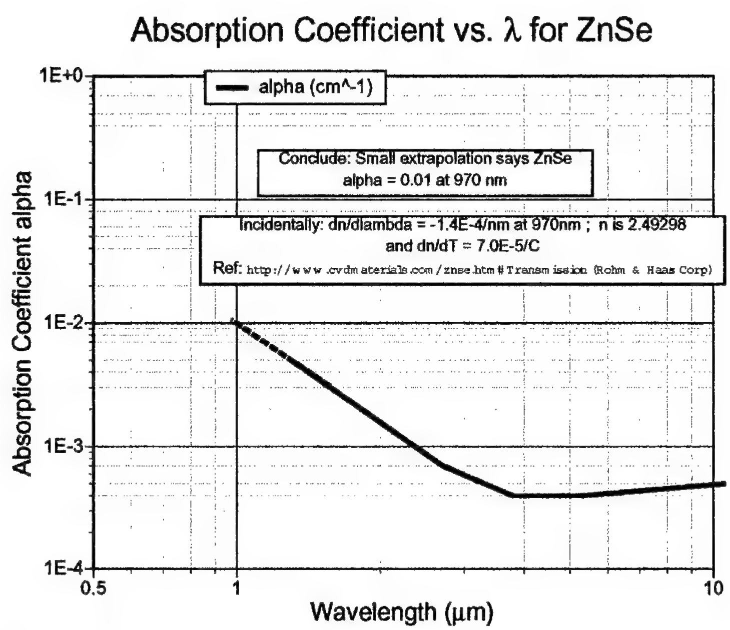

Figure 28. ZnSe absorption coefficient vs. wavelength

The end of the fuel fiber is presented to the laser radiation distribution developed by the ellipsoidal mirror. With just the right fuel fiber velocity, this end will be planar during ablation, and we will be able to take advantage of grazing incidence on this plane to reduce optic contamination from the R-mode jet [inset, Figure 26]. Unlike the T-mode case, the entire fuel fiber is consumed, not just some ablative coating.

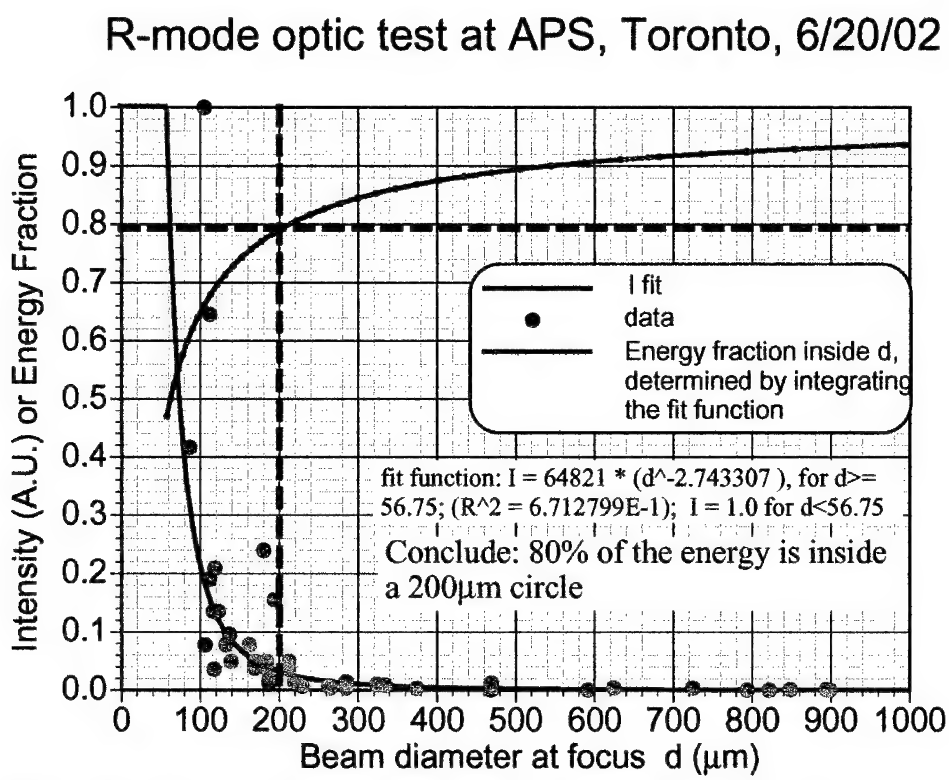

Figure 29. Results of R-mode optic tests at Applied Physics Specialties showed the device met our specifications.

Distance between the ellipsoidal mirror foci is chosen such that the fuel fiber injector can be inserted in the system without occluding more than 2% of the beam.

Because average incidence angle θ on the fuel surface will be 73° in the design, the anticipated lifetime of the mylar shield shown in Figure 26 based on Eq. (26) is 96 hours.

5.0 Major Achievements – Scientific

5.1 Passive ablatant development

Our best passive ablatant material is PVC, whether in T-mode or R-mode.

The laser plasma thruster fuel is very similar to audio/video recording tape except in the coating. Conventional recording tape uses a Mylar substrate with a ferrite based coating. Initially Mylar was used in the thruster development and a PVC coating was used in place of the ferrous type in recording tape. Numerous polymer tapes were investigated for use as the fuel substrate, and hundreds of combinations of tape and ablative coating [Appendix I, II]. Requirements for the tape are listed in Table 10. All but the outgassing rate specification have been achieved in this program.

Mylar was the prime candidate as a fuel substrate because of ruggedness and cost. There are over 100 different Mylar derivatives available commercially. Several different types were investigated. Although satisfactory, the Mylar poses two substantial detrimental traits. The best Mylar exhibits laser damage and fuel coating adhesion is difficult. Even with advanced surface preparation compounds, adhesion to Mylar is marginal at best. After several weeks, the fuel coating would detach from Mylar substrate. Surface preparations used in the automotive industry improved adhesion somewhat but the laser damage problem persisted.

Table 10. Tape specifications

Backing thickness	75-125μm
Backing transparency at 920nm	92%
Backing optical damage threshold	3MW/cm^2 for 5 ms at 920nm
Bending	Able to be bent 300 times around a 1-cm radius without cracking or delaminating
Temperature range	Able to satisfy all other requirements from 0 - 95C
Coating adhesion	Standard scotch tape test
Outgassing rate	$\Delta m/m \leq$ 1E-5 per hour
Minimum coupling coefficient C_m	60 μN/W
Minimum thrust	75 μN
Minimum specific impulse I_{sp}	200 seconds

Although not as resilient and rugged, acetate has far better optical properties than the best Mylar tested. To date, optically clear acetate (similar to motion picture film) has proven to be the best substrate candidate. Optical damage to the substrate must be avoided to insure long lens and laser life. Acetate is as inexpensive as Mylar and far easier to coat. Modern acetate used for motion picture film has life expectancy of 50 years and over 1000 showings. Since the thruster fuel tape has a maximum of 250 passes, tape substrate life should be no problem. In addition, the tape path in the thruster is far less arduous than through a motion picture projector. This leaves only one serious consideration, ablatant adhesion. Again, turning to the automotive paint experts, a surface preparation was acquire to enhance the PVC fuel adhesion. Using SEM Flexible Bonding Clear #39863, adhesion of the vinyl coating to the acetate was superb. With only qualitative examination, no means was found to remove the fuel from the acetate without destruction of the tape. Drawing on years of development in the automotive industry, bonding of fuel to the substrate is not a serious issue. Several coated samples have been set aside to evaluate the effect of time, temperature, and environment on adhesion properties. The adhesion mechanism is a chemical process and not strongly dependant on temperature or pressure. Forced air drying is the recommended method to expedite curing. The most favored passive fuel at this time is Plasi-Kote® Ultra™ Vinyl #405. Preliminary test show no difference in air cured or vacuum cured fuel tapes. However, adhesion decreases unacceptably with longterm vacuum exposure due to outgassing of the binder.

5.1.1 Static (single Impulse) measurements

Desirable properties for the ablator are high C_m and I_{sp}. Figure 30 shows typical static performance of tape made with acetate backing and black PVC ablator in T-mode, using a 5μm diameter laser irradiation spot. Figure 31 shows data for the same situation, except that the laser spot size is now 100μm instead of 5μm. As expected, the I_{sp} value is lower, and C_m about the same.

Figure 32 demonstrates that R-mode illumination of the PVC coating system gives better coupling coefficient, and motivates the effort to develop an R-mode microthruster which is reported here.

A total of 76 single-impulse tests were done in addition to those reported in Figures 30 and 31 [see Appendix I]. Table 11 summarizes the types of substrates and coatings investigated. Graphic results for other some of the most interesting of these passive coating systems are presented in Figures 33 – 37.

Table 11. Summary of substrates and passive ablatants studied	
Transparent substrates	**Absorbing passive ablatant coatings**
Polyethyleneterephthalate (PET)	Polyoxymethylene (Delrin™)
Cellulose acetate	Krylon™ matte black
Polyimide (Kapton™)	Black polyvinylchloride (Plastikote #405 matte black ultravinyl)
Fluorinated ethylpropylene (Teflon™)	Sheldahl proprietary black
	Black cellulose nitrate
	PMMA (Lucite™)/carbon black
	Fe_3O_4
	Aluminum
	Black nitrocellulose & binders (BNP)
	Plastikote #340 black lacquer
	Plastikote #611 trim black
	Plastikote #215 black engine enamel
	Black polyvinylchloride (Plastikote #411 gloss black ultravinyl)
	Smith-Corona typewriter ink
	Epson black printer ink
	Black vinyl bumper paint

Of all of the combinations of substrates and passive coatings tested, black PVC on acetate showed the best overall performance. As indicated in section 5.1.6, its outgassing properties do not meet our requirements at the current level of development, but no other passive tape system showed the combination of desirable performance in so many parameters.

Development of all passive coating systems was interrupted when we began obtaining the much better results with the exothermic designer polymer coatings reported in section 5.2. However, further work deserves to be done on low outgassing black coatings, such as the Sheldahl coating, and thicker aluminum coatings on Kapton™ or cellulose acetate substrates.

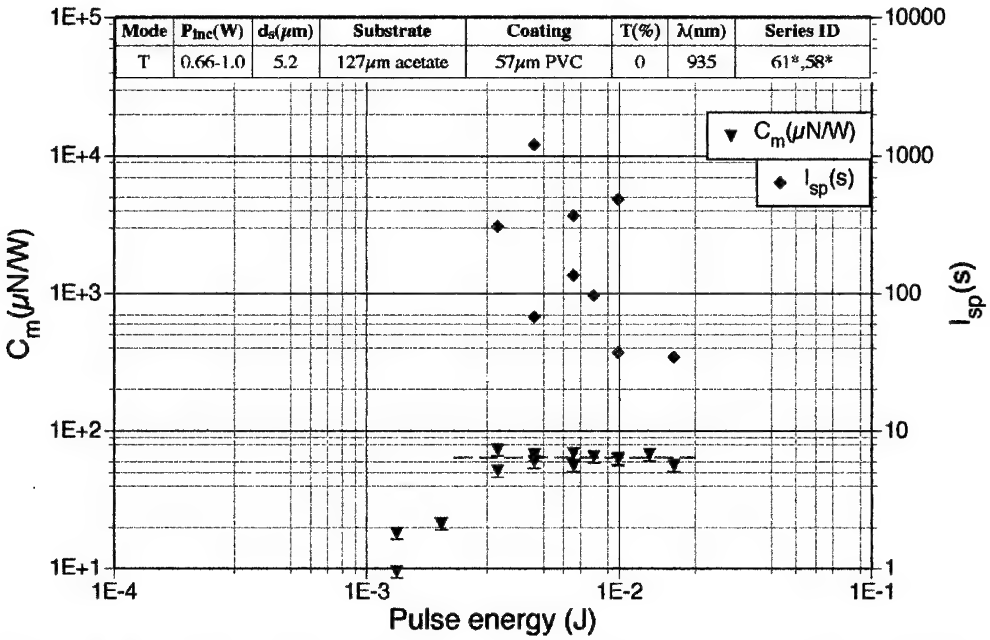

Figure 30. PVC/Acetate C_m and I_{sp} measured in static tests with single pulses from the single-mode research laser focused to 5μm spot diameter, in T mode. Note the nearly constant C_m value of about 70 μN/W above threshold. Similar C_m values are obtained with 100-μm spot diameter [see below] but the maximum I_{sp} value is

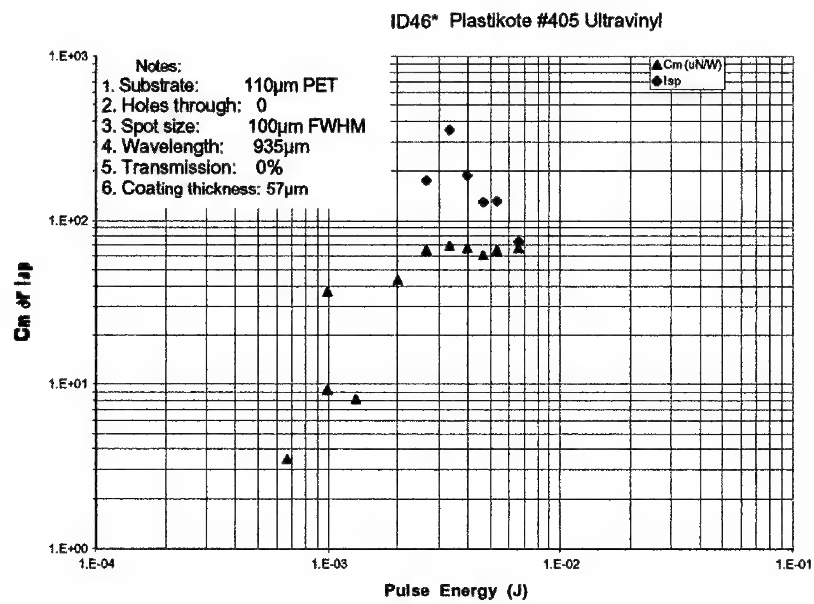

Figure 31. PVC/Acetate C_m and I_{sp} measured in static tests with single pulses from the single-mode research laser focused to 100μm spot diameter, in T mode. Notice that maximum I_{sp} has decreased to 350 seconds from 1250 seconds in Figure 30, while the similar C_m value is unchanged at about 70 μN/W above threshold.

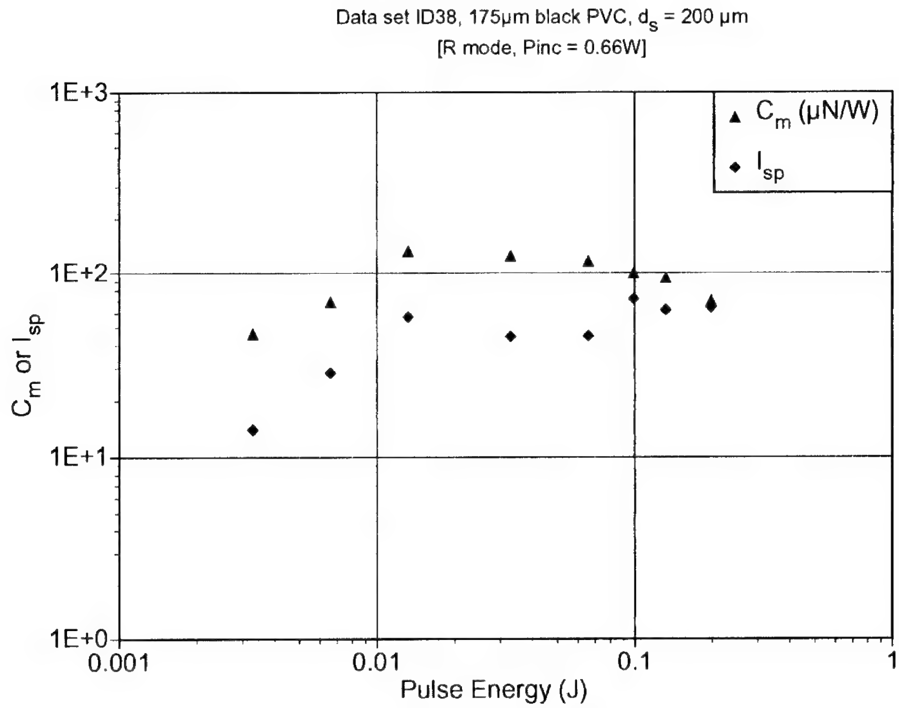

Figure 32. Results with PVC coating in R-mode. C_m values are approximately twice as large as in T-mode. Compare Figure 30.

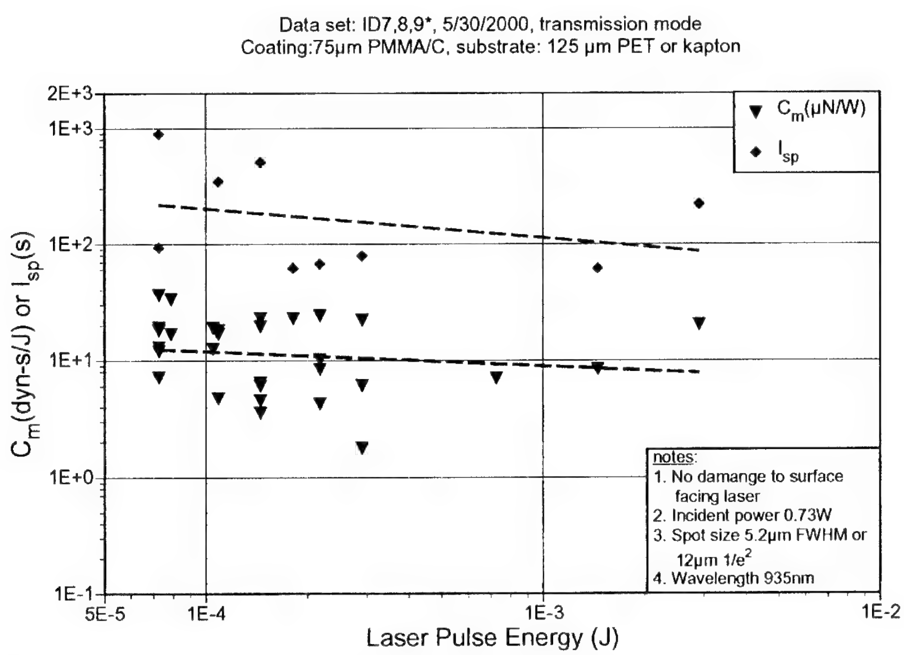

Figure 33. Results for carbon-doped PMMA on PET substrate

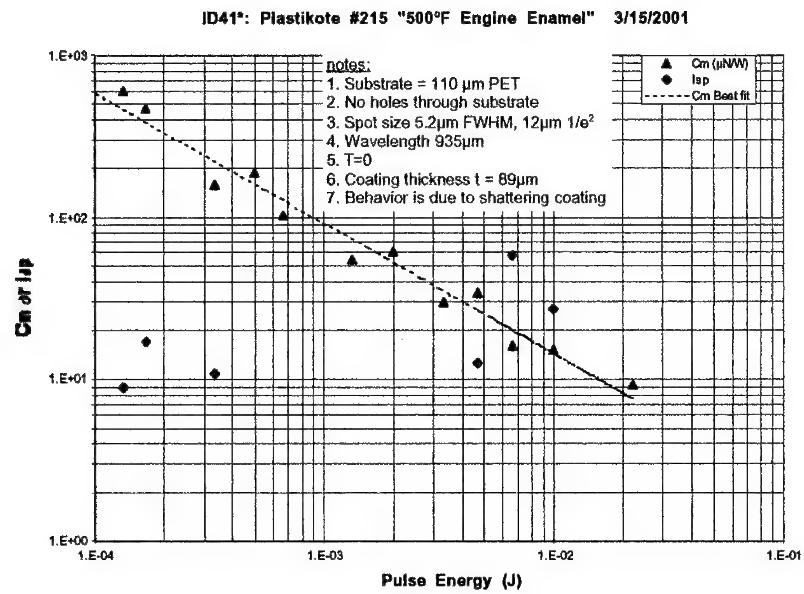

Figure 34. Results with Plastikote™ #215 black engine enamel are fascinating because of the extremely large C_m values obtained, even though I_{sp} is not interesting. Microscopic examination revealed the reason: at low fluence, the brittle coating was removed at radii well beyond the laser irradiation distribution, like a shattered coating on enameled steel.

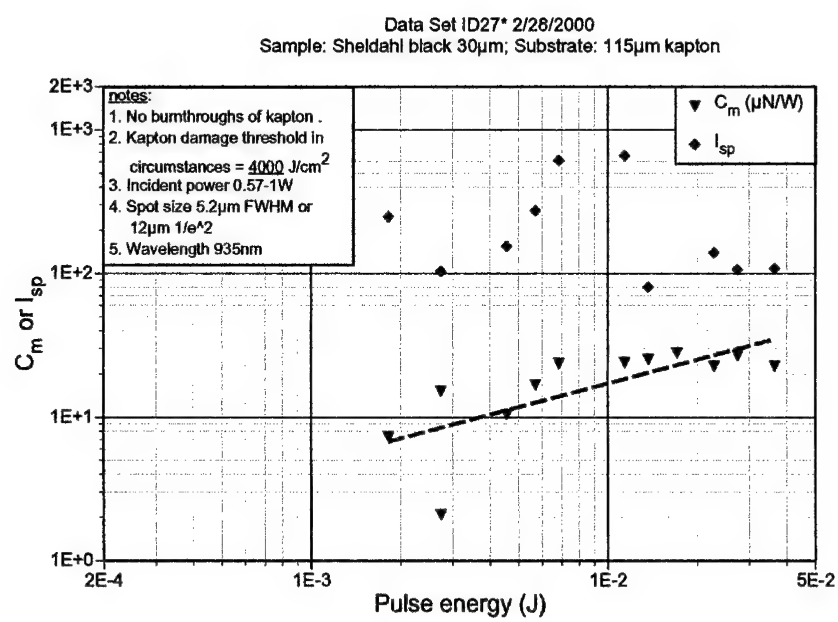

Figure 35. Results for Sheldahl™ black coating on Kapton™

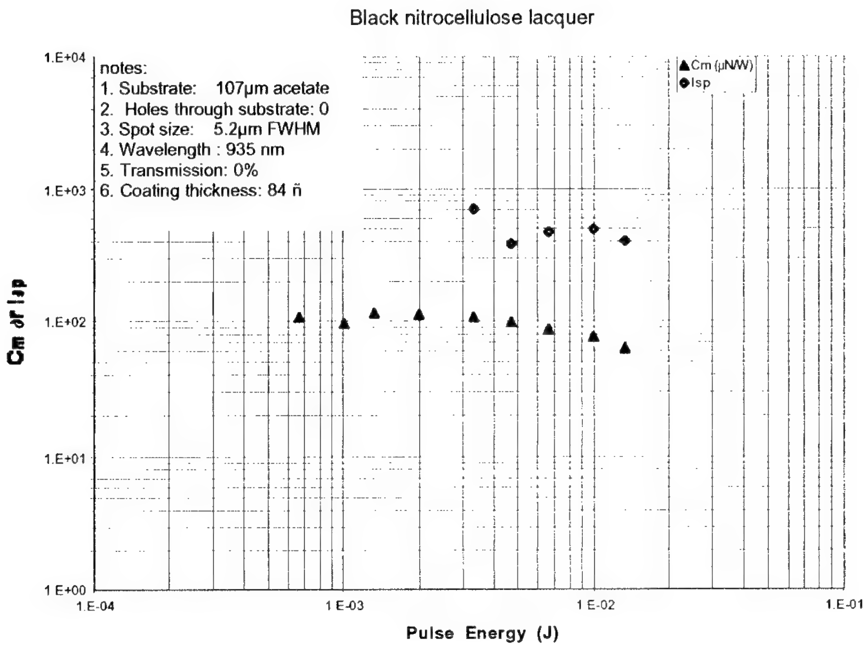

Figure 36. Results with black nitrocellulose lacquer

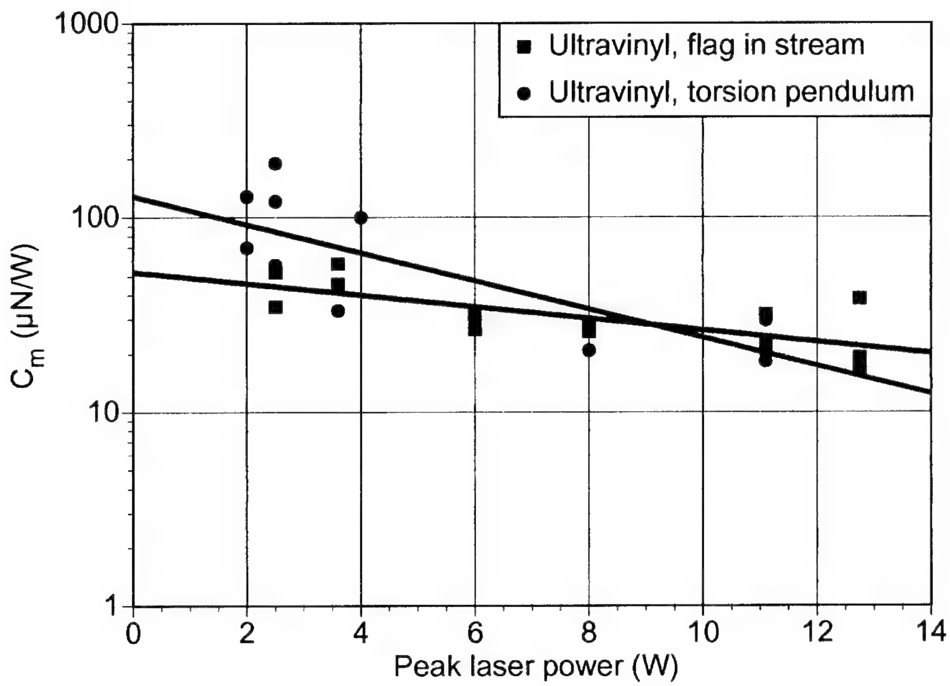

Figure 37. Comparing results obtained with the flag and torsion pendula shows good agreement on C_m, with somewhat higher results at low peak power obtained by the torsion pendulum [BT62(x) in Appendix II].

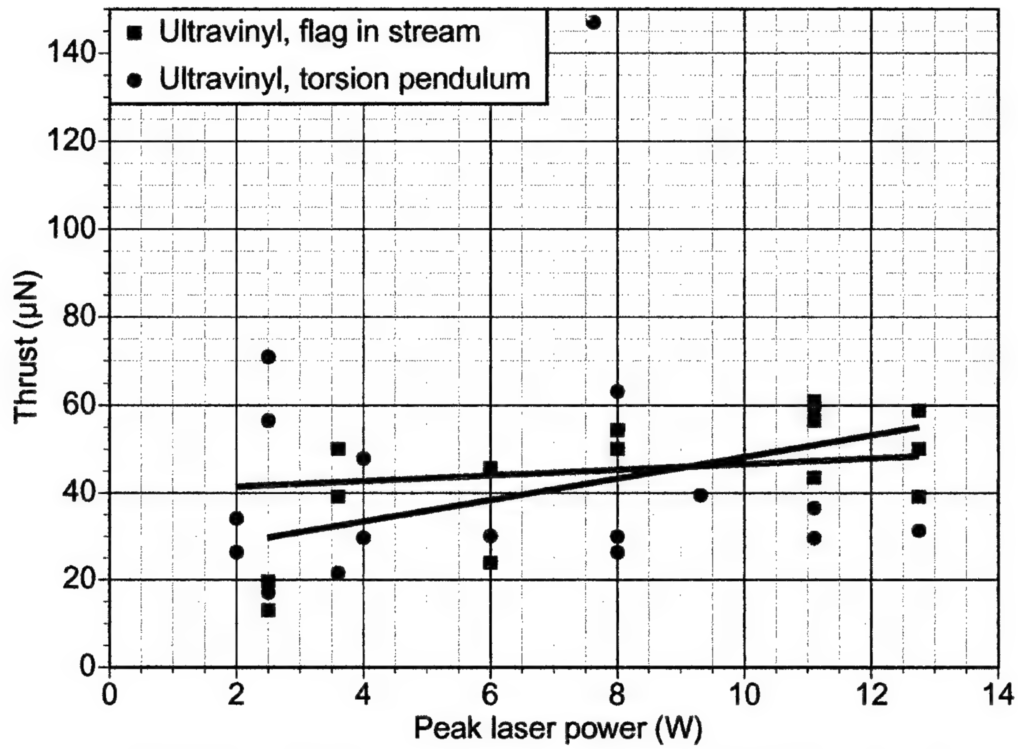

Figure 38. Thrust vs. peak laser power for the Figure 32 data [BT62(x) in App. II].

5.1.2 Dynamic (thrust) measurements

Figure 37 summarizes coupling coefficient values obtained during passive coating thrust measurements for this contract. The Figure also shows the reasonable agreement we obtained between results from the flag and torsion pendula. Key features of the data are a) C_m values up to 200μN/W were obtained from the PVC coatings, b) For torsion pendulum data, C_m decreases with increasing peak laser power, above an optimum value in the vicinity of 2.5W, c) flag pendulum data decreases less rapidly with laser power and d) since the maximum-C_m data point was obtained with 3ms pulses, pulse energy seems to be optimum around 7.5mJ. This is mainly due to the flag pendulum collecting less than 100% of the ejecta in the poorly-collimated low power jet. Despite the flag pendulum's large acceptance angle, the low power jet deposits a significant amount of material on the thruster apparatus beyond that angle.

Figure 38 shows thrust vs. power for the same data points. The largest thrust recorded was 147μN at a peak power of 7.6W and 23 mJ pulse energy. However, assuming this point is spurious, the low-scatter flag pendulum data indicates best thrust at around 12.6W peak power and 38mJ pulse energy, for 3ms pulses.

Figure 39 shows the measurements which proved that our preprototype can meet the thrust requirements set out in the Program Objectives using the passive PVC ablatatant.

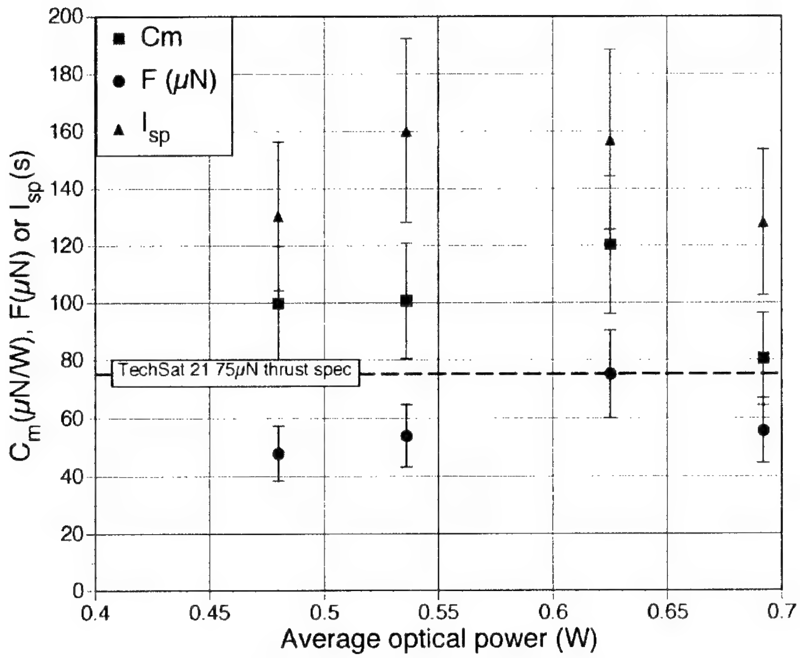

Figure 39. Measurements on the preprototype using PVC ablatant gives 75μN thrust, with C_m=120 μN/W and I_{sp}=160 s.

Results to be reported in section 5.2 below for our exothermic ablatant will far exceed requirements.

Figure 40 shows the well-defined track created in continuous-burn (CW) operation of the thruster. Figure 41 shows related measurements of CW tracks, giving the width at the bottom and top, the track depth, the penetration of the transparent substrate and the mass ablation rate as functions of deposited energy per unit length. An interesting feature is that the burn rate decreases above P/v = 1.5J/cm. This is because this level of energy deposition is sufficient to remove the ablatant, after which the laser energy is much less efficient in removing the remaining transparent material. It is seen that, even with CW (rather than the cleaner-cutting repetitive-pulse illumination), the width of the track at the bottom is very close to 100μm. Of more interest is the fact that in the range above 2 J/cm, about 20μm of the transparent backing is also ablated. This indicates that tape mass utilization is higher than one would assume by considering only the mass of the ablatant coating. We see similar results for mass utilization in repetitive-pulse tests.

One of the more interesting results was obtaining C_m= 50μN/W and 26μN thrust with a 0.2 μm aluminum flash-coating on Kapton™ (Appendix II, BT44*). The mass of the aluminum coating by itself is completely inadequate to produce the observed thrust. Instead, 25μm of the kapton material at the interface is vaporized, by the combined effects of the factor-of-4 light intensification in the standing waves created by reflection at the interface, and thermal conduction and reradiation by the hot aluminum coating.

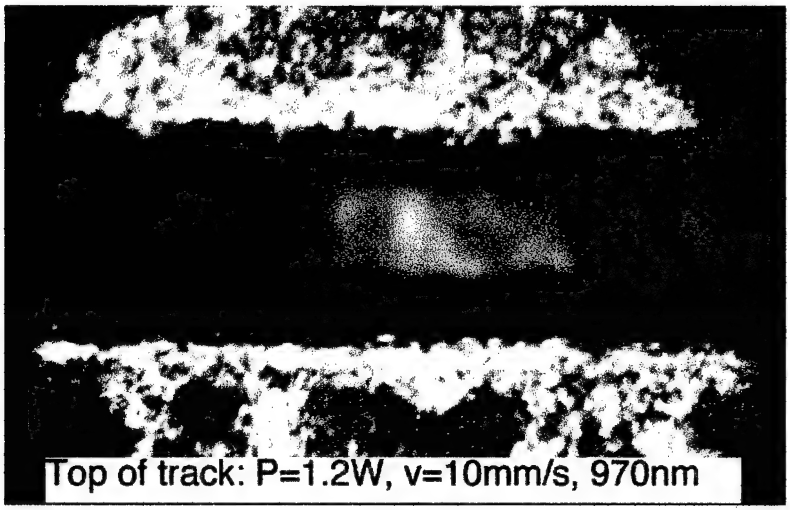

Figure 40. Photomicrograph of CW target tape track

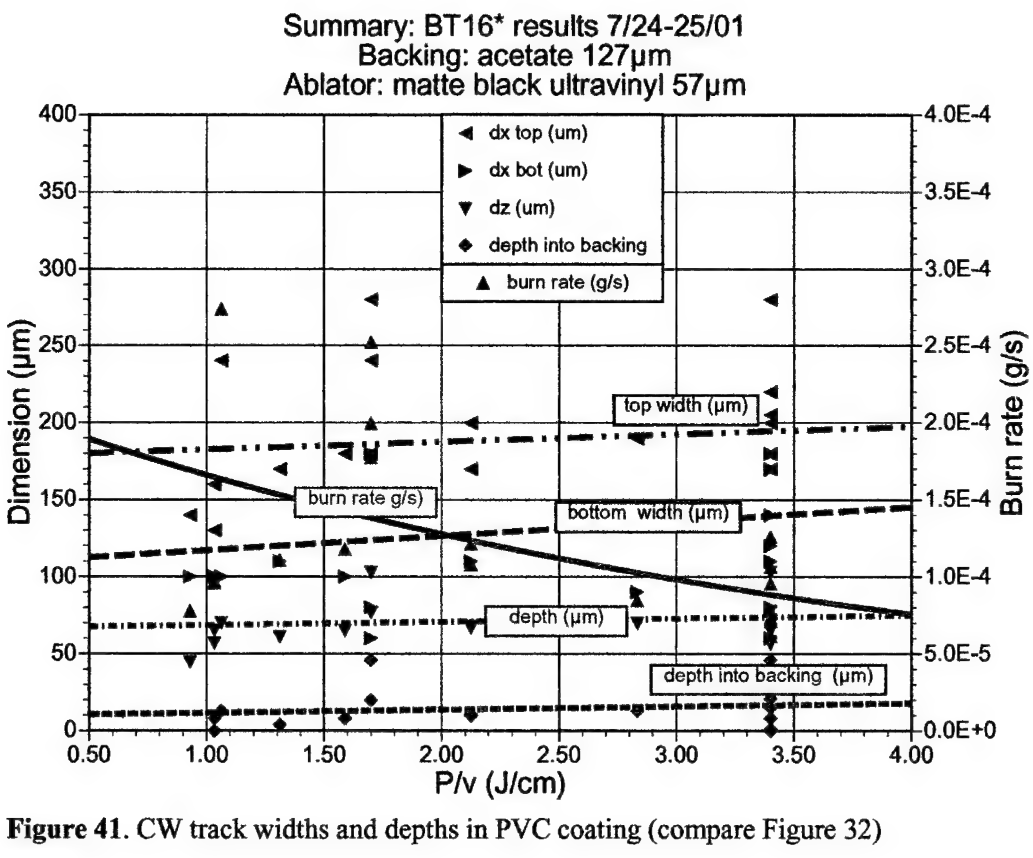

Figure 41. CW track widths and depths in PVC coating (compare Figure 32)

5.1.3 Plume contaminant distribution measurements

We took data on far-field plume contaminant distribution on nearly every thrust test. Figure 42 shows the most interesting of these results. In CW operation, we found strong plume steering, as indicated by the contaminant distribution, and a very sharp profile near 90°. The density indicates that a majority of the ablated material was ejected within 20° of the tape plane. This feature arises from guiding of the plume by the groove dug in the PVC material during the CW ablation process. It is essentially a magnified shadow of that groove.

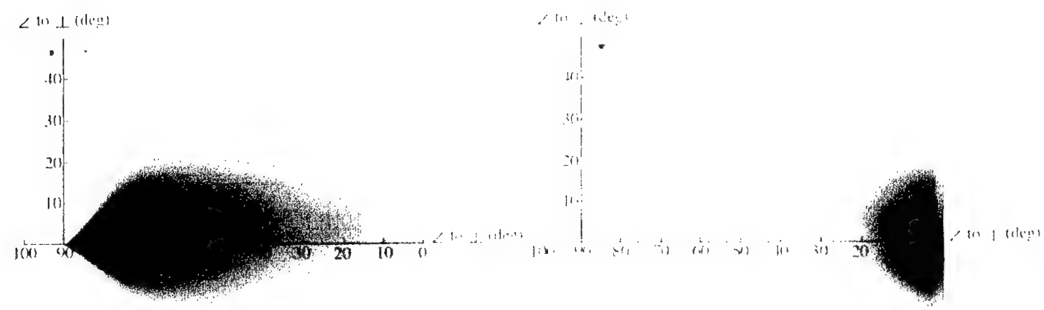

Figure 42. Plume steering in CW operation (left) vs. in repetitive-pulse operation for PVC.

5.1.4 Plume steering in CW operation and its solution

The solution to this problem was repetitive-pulse operation [Figures 43 – 44]. Pulses of 1 to 2ms duration were sufficiently short to prevent significant tape motion during the pulse and consequent steering of the ablation jet by the steady-state cavity sculpted into the relatively thick ablatant coating in CW operation.

Fortunately, our diode drive circuit was designed to have an option for repetitive-pulse operation at a time when we still planned to operate CW. In pulsed mode, measurements show the electronics are able to make square laser pulses with duration as short as 1ms at repetition frequency up to 200Hz. We typically operate at 100Hz and 1-2ms. To achieve 14W peak optical power (requiring 10V at 18A), a power transistor was added to the circuit board.

Subsequent laser power output calibrations showed a highly reproducible, essentially linear variation of average power with applied voltage above laser oscillation threshold. In addition, the measurements we made of the laser output and applied voltage pulse shapes guaranteed that peak power could be extrapolated from average power measurements.

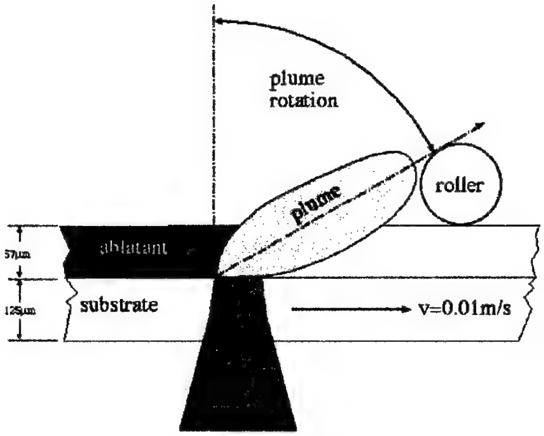

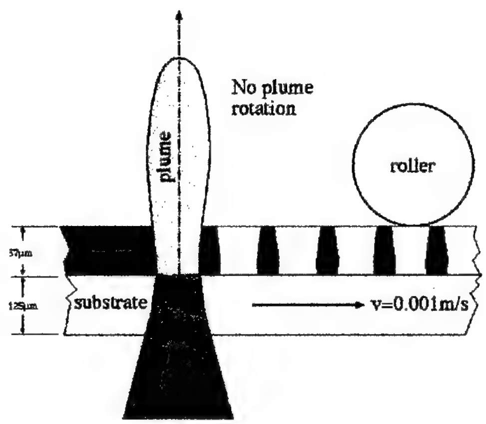

Figure 43a. Illustrating CW plume rotation. Tape motion during continuous ablation forms a ledge which steers the plume.

Figure 43b. Illustrating repetitive-pulse operation as the solution to the plume steering problem.

5.1.5 Effect of focusing and other parameters on the ablation jet

Figure 44a and b are two views of the thruster in operation, corresponding to the two situations shown in Figure 42. In CW operation, we see the badly rotated jet shown in Figure 44a. Under ideal focusing conditions and repetitive-pulse operation, the well collimated jet shown in Figure 44b is obtained. Figure 44c shows a third possibility: repetitive-pulse operation with excessive repetition rate such that the ablation holes overlap. The jet typically has a bright white spot right at the laser focus spot, and a cone of ejecta. The cone is usually orange in color, and is difficult to photograph because it is much less bright than the central spot. Depending on the coating material, the cone may include bright sparks. Material properties also strongly affect the shape of the jet. The well-collimated jet in Figure 44b is obtained with PVC ablatant. Tests with changing focus on PVC ablatant at 6W peak, 4ms showed a complete change in the jet character from barely visible to well developed in 500μm of focus travel.

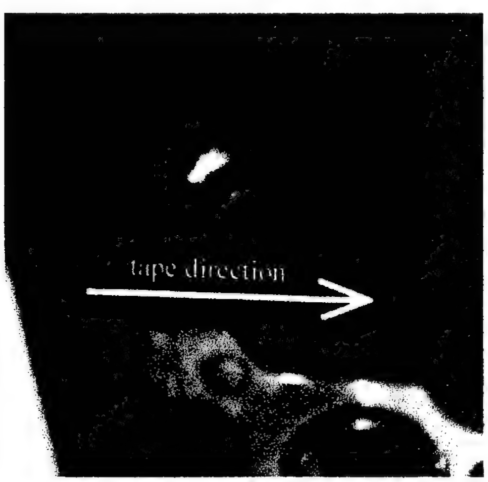

Figure 44a. Plume steering in CW operation

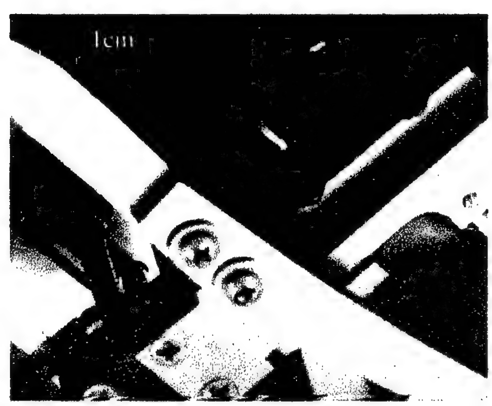

Figure 44b. Well-collimated jet in repetitive-pulse operation

5.1.6 Outgassing data

Figure 44c. Plume steering from overlapping pulses

Outgassing was a major issue with nearly all the passive ablatants. Only the Sheldahl proprietary black came close to meeting our requirements. However, the Sheldahl coating had several distinct. These were a) standard availability in maximum 15μm thickness b) coatings with greater thickness had bad adhesion c) coarse-grained features within the coating caused the ablation jet to point erratically, be broad rather than collimated and emit copious sparks of hot (but not vaporized) material. Figure 45 shows typical outgassing data for the PVC-type coatings.

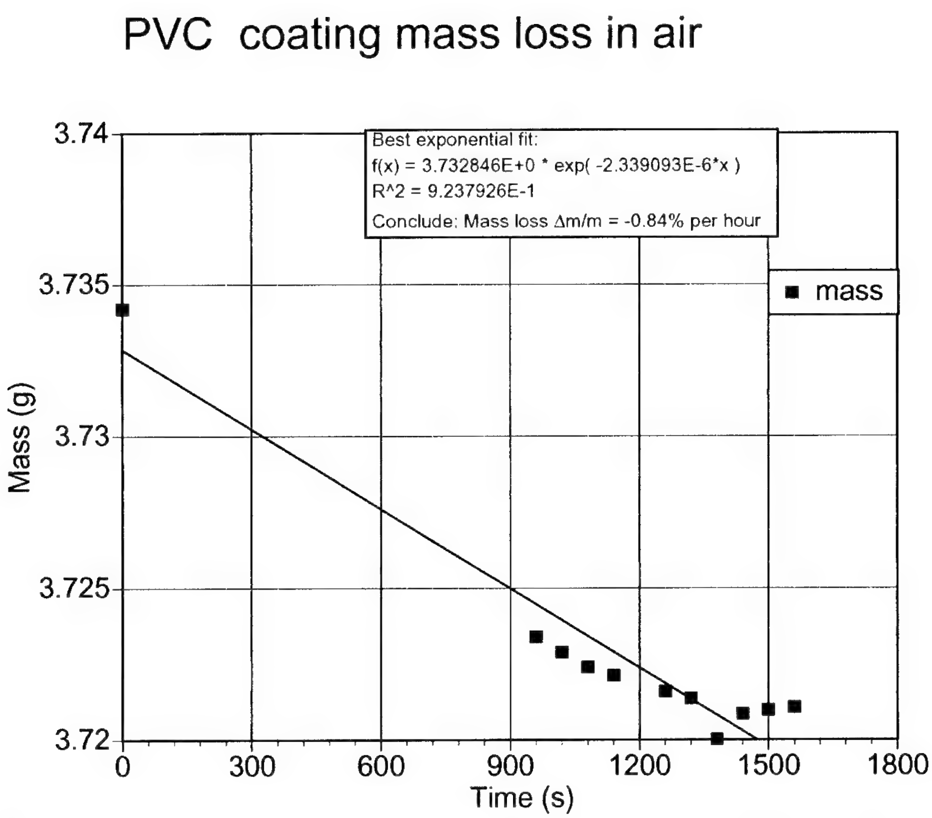

Figure 45. Outgassing mass loss Δm/m for the "Ultravinyl" PVC coating is 8.4E-3 per hour, a factor of 840 greater than our goal.

Sheldahl Corp. proprietary black is a carbon-loaded polyester-based thermo-setting adhesive. In our measurements, it achieved a value of $\Delta m/m$ = 2.4E-4 per hour, only slightly larger than that achieved by the designer polymer coating, and well within reach of our 1E-5/hour goal.

With further development, this material could make a good target tape. In particular, further work to reduce grain size and increase coating thickness without sacrificing adhesion would be worthwhile [see Figure 35 for its static performance, and App. II].

The material is available on 12, 25 and 50μm Kapton™ in 33m lengths. Its operating temperature range is -45 to 105C.

The Sheldahl black coating is also available on PEN, PET and polyethylamide (GE's "Ultem").

5.2 Exothermic Polymer Program – Paul Scherrer Institut

During the report period, we worked closely with the team of Dr. Thomas Lippert at the Paul Scherrer Institut, Villigen, Switzerland to develop exothermic "designer polymers" for our program. Such polymers would "unzip" gracefully, requiring a minimum of laser energy to initiate ablation. ETH is a world-renowned research center, essentially the Los Alamos of Switzerland. Dr. Lippert's specialty is polymer design [see related publications, section 8]. Dr. Lippert had a number of samples available to test, and developed others during the program [see Table 12]. Thirty-five samples were tested. Variations studied were the effect of absorbance, thickness, substrate and type of carbon absorber entrained. In general, the exothermic materials gave outstanding performance.

The proprietary material has a molecular weight of around 5000 g/mol, and releases 3100J/g on thermal decomposition, at a relatively high burning rate. We observe some ash left on the fuel tapes and deposited on adjacent surfaces with our 920nm irradiation. This is not seen with wavelengths shorter than about 350 nm [Lippert 2002].

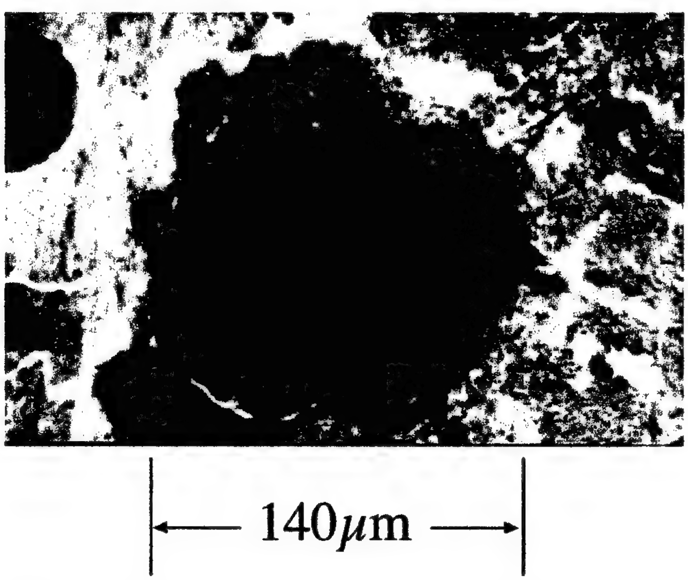

Figure 46. Image of a clean ablation hole in exothermic target material matches size of laser irradiation distribution, shows no self-initiation.

Figure 46 demonstrates that the laser cleanly initiates ablation, without causing uncontrolled detonation or self-ignition, in agreement with the discussion in section 2.2.

Support for the PSI work was provided by EOARD.

Table 12. Static measurements summary: PSI designer polymers

Order No.	Substrate	Ablator	Max C_m (μN/W)	Max I_{sp}(s)
PSNIR.001	125μm Acetate	50μm carbon T=0	14.7	200
	175μm Acetate	50μm carbon T=0	47.3	270
	25μm PET	64μm carbon T=0.15	8.3	----
	25μm PET	33μm carbon T=0.07	5.2	20
	150μm PET	40μm "exothermic" TP6	67.2	180
	150μm PET	40μm "exothermic" TP6	----	----
PSNIR.002	100μm PET	20μm TP1, T=0.38	16	14
	100μm PET	40μm TP2, T=0.27	28	27
	100μm PET	45μm TP3, T=0.34	29	34
	100μm PET	59μm CL1, T=0.50	8.4	19
	100μm PET	67μm CL2, T=0.26	12	19
	100μm PET	70μm CL1B45M, T=0.39	14	----
	75μm PET	65μm CL1B75My,T=0.38	11	155
	75μm Kapton™	64μm CL1B75PI,T=0.40	14	255
	100μm PET	70μm CL5, T=0.077	29	105
	100μm PET	68μm CB1, T=0.50	5	69
	100μm PET	69μm CB2, T=0.26	10	11
	100μm PET	68μm CB9/45S, T=0.36	7	28
	100μm PET	66μm CP1, T=0.38	17	85
PSNIR.003	110μm PET	70μm CL5, T=0.077	19	----
	110μm PET	66μm CP1, =0.38	10	76
	75μm Kapton™	54μm PVC/CL	75	5000
	75μm Kapton™	74μmBuna/CP	35	----
	75μm Kapton™	86μm PANI1	37	580
	75μm Kapton™	59μm Buna/CP	30	200
PSNIR.004	80μm Kapton™	230μm Proprietary "A"	520	546
	80μm Kapton™	142μm Proprietary "B"	370	450
	80μm Kapton™	371μm Proprietary "C"	510	330
	80μm Kapton™	224μm Proprietary "D"	370	----
	80μm Kapton™	102μm Proprietary "E"	220	140
	80μm Kapton™	193μm Proprietary "F"	370	180
	80μm Kapton™	226μm Proprietary "G"	200	650
	85μm Kapton™	490μm Proprietary/0.65% CP	2520	649
	81μm Kapton™	313μm Proprietary/0.65% CP	1170	254
	83μm Kapton™	145μm Proprietary/0.65% CP	215	540

Key:
CB= Alcotex with basic carbon
CP = Alcotex with carbon pearls
CL = Alcotex with conducting carbon
TP = Triazenepolymer with conducting carbon

5.2.1 Relative importance of chemical and laser energy inputs

Knowing that the thermal decomposition energy of the exothermic ablatant is 3.1kJ/g, and the typical Q* in our measurements with this material is in the range 1.0 – 2.5 kJ/g, it is easy to estimate the relative fraction of chemical energy input to the total involved in the interaction as being 10 – 25%.

5.2.2 Static (single impulse) measurements

Table 12 summarizes maximum values of C_m and I_{sp} obtained individually in static impulse measurements for our exothermic materials. The data for the Table is extracted from Appendix I to highlight performance of this material. It is seen that isolated measurements of C_m as high as 2500μN/W and I_{sp} as large as 5000 seconds were

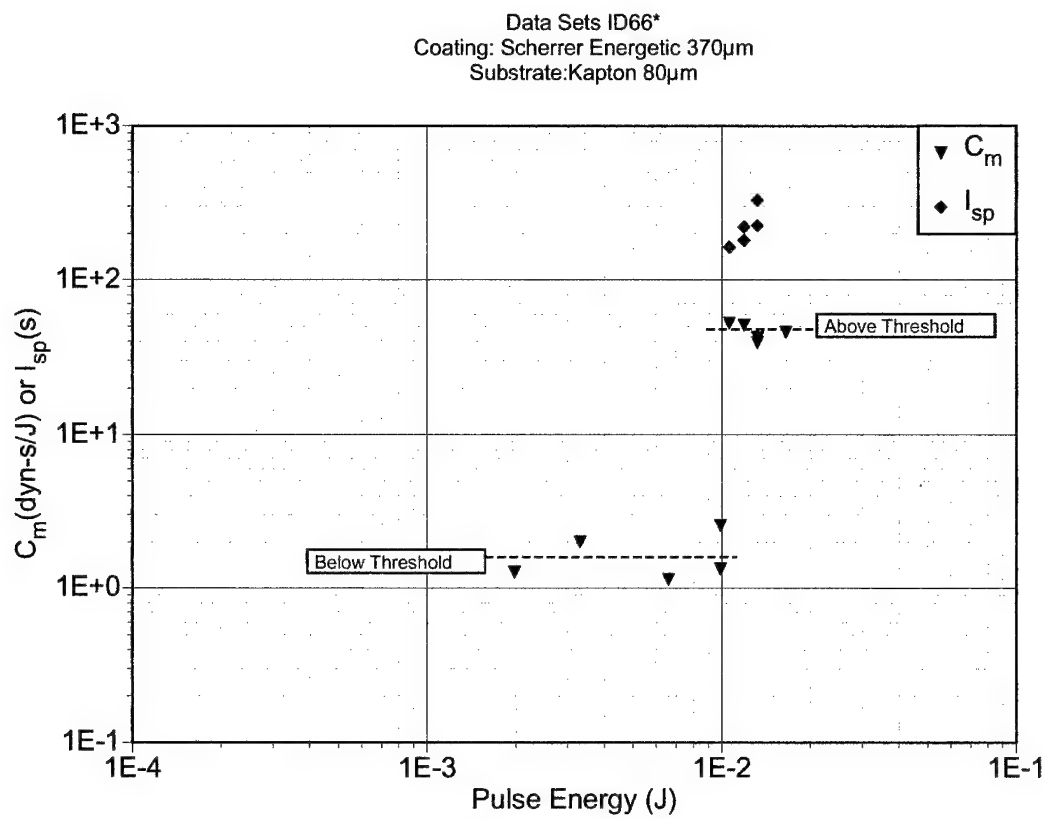

Figure 47. Illustrating strong threshold behavior in static tests of coupling coefficient for exothermic target material. Here, C_m increases abruptly by a factor of 30 at the threshold fluence for the exothermic detonation [compare Figure 30].

obtained in the static test program.

The largest product of C_m and I_{sp} obtained was 0.49 (1170μN/W, 422seconds) for the test described in the third row from the bottom of Table 12 (proprietary material with 0.65% carbon pearls). This product is 2.4 times the maximum permitted for a passive (nonexothermic) material.

Static data for exothermic materials shows a markedly different behavior from that for passive materials, in that a dramatic detonation threshold exists [Figure 47]. This particular test result is the end result of an arduous R&D process at PSI and NMERI/IERA. The material performs markedly better than previous PSI materials, of which Figure 48 is included as an example, showing the performance of the triazene polymer "TP6". The same threshold behavior occurs, but the C_m and I_{sp} levels achieved are much less interesting.

5.2.3 Dynamic (thrust) measurements

Armed with these results, we went on to create tapes from the PSI materials in order to do thrust measurements in the preprototype testbed thruster. Table 13 summarizes these results. Figure 49, following a format suggested by Larson *et al.* 2002, shows the portion of the data which was taken for the AFOSR Phase II program.

The Table 13 data is extracted from Appendix II to highlight performance of this material. From the Table, it is seen that isolated measurements of C_m as high as 350μN/W and I_{sp} as large as 360 seconds were obtained in the dynamic test program.

The largest product of C_m and I_{sp} obtained was 0.08 (274μN/W, 300 seconds) for the proprietary material, measured with the flag pendulum. This product is 40% of the maximum permitted for a nonexothermic material. It is noteworthy that the best results occurred for the samples with the thinnest coatings (see section 5.2.4 below).

The largest thrust we obtained from the exothermic ablatant tapes (on Kapton™) was 560μN, 7.5 times the requirement set out in the program objectives [Phipps and Luke 2002a].

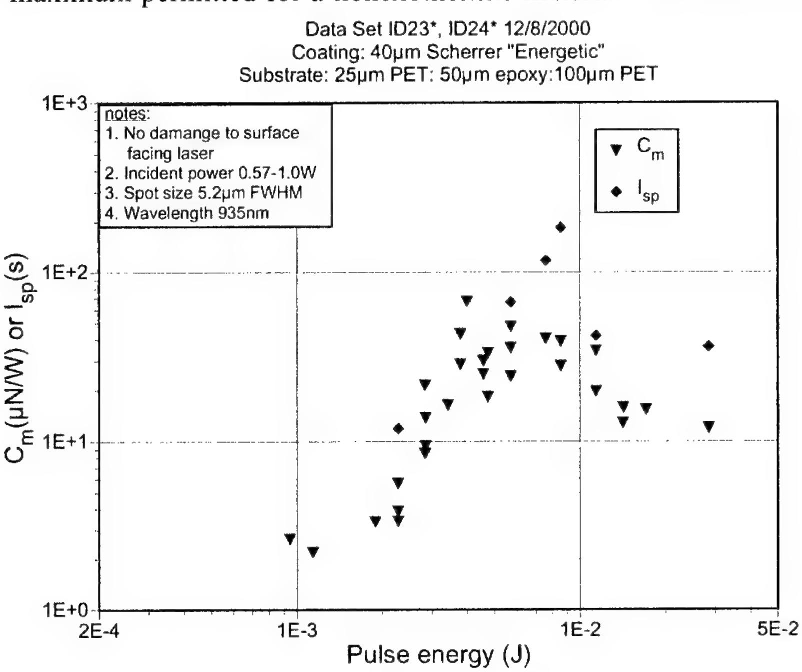

Figure 48. PSI's triazene polymer "TP6" showed the same threshold behavior, but failed to perform well.

Table 13. Dynamic measurements summary: PSI designer polymers

Order No.	Substrate	Ablator	Max C_m (μN/W)	Max I_{sp}(s)
PSNIR.004	80μm Kapton™	313μm Proprietary	277	----
	80μm Kapton™	313μm Proprietary	185	360
	80μm Kapton™	313μm Proprietary	330	78
	80μm Kapton™	370μm Proprietary	84	36
	80μm Kapton™	370μm Proprietary	277	117
	80μm Kapton™	370μm Proprietary	327	38
	80μm Kapton™	370μm Proprietary	313	108
	80μm Kapton™	370μm Proprietary	268	----
	80μm Kapton™	370μm Proprietary	92	----
	80μm Kapton™	370μm Proprietary	349	151
	80μm Kapton™	370μm Proprietary	326	151
	80μm Kapton™	145μm Proprietary	179	347
	80μm Kapton™	145μm Proprietary	274	300
	80μm Kapton™	145μm Proprietary	364	393
	80μm Kapton™	145μm Proprietary	120	283

5.2.4 Discrepancies between static and dynamic measurements

It is easily seen that both specific impulse and coupling coefficient are substantially higher in static compared to dynamic measurements.

To explain this, it is important to note important differences in the test setups.

Specific impulse and coupling coefficient are higher in the static tests for three reasons, and two of them derive from the fact that the static test laser is single mode, while the thrust or "dynamic" test laser is multimode and has to be focused more strongly to reach a useful intensity. These reasons are:

a) The laser spot size in the static test setup is 5um rather than 25um as in the dynamic tests. As a result of the broader illumination spot in the dynamic test setup, even though the laser power is 5 times higher, the intensity on target (W/cm^2) is 5 times lower and the target material which is illuminated is not heated to such a high temperature.

b) In the static tests, the laser beam can be focused on the target with a more relaxed numerical aperture of 0.2 (rather than 0.68 which is necessary in the dynamic test setup). The result is a substantially more cone-shaped beam within the ablatant coating in the dynamic setup.

This means, for example, that on passing through 340um of absorbing coating in dynamic test BT74A*, the majority of the coating material included in the illumination cone sees only 17% of the nominal incident intensity. This effect is responsible for a substantial sacrifice of I_{sp}. On the other hand, for the static test, all the material in the

illuminated cone in the same target would at least see 45% of the nominal incident intensity.

Summarizing these effects, for the thick energetic targets, a lot of the material sees more than 10 times less intensity in the dynamic or thrust test setup.

Part of the solution is to use thinner coatings. The coating thickness is currently something we cannot control, since we don't make them in-house. However, we note that the best results reported in Table 13 were for the 145μm thick coatings.

c) A further input to the difference in I_{sp} in the two cases, which we have not been able to quantify, are the different ways we measure I_{sp} in the two cases. For the static case, we have to measure the size of the cavity produced with a microscope to determine mass loss and I_{sp}, since it is not possible to measure the nanogram mass loss directly. This ignores the mass of gas that leaks out of the coating after the detonation, and gives higher than the true value for I_{sp}.

d) The fact that the particles in the coating are exposed to widely different intensities during illumination in the dynamic test setup produces a range of velocity distributions, and so is also an important reason for lower C_m in that case. For the energetic materials, this is an especially important factor for the C_m discrepancy, because the materials have a dramatic threshold for detonation [Figure 47]. Since impulse or force is measured directly

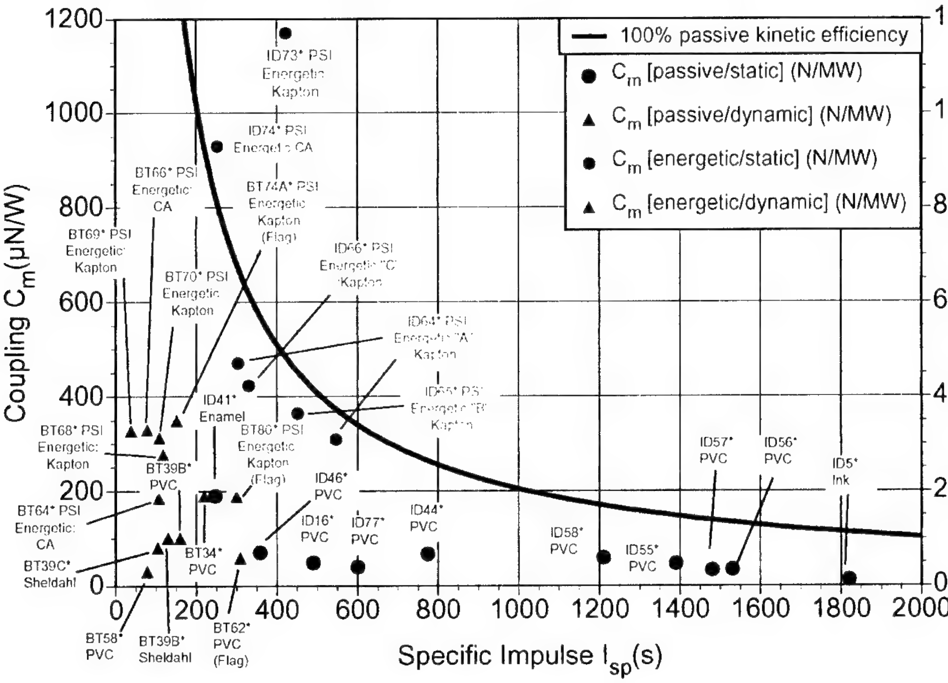

Figure 49. Compilation of data taken during the Phase II program [Phipps and Luke 2002a]. Several of the static test results for the exothermic coatings approach or exceed the product C_m*I_{sp} permitted for a passive material with 100% ablation efficiency. This product is generally a factor of two larger for static vs. dynamic measurements of the same type of material. This discrepancy is discussed in section 5.2.4.

in the static and dynamic test setups, the measurement is not part of the C_m discrepancy.

Having said all this, there are probably other reasons for this discrepancy that we don't fully understand.

5.2.4 Plume contaminant distribution measurements

Figure 50 shows the plume deposit distribution for exothermic targets on Kapton™. In comparison with Figure 42, the yellow rather than black coloration is noted, and a similar to perhaps slightly broader distribution. However, the widths of the distributions in Figures 42 and 50 are not statistically significant.

5.2.5 Outgassing data

In this program, we performed preliminary measurements of exothermic material outgassing which indicated a rate of 0.02%/hour, a very encouraging result just a factor of 20 above our goal.

6.0 Relationship of Accomplishments to AF Mission

The micro-LPT is potentially competitive with the micro-Pulsed Plasma Thruster [micro-PPT] on TechSat21-type microsatellite platforms. ACS propulsion system requirements for the TechSat 21 mission include 4 axis thrust, 0-75 μN thrust per axis, 100 N-s impulse per axis, 320N-s total impulse, 2mN-s minimum impulse bit, less than 20W electrical

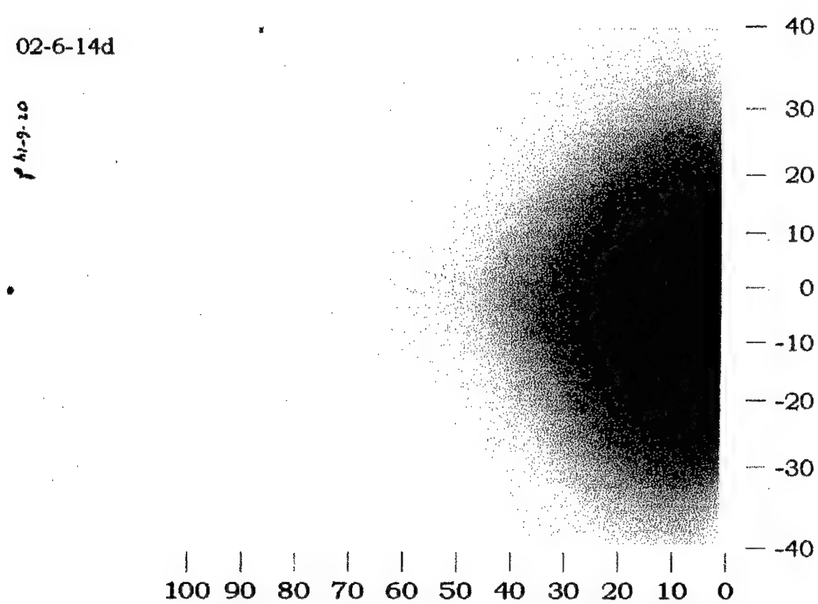

Figure 50. Plume deposit distribution in vertical and horizontal directions 6 cm from the target for PSI energetic target on Kapton. Dimensions are degrees away from target normal. Color is true. Compare Figure 42.

power input and less than 1kg system mass.

At this time, we see no reason why the micro-LPT commercial product cannot meet each of these requirements.

Obvious advantages are physical isolation of the source of energy from the ablation process, low voltage operation, etc. Some potential advantages have been demonstrated under this R&D program. These include lower mass, higher thrust to power ratio and higher system I_{sp}. The main difficulties we face are optics contamination and developing flight-qualified system components.

The micro-PPT has a much longer history. Its other advantages are direct drive, avoiding of intermediate conversion of energy to another form. Difficulties are that the propulsion source is itself consumed, both electrodes must be consumed at the same rate to maintain performance, and it has been difficult to build a reliable system with large ablated mass.

7.0 Personnel Supported:

Dr. Claude Phipps, prime PI, Photonic Associates, Santa Fe NM
Dr. James Luke, co-PI for NMERI/IERA, Albuquerque NM
Dr. Glen McDuff, Senior Research Engineer, NMERI/IERA, Albuquerque NM
Mr. Wesley Helgeson, Senior Technician, Team Specialties, Albuquerque NM
Mr. Ryan McNeal, University of New Mexico student and 3D CADCAM designer

8.0 Publications directly related to this work

8.1 Refereed journal articles

T. Lippert and A. Wokaun, "Laser processing of novel functional materials", *Chimia* **55**, 783-6 (2001)

T. Lippert, C. David, M. Hauer, A. Wokaun, J. Robert, O. Nuyken and C.R. Phipps, "Polymers for UV and Near-IR Irradiation", invited paper for special issue of *J. Photochem. Photobiol. Chem. Sec.*, **145**, 87-92 (2001)

T. Lippert, C. David, M. Hauer, T. Masubuchi, H. Masuhara, O. Nuyken, C. R. Phipps, J. Robert, T. Tada, K. Tomita, A. Wokaun, Novel applications for laser ablation of photopolymers, invited paper, special issue of *Appl. Surf. Sci.*, **186**, 14-23 (2002)

T. Lippert, C. David, M. Hauer, C. Phipps, A. Wokaun, Tailor-Made Polymers for Laser Applications, [invited paper for special issue] *Review of Laser Engineering*, **29**, no. 11, pp 734-738 (2001)

T. Lippert, C. David, J. T. Dickinson, M. Hauer, U. Kogelschatz, S. C. Langford, O. Nuyken, C. Phipps, J. Robert, A. Wokaun, Structure property relations of photoreactive polymers designed for laser ablation, invited paper for special issue of "Photoablation of Materials" in *J. Photochem. Photobiol. Chem. Sec.*, **145**, 145-157 (2001).

C. R. Phipps and J. Luke, "Diode Laser-driven Microthrusters: A New Departure for Micropropulsion", *J. AIAA* **40**, no. 2, pp. 310-318 (2002)

T.Yabe, C.Phipps, K.Aoki, M.Yamaguchi, R.Nakagawa , H.Mine , Y.Ogata , C.Baasandash , M.Nakagawa, E.Fujiwara, K.Yoshida , A.Nishiguchi and I.Kajiwara,

"Micro-airplane Propelled by Laser-Driven Exotic Target", Applied Physics Letters, **80**, 4318-20 (2002)

8.2 Reports

T. Lippert, Interim Reports 1 & 2, Project SPC 02-4038, contract F61775-02-WE-038, "Polymers used as fuels for Laser Plasma Thrusters in small satellites", available from EOARD

C. R. Phipps, and J. R. Luke, "Micro Laser Plasma Thrusters for Small Satellites", presentation at AFOSR Space Propulsion and Power Program, Contractors' Meeting 2002, 19-21 August 2002, Colorado Springs, CO

8.3 Presentations

T. Lippert, C. David, M. Hauer, O. Nuyken, C. Phipps, J. Robert, A. Wokaun, Polymers for UV and near-IR irradiation, 4th International Symposium PCPM 2001 (International Symposium on Photoreaction Control and Photofunctional Materials), Tsukuba, Japan, March 2001. **[invited]**

C. R. Phipps, J. Luke and G. McDuff, "A Diode-laser-driven Microthruster", *Proc. 27th International Electric Propulsion Conference, Pasadena CA, October 15-19, 2001,* Electric Propulsion Rocket Society (2002)

J. Luke, C. R. Phipps and G. McDuff, "Diode Laser Driven Microthruster Prototype", *Proc. 27th International Electric Propulsion Conference, Pasadena CA, October 15-19, 2001* , Electric Propulsion Rocket Society (2002)

T. Yabe, C. Phipps, R. Nakagawa, M. Yamaguchi K. Aoki, C. Baasandash, H. Abe, N. Yoshida, Y. Ogata, M. Nakagawa, E. Fujiwara, K. Yoshida, A. Nishiguchi, K. Ochi and I. Kajiwara, "Numerical and Experimental Analysis of Laser-Driven Rocket and Micro-Airplane", *Proc. 2nd International Conference on inertial Fusion Sciences and Applications, Kyoto Japan,* Elsevier, Paris (2002)

C. R. Phipps, J. R. Luke and G. G. McDuff, "A laser-ablation-based micro-rocket", paper AIAA 2002-2152, *Proc. 33rd AIAA Plasmadynamics and Lasers Conf., Maui* (2002)

C. R. Phipps, " Overview of Laser Applications: the State of the Art and the Future Trend", *Proc. International Congress on Laser Advanced Materials Processing 2002,* Osaka, May 27-31, 2002 **[invited keynote]**

M. Hauer, D. J. Funk, T. Lippert and A. Wokaun, "Laser ablation of a triazene polymer studied by ns-interferometry and shadowgraphy", *Proc. SPIE Conference on High Power Laser Ablation IV,* April 21-26, 2002 **SPIE 4760** pp. 259-268 (2002)

T. Lippert, M. Hauer, C. Phipps and A. Wokaun, "Polymers designed for laser applications - fundamentals and applications", *Proc. SPIE Conference on High Power Laser Ablation IV,* April 21-26, 2002 **SPIE 4760** pp. 63-71 (2002)

C. R. Phipps, J. R. Luke and T. Lippert, "Laser Ablation Powered Mini-Thruster", *Proc. SPIE Conference on High Power Laser Ablation IV,* April 21-26, 2002 **SPIE 4760** pp. 833-842 (2002)

C. R. Phipps, J. R. Luke, G.G. McDuff and T. Lippert, "Diode-laser-driven Micro-propulsion Engine", AAAF 6th International Symposium on Propulsion for Space Transportation of the XXIst Century, Palais de Congres, Versailles, France May 14-17, 2002

J. Luke and C. Phipps, "Laser plasma microthruster performance evaluation", First International Symposium on Beamed Energy Propulsion, Huntsville, AL, November 5-7, 2002

C. Phipps and J. Luke, "Advantages of a ns-pulse micro-Laser Plasma Thruster", First International Symposium on Beamed Energy Propulsion, Huntsville, AL, November 5-7, 2002

C. R. Phipps and J. Luke, "Micro Laser Plasma Thrusters for Small Satellites", *Proc. Santa Fe High Power Laser Ablation Conference*, April 23-28, 2000, SPIE **4065** pp. 801-5 (2000)

C. R. Phipps, "Realistic Laser Ablation Space Propulsion Concepts – Watts to Megawatts," Gordon Research Conference on Laser Interaction with Materials, Andover, NH June 11-15, 2000 **[invited]**

C. R. Phipps, J. Luke and J. Marquis, "Diode Laser-based Microthrusters: A New Alternative for High I_{sp}, Long-life Engines," 36th AIAA/ASME/SAE/ASEE Joint Propulsion Conference, Huntsville, AL July 18, 2000

9.0 Patents

Patent application filed: Phipps, Claude R. and Luke, James R., "Laser Plasma Thruster" [reported on form 882, 4/16/2001]. Anticipated to be awarded in early 2003.

10.0 Further Work

At the conclusion of the Phase II effort, we can identify some items which deserve further pursuit.

As discussed in section 5.1.6, the Sheldahl Corporation proprietary black coatings on various substrates hold future promise for development into a useful fuel tape.

The μLPT concept is extensible to operation with continuously repetitive short pulses, in which regime I_{sp} as high as 7000 seconds has been observed [Phipps and Michaelis 1994]. Appropriate lasers now exist with 15-gram mass, 100mW average power and 1ns pulse duration. Development of these to the 1W average power level is expected within a year [Dunton 2001]. This avenue should be aggressively pursued.

Throughout this program, we have been limited in our ability to do quantitative diagnostics on the microthruster plasma plume. This is because we needed almost all of the financial resources provided in this Phase II contract for direct labor and materials, and could not afford to buy lasers and other equipment required for diagnostics. The laboratory in which we work is at present supplied with only the most basic equipment which would be appropriate for such work. However, diagnostic data is crucial for the

modeling effort being pursued under Air Force funding at the University of Michigan. We hope that future funding will permit us to do a proper job of plasma diagnostics.

11.0 References

Cubbin, E.A., Ziemer, J.K., Choueri, E.Y., and Jahn, R.G. (1997) "Pulsed thrust measurements using laser interferometry", Rev. Sci. Inst. **68**, 2339-2346

Dreyfus, R.W. (1991)*J. Appl. Phys.* **69** 1721-9

Dunton, E., Litton-Airtron Corp. (2001), private communication

Fabbro, R. Fournier, J. Ballard, P. Devaux D. and Virmont, J. (1990)*J. Appl. Phys.* **68**, 775-784

Koppel, C. "Electric Propulsion Subsystem Comparisons", paper IAF-99-A.1.08, 50th International Astronautical Congress, 4-8 October 199, Amsterdam, Netherlands

Larson, C.W., Kalliomaa, W. and Mead. F., (2002) paper AIAA2002-2206, AIAA Plasmadynamics and Lasers Conference, Maui, 20-23 May

Lippert, T., (2002) private communication

Phipps, C.R., (2002) "Study of reflection-mode target illumination in a micro-LPT", Final Report for ERC, Inc. under purchase order no. RP010341, 2 August 2002, available from Electric Propulsion Group, AFRL/PRRS, 1 Ara Road, Edwards AFB CA 93524-7013

Phipps, C. R., Luke J. R. and McDuff, G. G., (2002a) "A diode-laser-driven microthruster", paper IEPC-01-220 *Proc. International Electric Propulsion Conference, Pasadena 2001* (Electric Propulsion Rocket Society, published entirely on CD)

Phipps, C. R., Luke J. R., and McDuff, G. G., (2002b) "A laser-ablation-based micro-rocket", paper AIAA 2002-2152, *Proc. 33rd AIAA Plasmadynamics and Lasers Conf., Maui*

Phipps, C. R., and Luke, J. R., (2002a), "Micro Laser Plasma Thrusters for Small Satellites", presentation at AFOSR Space Propulsion and Power Program, Contractors' Meeting 2002, 19-21 August, Colorado Springs, CO

Phipps, C. R., and Luke, J.R., (2002b), "Diode Laser-driven Microthrusters: A New Departure for Micropropulsion", *J. AIAA* **40** no. 2, 310-318

Phipps, C., Seibert II, D., Royse, R., King, G. and Campbell, J. (2000) "Very High Coupling Coefficients at Low Laser Fluence with a Structured Target," Proc. Santa Fe High Power Laser Ablation Conference, April 23-28, 2000, SPIE **4065** pp. 931-7

Phipps, C. R. and Luke, J. (1999), "Micro Laser Plasma Thrusters for Small Satellites." Final report, AFOSR STTR Phase I contract F49620-98-C-0038, available from AFOSR

Phipps, C.R. and Michaelis, M. M. (1994), "Laser Impulse Space Propulsion", *J. Laser and Particle Beams* **12** no. 1, pp. 23-54

Phipps, C., Harrison, R., Shimada, T., York, G., Turner, T., Corlis, X., Steele, H., Haynes, L. and King, T. (1990)"Enhanced Vacuum Laser-impulse Coupling by Volume Absorption at Infrared Wavelengths", *Laser and Particle Beams,* **8**, 281

Phipps, C. R., Turner, T. P., Harrison, R. F., York, G. W., Osborne, W. Z., Anderson, G. K., Corlis, X. F., Haynes, L. C., Steele, H. S., Spicochi, K. C. and King, T. R., (1988) "Impulse Coupling to Targets in Vacuum by KrF, HF and CO_2 Lasers" , *J. Appl. Phys.*, **64**, pp. 1083-96

Phipps C. R. and Dreyfus, R. (1993) in *Laser Ionization Mass Analysis,* Akos Vertes, Renaat Gijbels and Fred Adams, eds., Wiley, New York, May,

Pirri, A., Root R. and Wu, P. (1978)*AIAA Journal*, **16**, 1296-1304

Raizer, Yu. (1977) *Laser-induced Discharge Phenomena*, Consultants Bureau, New York pp. 198-249

Saleres, A. *et al.*, (1992)*Revue Scientifique et Technique de la Defense*, *CEL-Valenton report 77*

Yabe, T., Phipps, C., Aoki, K., Yamaguchi, M., Nakagawa, R., Mine, H., Ogata, Y., Baasandash, C., Nakagawa, M., Fujiwara, E., Yoshida, K., Nishiguchi, A. and Kajiwara, I. (2002) "Micro-airplane Propelled by Laser-Driven Exotic Target", Applied Physics Letters, **80**, 4318-20 (2002)

Ziemer, J. K. (2000), private communication

Appendix I: Single-pulse Test Data

Notes	ID	Date	T	R	λ (nm)	d_s(μm) FWHM	Substrate	tk. (μm)	Coating	tk. (μm)	Max C_m	at W(mJ)	Max I_{sp}	at W(mJ)	Typ Q*
	1*	5/3/00	x		935	20	kapton	125	S/C carbon black	20	3.3	0.33	261	0.2	3.65E+04
See 1*	2*	5/5/00	x		935	20	kapton	125	S/C carbon black		0				3.65E+04
	3*	5/9/00	x		935	5.2	kapton	125	Krylon matte black	10	198	19.8			2.23E+04
	4*	5/11/00		x	935	5.2	none		delrin	150	26	2.6	45	0.66	3.16E+04
	5*	5/26/00	x		935	5.2	CA	125	Epson black ink	12	1.6	0.16	1820	0.17	2.55E+04
best focused data ever taken	6*	5/26/00	x		935	5.2	CA	115	S/C carbon black	45	0.66	0.066	295	0.099	4.68E+04
	7*	5/30/00	x		935	5.2	CA	125	Lucite/S/C carbon black	75	0.73	0.073	896	0.073	8.62E+04
See 7*	8*	5/30/00	x		935	5.2	CA	125	Lucite/S/C carbon black		0				8.62E+04
See 7*	9*	6/2/00	x		935	5.2	CA	125	Lucite/S/C carbon black		0				8.62E+04
	10*	6/3/00	x		935	5.2	CA	125	Plastikote #411 Ultravinyl	18	0.27	0.027	300	0.044	5.34E+04
Substrate much too thin, burnthrough	11*	6/2/00	x		935	5.2	CA	12.5	Sheldahl black	15	495	49.5			
	12*	8/10/00	x		935	5.2	CA	125	PSI carbon black	50	660	66	202	13.2	2.96E+04
See 12*	13*	8/10/00	x		935	5.2	CA	125	PSI carbon black	50	0				2.96E+04
	14*	8/11/00		x	935	5.2	CA	175	PSI carbon black	50	420	42	271	0.132	4.06E+04
floppy disk	15*	8/11/00	x		935	5.2	?	75	Fe_3O_4	2	2	0.2			
system continuity check	16*	8/11/00		x	935	5.2			black PVC film	175	66	6.6	2600	6.6	4.95E+04
bad data	17*	11/16/00			935						0				
thrust reversal and burnthrough	18*	11/16/00	x		935	5.2	PET	25	PSI dilute carbon black T=0.15	64	6.6	0.66			

Notes	ID	Date	T	R	λ (nm)	d_s(μm) FWHM	Substrate	tk. (μm)	Coating	tk. (μm)	Max C_m	at W(mJ)	Max I_{sp}	at W(mJ)	Typ Q*
Substrate much too thin, burnthrough	19*	11/16/00	x		935	5.2	PET	25	PSI dilute carbon black T=0.07	33	17.1	1.71	20	1.14	5.00E+04
Substrate much too thin, burnthrough	20*	11/16/00	x		935	5.2	PET	12	S/C carbon black	12	0				
Test: PET damage threshold>13.2mJ	21*	11/16/00			935	5.2	PET	25			0				
	22*	11/21/00	x		935	5.2	kapton	25	S/C carbon black	58	660	66			
epoxy sandwich	23*	12/7/00	x		935	5.2	PET & epoxy	150	PSI exothermic TP6	40	40	4	184	8.55	2.60E+04
See 23*	24*	12/8/00	x		935	5.2	PET & epoxy	150	PSI exothermic TP6	40	0				2.60E+04
	25*	1/18/01	x		935	5.2	CA	100	Plastikote #411 Ultravinyl	89	114	11.4	245	28.5	3.65E+04
	26*	1/30/01	x		935	5.2	kapton,CA &epoxy	157	Sheldahl black	15	114	11.4	517	3.99	2.75E+04
	27*	2/28/01	x		935	5.2	kapton	115	Sheldahl black	30	170	17	661	11.4	1.22E+05
	28*	3/6/01	x		935	5.2	PET	100	PSI TP1 T=0.38	20	33	3.3	13.5	1.32	1.69E+04
	29*	3/6/01	x		935	5.2	PET	100	PSI TP2 T=0.27	40	54.8	5.48	26.6	3.3	7.80E+03
	30*	3/6/01	x		935	5.2	PET	100	PSI TP3 T=0.34	45	46	4.6	34	4.62	1.05E+04
	31*	3/6/01	x		935	5.2	PET	100	PSI CL1 T=0.50	59	274	27.4	19.4	11	1.65E+04
	32*	3/6/01	x		935	5.2	PET	100	PSI CL2 T=0.26	67	330	33	18.9	21.9	1.47E+04
	33*	3/8/01	x		935	5.2	PET	100	PSI CL1B45M T=0.39	70	21.9	2.19			
	34*	3/8/01	x		935	5.2	PET	100	PSI CL1B75M T=0.38	65	33	3.3	155	21.9	1.64E+05
	35*	3/8/01	x		935	5.2	PET	100	PSICL1B75PI T=0.40	64	33	3.3	255	4.62	1.21E+05
	36*	3/8/01	x		935	5.2	PET	100	PSI CL5 T=0.077	70	66	6.6	105	1.98	4.08E+04
	37*	3/8/01	x		935	5.2	PET	100	PSI CB1 T=0.50	68	132	13.2	68.5	6.6	9.59E+04

Notes	ID	Date	T	R	λ (nm)	d_s(μm) FWHM	Substrate	tk. (μm)	Coating	tk. (μm)	Max C_m	at W(mJ)	Max I_{sp}	at W(mJ)	Typ Q*
	38*	3/8/01	x		935	5.2	PET	100	PSI CB2 T=0.26	69	66	6.6	10.5	21.9	1.72E+04
	39*	3/8/01	x		935	5.2	PET	100	PSI CB9/45S T=0.36	68	66	6.6	27.9	9.9	2.87E+04
	40*	3/8/01	x		935	5.2	PET	100	PSI CP1 T=0.38	66	33	3.3	85	21.9	1.09E+04
	41*	3/15/01	x		935	5.2	CA	110	Plastikote #215 500F Engine Enamel	89	1.32	0.132	247	0.495	5.65E+04
	42*	3/15/01	x		935	5.2	CA	110	Plastikote #340 Lacquer	95	13.2	1.32	60	1.32	7.33E+03
	43*	3/15/01	x		935	5.2	CA	110	Plastikote #611 Trim Black	82	19.8	1.98	336	0.396	4.19E+04
	44*	3/15/01	x		935	5.2	CA	110	Plastikote #405 Ultravinyl	57	19.8	1.98	774	1.98	4.44E+04
	45*	3/20/01	x		935	100	CA	110	Plastikote #405 Ultravinyl	89	164	16.4			
	46*	3/20/01	x		935	100	CA	110	Plastikote #405 Ultravinyl	57	33	3.3	358	3.3	2.57E+04
	47*	3/20/01	x		935	100	PET	110	PSI CL5 T=0.077	70	132	13.2			
	48*	3/20/01	x		935	100	PET	110	PSI CP1 T=0.38	66	330	33	76	9.9	5.68E+04
	49*	3/20/01		x	935	5.2	CA epoxy sandwich	175	none		0				
	50*	6/4/01	x		935	5.2&100	kapton	75	PVC/Alcotex/conducting C	54	13	1.3	5000	2	1.39E+05
	51*	6/4/01	x		935	5.2&100	kapton	75	Buna 3/50/Alcotex/carbon pearls	74	20	2			1.08E+04
	52*	6/4/01	x		935	5.2&100	kapton	75	PANI1	86	32	3.2	580	3.2	9.60E+04
	53*	6/6/01	x		935	5.2&100	capacitor PET	127	matte black ultravinyl	70	200	20	180	13	3.26E+04
	54*	6/6/01	x		935	5.2&100	kapton	75	Buna 3/35	59	80	8	200	2	1.61E+04
	55*	6/20/01	x		935	5.2&100	clear PET	127	bumper vinyl paint	66	75	7.5	2000	10	7.26E+04
	56*	6/20/01	x		935	5.2&100	clear PET	127	matte black ultravinyl	76	100	10	1600	6.5	1.88E+05

Notes	ID	Date	T	R	λ (nm)	d_S(μm) FWHM	Substrate	tk. (μm)	Coating	tk. (μm)	Max C_m	at W(mJ)	Max I_{sp}	at W(mJ)	Typ Q*
	57*	6/26/01	x		935	5.2&101	clear PET	127	matte black ultravinyl	53	10	1	1600	1	2.93E+04
	58*	6/27/01	x		935	5.2	clear PET	127	fresh matte black ultravinyl	55	100	10	6000	3	6.86E+04
	59*	6/28/01	x		935	5.2	clear PET	127	matte black ultravinyl	55	70	7	90	10	2.11E+04
	60*	7/1/01	x		935	5.2&90	clear CA	127	matte black ultravinyl	57	100	10	300	4	2.80E+04
	61*	7/19/01	x		935	5.2&90	clear A	127	matte black ultravinyl	57	33	3.3	500	9.9	1.31E+04
	62*	1/29/02	x		935	5.2	kapton	80	PSI sample "F"	193	80	8	180	10	4500
	63*	1/29/02	x		935	5.2	kapton	80	PSI sample "G"	226	100	10	650	3.3	7.30E+04
	64*	1/29/02	x		935	5.2	kapton	80	PSI sample "A"	230	130	13	546	6.6	1.70E+04
	65*	1/30/02	x		935	5.2	kapton	80	PSI sample "B"	142	80	8	450	4.6	1.40E+04
	66*	1/30/02	x		935	5.2	kapton	80	PSI sample "C"	371	120	12	330	13	7.60E+03
	67*	1/30/02	x		935	5.2	kapton	80	PSI sample "D"	224	26	2.6	----	----	4.44E+03
	68*	1/30/02	x		935	5.2	kapton	80	PSI sample "E"	102	130	13	140	3.3	8.40E+03
	69*	1/30/02	x		935	5.2	CA	107	Black nail polish	84	20	2	71	3	6.40E+03
	70*	6/7/02	x		935	5.2	CA	125	1/3BNP, 2/3NC	37	20	2	132	2	2.14E+04
	72*	6/7/02	x		935	5.2	CA	125	2/3BNP. 1/3NC	30	66	6.6	58	16.5	1.40E+04
	73*	6/7/02	x		935	5.2	kapton	86	Prop. with 0.65%CP	490	66	6.6	649	13.2	1.40E+03
	74*	6/7/02	x		935	5.2	CA	81	Prop. with 0.65%CP	313	26	2.6	254	2	3.00E+03
negative coupling	75*	7/9/02	x		935	5.2	kapton	64	resistor ink	71	0				
no coupling	76*	7/9/02	x		935	5.2	teflon	125	Al	2	0				
	77*	7/19/02	x		935	5.2	kapton	64	custom non plasticized PVC	93	33	3.3	60	1.3	1.50E+04
	78*	7/19/02	x		935	5.2	kapton	83	Prop. with 0.65%CP	145	10	1	540	1.5	6.00E+04

Key to Tables:

Alcotex™ =	Carbon-doped polyvinyl alcohol, Hoechst
BT=	Thrust test identification number. Asterisk inidicates Phase II work
CA =	Cellulose acetate
CB=	Alcotex™ with basic carbon
CL =	Alcotex™ with conducting carbon
CP =	Alcotex™ with carbon pearls
C_m =	Momentum coupling coefficient or thrust to power ratio (μN/W)
d_s (μm) =	Spot diameter on target at full width half maximum
f =	Pulse frequency in thrust tests (Hz)
F =	Thrust (μN)
ID =	Static experiment identification number. Asterisk indicates Phase II work
I_{sp} =	Specific impulse (s)
Kapton™=	Polyimide
PANi =	Polyaniline
PET =	Polyethyleneterephthalate
Prop. =	Proprietary exothermic coating
PSI =	Paul Scherrer Institut
Q* =	Specific ablation energy (kJ/kg)
R =	Reflection mode measurement
S/C =	Black pigment from Smith-Corona typewriter tape
T =	Transmission mode measurement
τ=	Pulse duration for thrust measurements (ms) [static measurements have various pulsewidths]
T_{op} =	Run time for a thrust measurement
tk. =	Substrate or coating thickness
TP =	Triazenepolymer with conducting carbon
v =	Tape speed (mm/s) in thrust tests
W(mJ) =	Incident pulse energy

Appendix II: Thrust Test Data

Notes	BT	Date	λ (nm)	v(mm/s)	Sub-strate	tk. (μm)	Coating	tk. (μm)	P_{pk}(W)	τ(ms)	f(Hz)	<P>(W)	C_m (μN/W)	I_{sp} (s)	Q* (kJ/kg)	F(μN)	T_{op}(s)
Realized rep-pulse operation is necessary to avoid plume steering	29*	10/13/01	980	1	CA	125	Plastikote 405	91	2	20	6.7	0.268	127.7	----	----	34.21	150
Hg friction makes this point dubious	30*	10/13/01	980	1	CA	125	Plastikote 405	91	2	20	3	0.12	65.8	----	----	7.89	300
Hg friction and outgassing make this point dubious	31*	10/13/01	980	1	CA	125	Plastikote 405	91	2.5	20	7	0.35	28.2	----	3946	9.87	1200
Beautiful jet! Fixed spot overlap, no plume steering	32*	10/25/01	980	3	CA	125	Plastikote 405	83	2.5	10	10	0.25	----	----	8790	----	336
Plume steering because of spot overlap	33*	10/26/01	980	12	CA	125	Plastikote 405	83	2.5	10	12	0.3	57.0	36.6	6292	17.11	375
Very nice jet! Conference material! Slight steering.	34*	10/30/01	980	5	CA	125	Plastikote 405	67 to 78	2.5	10	15	0.375	189.5	220.4	1.14E+04	71.05	380
	35*	10/30/01	980	10	CA	125	Plastikote 405	67	2.5	10	25	0.625	120.5	157.4	1.28E+04	75.32	350
NB: points 1-4 reduced with calibration factors deduced from measurements of nonlinear force response due to mercury stiction.	36*	10/30/01	980	5	CA	125	Plastikote 405	78	2.5	10	15	0.375	70.2	----	----	26.32	272

Notes	BT	Date	λ (nm)	v(mm/s)	Sub-strate	tk. (µm)	Coating	tk. (µm)	P_{pk}(W)	τ(ms)	f(Hz)	<P>(W)	C_m (µN/W)	I_{sp} (s)	Q* (kJ/kg)	F(µN)	T_{op}(s)
Beautiful jet! no plume steering; new power circuit permits high peak currents	37*	11/20/01	980	13	CA	125	Plastikote 405	78	4	2	40	0.32	---	---	---	---	66.7
helical illumination mode	38*	11/20/01	980	18.1	CA	125	Plastikote 405	53	4	2	60	0.48	99.8	130.3	1.28E+04	47.89	105
bad jet. Lens not properly focused	39A*	11/20/01	980	12.1	kapton	125	Sheldahl black	15	5.96	3	40	0.7152	---	---	1.47E+04	---	175
	39B*	11/20/01	980	12.1	kapton	125	Sheldahl black	15	5.96	3	30	0.5364	100.6	160.1	1.56E+04	53.95	180
	39C*	11/20/01	980	12.1	kapton	125	Sheldahl black	15	7.69	3	30	0.6921	80.3	104.9	1.28E+04	55.58	180
catastrophic lens failure	40*	11/21/01	980	12.1	kapton	125	Sheldahl black	15	6.83	3	32	0.65568	---	---	---	---	75
Beautiful jet! But excessive outgassing	41*	11/21/01	980	12.1	CA	125	Plastikote 405	60	5.96	2	32	0.38144	---	---	---	---	30
Best spots yet: 40x100x64 deep but blast shield destroyed	42*	11/30/01	980	10	CA	125	Plastikote 405	60	5.1	2	20	0.204	---	---	---	---	50
CW R-mode test (failure)	43*	12/3/01	980	20	CA	125	Plastikote 405	78	---	---	---	4	---	---	---	---	16
Etch depth in kapton: 15µm NB	44*	1/22/02	980	12.1	kapton	125	Aluminum	0.2	5.96	3	30	0.5364	49.1	---	---	26.32	167
No measurable deposits; however, very poor adhesion	45*	1/12/02	980	12.1	CA	125	bumper paint	69	5.96	3	30	0.5364	132.5	---	---	71.05	167
No Q* because ended with tape 40% bare;	46*	1/22/02	980	12.1	CA	125	bumper paint	69	5.96	4	30	0.7152	67.5	---	---	48.25	167

Notes	BT	Date	λ (nm)	v(mm/s)	Sub-strate	tk. (µm)	Coating	tk. (µm)	P_{pk}(W)	τ(ms)	f(Hz)	<P>(W)	C_m (µN/W)	I_{sp} (s)	Q* (kJ/kg)	F(µN)	T_{op}(s)
Lens died: tried 3 times, found kapton was burning on front side	47*	1/23/02	980	12.1	kapton	125	bumper paint	15	5.96	4	45	1.0728	----	----	----	----	11
Burned 4th lens, gave up	48*	1/23/02	980	12.1	kapton	125	Sheldahl black	15	5.96	4	30	0.7152	----	----	----	----	----
Refocused in error, so large spot, overlaps, bad plume steering at 90 °; still, good jet!	49*	1/23/02	980	12.1	CA	125	ultravinyl:PMMA 8:1	46	5.96	4	30	0.7152	65.9	----	----	47.11	300
Outgassing makes delta-m & Q* measurement inaccurate	50*	1/30/02	980	12.1	CA	125	ultravinyl:PMMA 8:1	46	5.96	4	30	0.7152	60.7	86.4	13949	43.42	300
Lots of sparks, some beam steering; Outgassing makes delta-m & Q* measurement inaccurate	51*	1/30/02	980	12.1	CA	107	black nail polish	84	5.96	4	40	0.9536	124.2	81.1	6404	118.42	250
Jet is very broad and stutters. Also saw kapton damage: tiny 100µm holes on FS.	52*	2/5/02	980	12.1	kapton	50	bumper paint	86	5.96	4	35	0.8344	----	----	----	----	286
BT37* tape; highest Q* recorded; Isp = 431 if Cm=6.5.	53*	2/5/02	980	12.1	CA	125	Plastikote 405	78	5.96	4	35	0.8344	----	----	6.50E+04	----	286
BT52* tape	54*A	2/5/02	980	12.1	kapton	125	bumper paint	86	5.96	4	45	1.0728	22.1	----	----	23.68	120
BT52* tape	54*B	2/5/02	980	3	kapton	125	bumper	86	3	10	12	0.36	51.2	----	----	18.42	450

Notes	BT	Date	λ (nm)	v(mm/s)	Sub-strate	tk. (µm)	Coating	tk. (µm)	P_{pk}(W)	τ(ms)	f(Hz)	<P>(W)	C_m (µN/W)	I_{sp} (s)	Q* (kJ/kg)	F(µN)	T_{op}(s)
BT52* tape	54* C	2/5/02	980	12.1	kapton	125	bumper paint	86	5.34	4	45	0.9612	68.4	---	---	65.79	450
Focus tests with focal dial settings from 0.090 to 0.054"	55*	4/4/02	920	12.1	CA	125	Plastikote 405	60	5.3	4	20	0.424	---	---	---	---	5
Beautiful jets with zfoc=0.082. First run with focus motor installed. Jet quality tests with various focal dial settings, <P> up to 2.0W, vtape up to 20. All foci beyond tape.	56*	4/17/02	920	12.1	CA	125	Plastikote 405	83	various 3.6-11.1	2	40 to 60	---	---	---	---	---	80
First accurate thrust measurement. First accurate Q* meast. Excellent Q* for this tape. Cm meast inhibited by dirty mercury cup.	57*	4/17/02	920	20	CA	125	Plastikote 405	83	11.1	2	90	1.998	4.0	10.6	2.63E+04	7.89	500
First believable Cm meast.	58*	4/18/02	920	20	CA	125	Plastikote 405	83	11.1	2	90	1.998	29.8	78.4	2.58E+04	59.47	500
	59*A	4/18/02	920	20	CA	125	Plastikote 405	83	3.6	2	90	0.648	33.3	33.9	9967	21.58	200
	59*B	4/18/02	920	20	CA	125	Plastikote 405	83	6	2	90	1.08	27.9	28.4	9967	30.13	200
	59* C	4/18/02	920	20	CA	125	Plastikote 405	83	8	2	90	1.44	20.8	21.2	9967	30.00	200
	59* D	4/18/02	920	20	CA	125	Plastikote 405	83	11.1	2	90	1.998	18.3	18.6	9967	36.58	200

Notes	BT	Date	λ (nm)	v(mm/s)	Sub-strate	tk. (μm)	Coating	tk. (μm)	P_{pk}(W)	τ(ms)	f(Hz)	<P>(W)	C_m (μN/W)	I_{sp} (s)	Q* (kJ/kg)	F(μN)	T_{op}(s)
	59*E	4/18/02	920	20	CA	125	Plastikote 405	83	11.1	2	65	1.443	20.5	27.6	1.32E+04	29.61	300
Best looking jet in the bunch	59*F	4/18/02	920	20	CA	125	Plastikote 405	83	12.75	2	65	1.6575	18.9	25.4	1.32E+04	31.32	300
Tiny pillshaped flash, no FS flash, lots of smoke	59*G	4/18/02	920	20	CA	125	Plastikote 405	83	12.75	2	65	1.6575	----	----	1.32E+04	----	1
Tapebacking fell apart before we could shoot.	60*	4/18/02	920	----	kapton	75	Lippert "A" and "B"	240-350	12.75	2	----	----	----	----	----	----	----
Lots of sparks; 5s track;Track is 250wx120d, burning to within 60 of front surface	61*	4/18/02	920	20	CA	125	BNP	83	11.1	4	90	3.996	12.5	----	----	50.00	250
	61*B	4/18/02	920	20	CA	125	BNP	83	12.75	4	90	4.59	10.3	----	----	47.37	250
FLAG PENDULUM; all at z=0.082; purpose: optimization run vs. W	62*(1)	4/19/02	920	20	CA	125	Plastikote 405	91	11.1	2	90	2	22.8	----	----	46.00	15
FLAG PENDULUM	62*(2)	4/19/02	920	20	CA	125	Plastikote 405	91	11.1	2	80	1.78	33.3	----	----	59.00	15
FLAG PENDULUM	62*(3)	4/19/02	920	20	CA	125	Plastikote 405	91	11.1	3	80	2.66	24	----	----	64.00	15
FLAG PENDULUM	62*(4)	4/19/02	920	20	CA	125	Plastikote 405	91	8	3	80	1.92	27.3	----	----	52.00	15
FLAG PENDULUM	62*(5)	4/19/02	920	20	CA	125	Plastikote 405	91	6	3	80	1.44	24.7	----	----	36.00	30
FLAG PENDULUM	62*(6)	4/19/02	920	20	CA	125	Plastikote 405	91	3.6	3	80	0.86	47.7	----	----	41.00	30

Notes	BT	Date	λ (nm)	v(mm/s)	Sub-strate	tk. (μm)	Coating	tk. (μm)	P_{pk}(W)	τ(ms)	f(Hz)	<P>(W)	C_m (μN/W)	I_{sp} (s)	Q* (kJ/kg)	F(μN)	T_{op}(s)
FLAG PENDULUM	62*(7)	4/19/02	920	20	CA	125	Plastikote 405	91	12.75	1	80	1.02	40.2	----	----	41.00	30
45° steering, FLAG PENDULUM	62*(8)	4/19/02	920	20	CA	125	Plastikote 405	91	2.5	10	15	0.375	54.7	----	----	21.00	30
30° steering, FLAG PENDULUM	62*(9)	4/19/02	920	4	CA	125	Plastikote 405	91	2.5	10	15	0.375	36.4	----	----	14.00	45
FLAG PENDULUM	62*(10)	4/19/02	920	4	CA	125	Plastikote 405	91	6	10	15	0.9	27.8	231	8.13E+04	25.00	45
best Cm result in optimization run, cf. Done with FLAG PENDULUM; very nice jet!	62*(11)	4/19/02	920	20	CA	125	Plastikote 405	91	3.6	3	80	0.86	58.3	309	5.19E+04	50.00	300
best Isp result in optimization run, FLAG PENDULUM	62*(12)	4/19/02	920	20	CA	125	Plastikote 405	91	8	3	80	1.92	28.4	313	1.08E+05	55.00	300
FLAG PENDULUM	62*(13)	4/19/02	920	20	CA	125	Plastikote 405	91	12.75	3	80	3.06	19.2			59.00	30
FLAG PENDULUM	62*(14)	4/19/02	920	20	CA	125	Plastikote 405	91	12.75	3	80	3.06	16.4			50.00	30
	63*	6/7/02	920	19.2	CA	81	Lippert "GP"	313		2	60	0.6	277	----	----	166	16
unreliable result	64*	6/13/02	920	19.2	CA	81	Lippert "GP"	313	4.8	2	60	0.58	185	360	1.93E+04	107	180
outgassing makes delta-m & Q* measurement somewhat inaccurate	65*	6/13/02	920	19.2	CA	125	Plastikote 405	56	11.1	2	65	1.44	62	51	----	89	600
best performance yet	66*	6/14/02	920	19.2	CA	81	Lippert Prop.	313	11.1	2	65	1.44	330	78	----	475	70

Notes	BT	Date	λ (nm)	v(mm/s)	Sub-strate	tk. (μm)	Coating	tk. (μm)	P_{pk}(W)	τ(ms)	f(Hz)	<P>(W)	C_m (μN/W)	I_{sp} (s)	Q* (kJ/kg)	F(μN)	T_{op}(s)
	67*	6/14/02	920	19.2	kapton	81	Lippert Prop.	370	4.8	2	65	0.624	84	36	4158	52	40
	68*	6/14/02	920	19.2	kapton	81	Lippert Prop.	370	8	2	65	1.04	277	117	----	288	300
	69*	6/14/02	920	19.2	kapton	81	Lippert Prop.	370	8	2	65	1.04	327	38	----	340	270
this is the best performance yet	70*	6/14/02	920	19.2	kapton	81	Lippert Prop.	370	11.1	2	65	1.44	313	108	----	450	60
z=0.063	72*	6/14/02	920	19.2	kapton	81	Lippert Prop.	370	13	2.5	65	2.11	268	----	----	566	180
still no visible jet. Thick coating.	73*	7/9/02	920	10	kapton	81	Lippert Prop.	370	6	10	20	1.2	92	----	----	110	10
FLAG PENDULUM	74A*	7/18/02	920	20	kapton	81	Lippert Prop.	370	8	2	65	1.04	349	151	4230	363	30
FLAG PENDULUM	74B*	7/18/02	920	20	kapton	81	Lippert Prop.	370	8	2	65	1.04	326	151	4230	339	75
saw negative displacement. Burned output lens.	75*	7/18/02	920	20	CA	107	BNP, sprayed	53	10	10	30	3	0	0	0	0	300
	76*	7/18/02	920	20	CA	107	BNP, sprayed	53	10	2	50	1	15.1	28.6	9243	30.3	300
terminated by tape catching in apparatus.	77*	7/18/02	920	20	CA	107	BNP, thick painted	115	10	3	50	1.5	35.1	----	----	52.6	180
Torsion (see flag result)	78*	8/7/02	920	20	kapton	83	PSI exothermic, thin	145	5.5	2	50	0.55	179	35	1.90E+03	99	200
FLAG PENDULUM	80*	8/8/02	920	20	kapton	83	PSI exothermic, thin	145	5.5	2	50	0.55	274	300	1.06E+04	150	60

Notes	BT	Date	λ (nm)	v(mm/s)	Sub-strate	tk. (μm)	Coating	tk. (μm)	P_{pk}(W)	τ(ms)	f(Hz)	<P>(W)	C_m (μN/W)	I_{sp} (s)	Q* (kJ/kg)	F(μN)	T_{op}(s)
Torsion; terminated by protector plate burn; best;z=0.056";η=70%.	81*	8/27/02	920	20	kapton	83	PSI exothermic, thin	145	5.5	2	50	0.55	364	39	1.06E+03	200	52
Torsion	82*	8/28/02	920	20	kapton	83	PSI exothermic, thin	145	5.5	2	50	0.55	120	28	2.31E+03	66	165
Torsion; longest run, 126μN thrust. BEST JET WE"VE SEEN; terminated by EOT.	83*	8/28/02	920	20	CA	83	Aged Plastikote 405	145	7.62	3	80	1.83	81	93	1.14E+04	147	960